

Distribution Agreement

In presenting this dissertation as a partial fulfillment of the requirements for an advanced degree from Emory University, I hereby grant to Emory University and its agents the non-exclusive license to archive, make accessible, and display my dissertation in whole or in part in all forms of media, now or hereafter known, including display on the world wide web. I understand that I may select some access restrictions as part of the online submission of this dissertation. I retain all ownership rights to the copyright of the dissertation. I also retain the right to use in future works (such as articles or books) all or part of this dissertation.

Signature:

Shannon Elisabeth Elf

Date

Development of Novel Targeted Anti-Leukemia Therapies

By

Shannon Elisabeth Elf
Doctor of Philosophy

Graduate Division of Biological and Biomedical Sciences
Molecular & Systems Pharmacology

Jing Chen, Ph.D.
Advisor

Lawrence Boise, Ph.D.
Committee Member

Haian Fu, Ph.D.
Committee Member

Sumin Kang, Ph.D.
Committee Member

Rita Nahta, Ph.D.
Committee Member

Accepted:

Lisa A. Tedesco, Ph.D.
Dean of the James T. Laney School of Graduate Studies

Date

Development of Novel Targeted Anti-Leukemia Therapies

By

Shannon Elisabeth Elf
Artium Baccalaureus (A.B.), Bowdoin College, 2003

Advisor:
Jing Chen, Ph.D.

An abstract of
A dissertation submitted to the Faculty of the James T. Laney School of Graduate
Studies of Emory University in partial fulfillment of the requirements for the degree
of
Doctor of Philosophy
in
Graduate Division of Biological and Biomedical Sciences
Molecular & Systems Pharmacology
2013

Development of Novel Targeted Anti-Leukemia Therapies

By

Shannon Elisabeth Elf

Constitutively activated tyrosine kinases are frequently implicated in the pathogenesis of human leukemia, making them attractive therapeutic targets. Though tyrosine kinase inhibitors have proven remarkably effective for leukemia treatment, they are disease-remitting rather than curative, and many patients develop overt resistance during therapy. This underscores the importance of designing alternate and/or complementary anti-leukemia therapeutic strategies. Our phospho-proteomics studies revealed that serine/threonine kinase p90RSK2 (RSK2) is a common substrate of distinct leukemogenic tyrosine kinases including BCR-ABL and FMS-like tyrosine kinase 3-internal tandem duplication (FLT3-ITD). We found that RSK2 is dispensable for BCR-ABL-induced myeloproliferative neoplasm, but required for FLT3-ITD-induced myeloid transformation in a murine bone marrow transplant assay. Moreover, inhibition of RSK2 by selective RSK inhibitor fmk induces significant apoptosis in FLT3-ITD-positive, but not BCR-ABL expressing leukemia cell lines and primary leukemia cells from human patients. These results suggest that RSK2 may represent an alternative therapeutic target in the treatment of FLT3-ITD-positive leukemia. Our phospho-proteomics studies also revealed a group of metabolic enzymes as tyrosine phosphorylated in leukemia cells transformed by different leukemogenic tyrosine kinases. Among those identified, we found that glycolytic enzyme phosphoglycerate mutase 1 (PGAM1) is important for the coordination of bioenergetic and anabolic biosynthetic pathways in leukemia cells, which is essential for cell proliferation and disease development. We developed a selective PGAM1 inhibitor, PGMI-004A, that effectively inhibits viability of diverse leukemia cell lines and primary leukemia cells from patients with no off-target activity and minimal toxicity. Additionally, we found that 6-phosphogluconate dehydrogenase (6PGD) in the pentose phosphate pathway (PPP) is commonly upregulated by lysine acetylation in cancer/leukemia cells. 6PGD provides an additional link between the oxidative PPP and lipogenesis through 6PGD product-dependent inhibition of LKB1-AMPK signaling, and represents a novel anti-cancer/leukemia target. We developed selective small molecule 6PGD inhibitors, Physcion and S3, and found that treatment with 6PGD inhibitors alone or in combination with anti-malarial drug dihydroartemisinin effectively inhibits cell viability in leukemia cell lines and patient samples, and attenuates leukemia cell-derived tumor growth in mice with minimal off-target toxicity. Collectively, these studies provide “proof of principle” for the development of RSK2, PGAM1 and 6PGD inhibitors as novel anti-leukemia agents.

Development of Novel Targeted Anti-Leukemia Therapies

By

Shannon Elisabeth Elf
Artium Baccalaureus (A.B.), Bowdoin College, 2003

Advisor:
Jing Chen, Ph.D.

A dissertation submitted to the Faculty of the James T. Laney School of Graduate
Studies of Emory University in partial fulfillment of the requirements for the degree
of
Doctor of Philosophy
in
Graduate Division of Biological and Biomedical Sciences
Molecular & Systems Pharmacology
2013

Acknowledgements

Many people are owed thanks for their contributions throughout the completion of this work and this degree.

My gratitude is owed first and foremost to my beloved father, a man of tremendous courage and character whom I miss so deeply each and every day. He has been my pillar of strength and inspiration throughout this five-year journey, and I could not have endured the inevitable periods of discouragement and emotional strain without his memory and spirit encouraging me to keep going. He is my hero, and I aspire to make him proud in everything I do.

To my mom, the pinnacle of tenacity and fortitude, and a constant role model for me throughout my life. Her unflagging optimism and positive outlook on life have deeply influenced the person I have become as an adult, as has her incredible strength of character. She is truly the most extraordinary person I know, and I am so blessed to be her daughter.

To Courtney and Caitlyn, my sanctuaries and sources of immeasurable comfort and solace. I can't begin to detail all that they've done for me over the past five years, but their love, support, thoughtfulness, encouragement, talks, and visits have meant the world to me, as have all the times they've talked me off the ledge. I am so fortunate to have been born in the middle of two such remarkable sisters.

To Ethan, for giving me a second home, for always lending an ear when I needed one, for feeding me, sharing good wine with me, and for giving me financial support when I needed it.

To Julia and Madeleine, for filling my heart with so much love it could burst, for all the hugs and snuggles and kisses, for all the pictures and surprises in the mail, for sharing their beds with me, taking walks with me, and letting me experience what it's like to love so intensely I could explode.

To Blake, who has been a source of constancy for me during a decade when little else has remained unchanged. His own accomplishments in life have continually served to motivate me, and I always have and continue to aspire towards his level of proficiency, skill, and talent not just academically and scientifically, but in everything he does. I'm so thankful for his presence in my life, for his love, his friendship, and for filling my life with happiness, laughter, comfort, and significance.

To Clara, for her boundless love and devotion, and for her effusive post-work greetings every day, that no matter how bad a day it was, she gifted me with a clean slate as soon as I walked through the door.

To my mentor, Jing Chen, for his faith in me, his patience with me, and his endless generosity and support. I am so grateful to have been trained by someone so wise, so gifted, and so excited by what we do that his enthusiasm was infectious.

To Sumin Kang, who was in many ways a second mentor to me, and a role model in her precision and unparalleled technical skill. She set an incredibly high standard in the lab and I strove to reach that standard in all that I did.

To my labmates, Changliang Shan, Jun Fan, and Heebum Kang, for their kindness, selflessness, and encouragement. I truly couldn't have asked for a better group of people to work with, and better friends to have both inside and outside the lab.

To my thesis committee members, Larry Boise, Haiyan Fu, Rita Nahta, and Sumin Kang, for making my committee meetings both pleasant and productive, for sharing with me their insight and wisdom, and for their support and encouragement along the way.

To John Hepler, for being a foundation of support and reassurance for me, for always leaving his door open to me, and for being a constant voice of both comfort and reason throughout the past five years.

To the MSP program, particularly Randy Hall, Eddie Morgan, and Susan Hoffstadter, for their outstanding leadership, and for their ability to strike a delicate balance between being a student-friendly program and one that is nationally recognized for its research impact and productivity.

To the patients who so bravely donated samples to the tissue bank for our use, their very existence reminded me on a daily basis why I'm doing what I do, and provided perspective when frustration or pessimism crept in. Their courage and optimism should remind us all that oftentimes the struggles we face on a daily basis pale in comparison to those faced by these patients. We must remember, in the grand scheme of things, why we come to lab every day, and why we work so hard - not for our own personal gain, but for those who are heroically battling cancer every single day, maintaining hope and faith in us that we will someday find a cure.

Table of Contents

Chapter 1: Introduction

1.1	Leukemia	p.1
1.2	Leukemia therapy in the pre-Gleevec® era: conventional treatment approaches	p. 2
1.3	The advent of targeted leukemia therapy	p. 3
1.4	Leukemia therapy: the Gleevec® era	p. 6
1.5	Clinical challenges in the Gleevec® era	p. 7
1.6	Leukemia therapy in the post-Gleevec® era	p. 9
1.7	Identifying pan-leukemia therapeutic targets	p. 14

Chapter 2: Targeting p90 ribosomal S6 kinase 2 in myeloid leukemia

2.1	Introduction	p. 18
2.2	Materials and Methods	p. 21
2.3	Results	p. 25
2.4	Discussion	p. 44

Chapter 3: Targeting leukemia metabolism as a novel therapeutic strategy

3.1	Signaling and targeting of phosphoglycerate mutase 1 in human cancer	
3.1.1	Introduction	p. 49
3.1.2	Materials and Methods	p. 52
3.1.3	Results	p. 55
3.1.4	Discussion	p. 73

3.2	Signaling and targeting of 6-phosphogluconate dehydrogenase in human leukemia	
3.2.1	Introduction	p. 79
3.2.2	Materials and methods	p. 81
3.2.3	Results	p. 87
3.2.4	Discussion	p. 103
3.3	Development of novel combinatorial anti-leukemia therapies: a lesson from dehydrogenase deficient hemolytic anemia	
3.3.1	Introduction	p. 107
3.3.2	Materials and methods	p. 110
3.3.3	Results	p. 115
3.3.4	Discussion	p. 135
Chapter 4: Discussion		
4.1	Summary	p. 138
4.2	Future Directions	p. 142
	References	p. 150

List of Figures

Figure 1.1.6. Current cornerstone treatments for leukemia depend on disease type.

Figure 1.2. RSK2 is activated in diverse human leukemia cells transformed by different leukemogenic tyrosine kinases including BCR-ABL and FLT3-ITD.

Figure 2.2. Targeting BCR-ABL by imatinib in K562 cells and FLT3-ITD by TKI258 in Molm14 and Mv(4;11) cells attenuates RSK2 activation in a dose dependent manner.

Figure 3.2. Targeting FLT3-ITD by CEP701 and MLN518 results in decreased RSK2 activation in FLT3-ITD positive human leukemia cell lines.

Figure 4.2. Genetic deficiency of RSK2 in donor bone marrow cells does not affect retroviral infection efficiency or hematopoietic reconstitution capability.

Figure 5.2. Genetic deficiency of RSK2 does not affect BCR-ABL induced myeloproliferative neoplasm in a murine bone marrow transplant (BMT) assay.

Figure 6.2. FLT3-ITD induced T-ALL in BMT mice using RSK2 KO BM cells, phenotypically distinct from the myeloproliferative neoplasm induced by FLT3-ITD using WT BM cells.

Figure 7.2. Targeting RSK2 by fmk attenuates cell viability and induces apoptosis in FLT3-ITD, but not BCR-ABL expressing Ba/F3 cells and human leukemia cells.

Figure 8.2. RNAi-mediated targeted down-regulation of RSK1 failed to significantly induce apoptosis or attenuate cell viability in BCR-ABL or FLT3-ITD expressing human leukemia cell lines.

Figure 9.2. Fmk treatment induces significant apoptosis in FLT3-ITD but not BCR-ABL-expressing primary human leukemia cells.

Figure 10.2. Proposed model: role of RSK2 in BCR-ABL and FLT3-ITD-induced myeloproliferative neoplasm (MPN).

Figure 1.3.1. PGAM1 is important for cancer cell proliferation and tumor growth.

Figure 2.3.1. Identification and characterization of a small molecule PGAM1 inhibitor, PGMI-004A.

Figure 3.3.1. Inhibition of PGAM1 by PGMI-004A decreases viability of diverse leukemia cells but not normal, proliferating human cells.

Figure 4.3.1. Chronic PGMI-004A treatment causes no off-target toxicity in nude mice.

Figure 5.3.1. PGMI-004A treatment results in attenuated tumor growth in xenograft nude mice *in vivo*.

Figure 6.3.1. PGMI-004A treatment results in reduced cell proliferation of primary leukemia cells from patients, but not hematopoietic cells from healthy human donors.

Figure 7.3.1. Proposed model: role of PGAM1 in cancer cell metabolism.

Figure 1.3.2. 6PGD is lysine acetylated in diverse human leukemia and solid tumor cell lines.

Figure 2.3.2. Protein levels and lysine acetylation of 6PGD are important for tumor growth *in vivo*.

Figure 3.3.2. Physcion and its derivative S3 are selective 6PGD inhibitors.

Figure 4.3.2. Chronic S3 treatment causes no off-target toxicity in nude mice

Figure 5.3.2. S3 treatment results in reduced leukemia K562 cell tumor growth *in vivo*.

Figure 6.3.2. 6PGD enzyme activity and lysine acetylation levels are commonly upregulated in human primary leukemia cells and Physcion treatment results in reduced cell proliferation of primary leukemia cells from human patients.

Figure 7.3.2. Proposed model: role of 6PGD in cancer cell metabolism.

Figure 1.3.3. Targeting the oxidative pentose phosphate pathway by stable knockdown of G6PD or 6PGD sensitizes K562 human leukemia cells to anti-malarial agent DHA.

Figure 2.3.3. G6PD inhibitor DHEA in combination with DHA does not synergistically inhibit K562 cell viability.

Figure 3.3.3. 6PGD inhibitor Physcion in combination with DHA leads to synergistic inhibition of K562 cell viability and induction of apoptosis.

Figure 4.3.3. Combination treatment with Physcion + DHA leads to synergistic inhibition of cell viability in diverse human leukemia cell lines.

Figure 5.3.3. Synergistic inhibition of cell viability in K562 leukemia cells treated with Physcion + DHA is mediated in part by activation of AMPK.

Figure 6.3.3. Synergistic inhibition of cell viability in K562 leukemia cells treated with Physcion + DHA is mediated in part by activation of AMPK.

Figure 7.3.3. Combination treatment with Physcion + AMPK activator A769662 leads to synergistic inhibition of cell viability in diverse human leukemia cell lines.

Figure 8.3.3. S3 + DHA combination treatment results in significantly attenuated leukemia K562 cell tumor growth *in vivo*.

Figure 9.3.3. Physcion + DHA leads to significant inhibition of cell viability in primary leukemia cells from human patients with a spectrum of disease types.

List of Abbreviations

In order of use:

AML: acute myeloid leukemia

ALL: acute lymphoid leukemia

CML: chronic myeloid leukemia

CLL: chronic lymphoid leukemia

BCR: breakpoint cluster region

ABL1: Abelson murine leukemia viral oncogene homolog 1

MAPK: Mitogen-activated protein kinase

PI3K: phosphatidylinositol 3-kinase

JAK: Janus kinase

STAT: Signal transducer and activator of transcription

FLT3: fms-like tyrosine kinase 3

ITD: internal tandem duplication

AML1: acute myeloid leukemia-1

ETO: co-repressor eight-twenty-one

PML: promyelocytic leukemia

RAR: retinoic acid receptor

APL: acute promyelocytic leukemia

TKI: tyrosine kinase inhibitor

ATP: adenosine triphosphate

LTK: leukemogenic tyrosine kinase

OTK: oncogenic tyrosine kinase

PDGFR: platelet-derived growth factor receptor

NADPH: nicotinamide adenine dinucleotide phosphate

ROS: reactive oxygen species

IDH1: isocitrate dehydrogenase 1

IDH2: isocitrate dehydrogenase 2

RSK2: p90 ribosomal S6 kinase 2

FGFR3: fibroblast growth factor receptor 3

PGAM1: phosphoglycerate mutase 1

PKM2: pyruvate kinase M2

LDHA: lactate dehydrogenase A

PDHK1: pyruvate dehydrogenase kinase 1

6PGD: 6-phosphogluconate dehydrogenase

PPP: pentose phosphate pathway

G6PD: glucose-6-phosphate dehydrogenase

DHA: dihydroartemisinin

RBC: red blood cell

CTK: C-terminal kinase

NTK: N-terminal kinase

CREB: cAMP-response element-binding protein

DAPK: death associated protein kinase

CLS: Coffin-Lowry syndrome

FGFR1: fibroblast growth factor receptor 1

MPN: myeloproliferative neoplasm

FBS: fetal bovine serum

IL-3: interleukin-3

IL-6: interleukin-6

KO: knockout

WT: wild type

SCF: stem cell factor

WBC: white blood cell

PI: propidium iodide

HES: hypereosinophilic syndrome

MPD: myeloproliferative disease

ALCL: anaplastic large-cell lymphoma

VEGFR: vascular endothelial growth factor receptor

BMT: bone marrow transplant

PB: peripheral blood

BM: bone marrow

T-ALL: T-cell acute lymphoid leukemia

TKD: tyrosine kinase domain

KD: knockdown

G-6-P: glucose-6-phosphate

R-5-P: ribose-5-phosphate

3-PG: 3-phosphoglycerate

2-PG: 2-phosphoglycerate

PHGDH: 3-phosphoglycerate dehydrogenase

NADH: nicotinamide adenine dinucleotide

DMSO: dimethyl sulfoxide

6-PG: 6-phosphogluconate

Ru-5-P: ribulose-5-phosphate

pPYR: 3-phosphohydroxypyruvate

FDA: Food and Drug Administration

HDF: human dermal fibroblasts

HFF: human foreskin fibroblasts

B-ALL: B-cell acute lymphoid leukemia

AMPK: adenine monophosphate-activated protein kinase

LKB1: liver kinase B1

TSA: trichostatin A

NAM: nicotinamide

NAC: N-acetyl-L-cysteine

SIRT: Sirtuin deacetylase

HDAC: histone deacetylase

DLAT: dihydrolipoamide S-acetyltransferase

ACAT2: acetyl-CoA acetyltransferase 2

ACC1: acetyl Co-A carboxylase 1

6-AN: 6-aminonicotinamide

GLUD1: glutamate dehydrogenase 1

IHC: immunohistochemistry

PFK: phosphofructokinase

6-PGL: 6-phosphogluconolactone

DHEA: dehydroepiandrosterone

CI: combination index

COX: cyclooxygenase

LSC: leukemia stem cell

SAR: structure-activity relationship

2-DG: 2-deoxyglucose

Chapter 1: Introduction

1.1. Leukemia

Leukemia is a progressive, malignant neoplasm of the blood-forming organs, characterized by abnormal hematopoietic development and uncontrolled proliferation of white blood cells and their precursors in the blood and bone marrow. It is frequently accompanied by a depletion of other hematopoietic cell types, including erythrocytes and platelets, resulting in anemia and increased susceptibility to infection and hemorrhage. In the United States, leukemia accounts for approximately 3% of all cancer deaths. Nearly 49,000 new cases and 24,000 deaths were estimated for 2013. Leukemia remains the leading cause of cancer deaths among children ages 15 and under, accounting for over one-third of all cancer deaths in this age group (1).

Leukemia classification is based on two principal determinants: the hematopoietic cell lineage in which the disease arises, and the level of maturation achieved by the affected cell type. Acute leukemias, which include acute myeloid leukemia (AML) and acute lymphoid leukemia (ALL), are characterized by the excessive production of immature myeloid or lymphoid blood cells ("blasts"), respectively. Chronic leukemias, including chronic myeloid leukemia (CML) and chronic lymphoid leukemia (CLL), are marked by the uncontrolled proliferation of mature but

nonfunctional blood cells of each corresponding lineage. Among these, myeloid leukemias have the worst prognosis based on a five-year survival rate (2).

1.2. Leukemia therapy in the pre-Gleevec® era: conventional treatment approaches

Though leukemia is considered a largely treatable disease, current therapeutic regimens can be highly aggressive and are associated with extremely adverse side effects. Cytotoxic chemotherapy, radiation therapy, and bone marrow transplantation remain the primary treatment options for most leukemia patients, each of which severely affects quality of life. Both chemotherapy and radiation therapy are typically used as first-line treatments for newly diagnosed leukemias, with an average remission rate of 50%. However, relapse rates range from 30-70% depending on the disease stage and type, and the side effects of both treatments, including hair loss, nausea and vomiting, fatigue, loss of appetite and weight loss, insomnia, and skin rash, can be tremendously distressing to the patient (1). Such therapies often prove too toxic for children and elderly patients, who are most prone to develop leukemia. For relapsed patients who would not benefit from prolonged treatment with chemotherapy or have already developed drug resistance, bone marrow transplantation remains the only conventional treatment option. Though substantial advances have been made in bone marrow transplantation practices over the past 60 years, it is still considered a dangerous procedure associated with high treatment-related mortality. Patients undergoing bone marrow

transplantation are subjected to “preparative treatment” involving high-dose chemotherapy and radiation, which attempts to clear the hematopoietic system of diseased cells and make space for the new bone marrow cells. Because this destroys the immune system, patients are subsequently at high risk for infection and must be kept in isolation prior to and following the procedure (4). Additionally, patients undergoing an allogenic transplant in which bone marrow cells are taken from a tissue matched donor are at risk for graft-versus-host disease in which the transplanted immune cells attack the host's body cells, leading to vital organ damage (5).

1.3. The advent of targeted leukemia therapy

During the past decade, anti-cancer therapies have seen a systematic shift from such conventional “one-size-fits-all” treatment strategies to the development of targeted agents aimed specifically at inhibiting proteins and pathways that are required by cancer cells, but not normal cells, for continued growth and survival. This approach, in theory, spares the body’s normal cells and thereby causes fewer adverse side effects for the patient. The foundation of targeted therapy rests primarily upon the identification of specific alterations in cancer cells that function to drive proliferation and survival, followed by the discovery and development of molecularly targeted drugs that exploit these vulnerabilities.

In leukemia, such alterations have been classically divided into two complementation groups: class I mutations and class II mutations (5-6). Class I mutations activate signal transduction pathways resulting in enhanced proliferation and survival of leukemic progenitor cells. Among these, mutations leading to the fusion tyrosine kinase BCR-ABL and constitutive activation of the receptor tyrosine kinase fms-like tyrosine kinase 3 (FLT3) are the most prevalent (7-8).

Class I mutations: BCR-ABL. BCR-ABL is a chimeric oncogene generated by the translocation of sequences from the Abelson murine leukemia viral oncogene homolog 1 (*ABL1*) tyrosine kinase gene on chromosome 9 into the breakpoint cluster region (*BCR*) gene on chromosome 22. Alternative isoforms, p210^{BCR-ABL} and p190^{BCR-ABL}, are produced that are characteristic of CML (found in 95% of patients) and ALL (found in 25-30% of patients), respectively (9). The head to tail fusion of *BCR* to *ABL1* causes loss of the negative regulatory SH3 domain on the tail of the ABL protein, which promotes autophosphorylation and constitutive ABL kinase activity (10-11). BCR-ABL activates various signaling pathways responsible for proliferation and survival, including Ras/Mitogen-activated protein kinase (MAPK), phosphatidylinositol 3-kinase (PI3K), and Janus kinase-Signal transducer and activator of transcription (JAK-STAT) pathways (12).

Class I mutations: FLT3-ITD. The FLT3 receptor plays a critical role in normal hematopoiesis and is expressed primarily on immature myeloid and lymphoid progenitors. Internal tandem duplications (ITDs) in the juxtamembrane domain of

FLT3 disrupt the autoinhibitory capacity of the receptor, ultimately leading to constitutive FLT3 signaling and activation of various downstream effectors of proliferation and survival, including the Ras/MAPK and PI3K pathways. FLT3-ITD mutations are found in approximately 25% of AML patients, and are typically associated with poor prognosis (5, 13-17).

Class II mutations. In contrast to class I mutations, class II mutations affect transcription factors or components of the transcriptional activation complex, resulting in impaired differentiation and/or the reacquisition of stem cell characteristics by hematopoietic progenitors (6-8). Notable examples include the t(8;21) chromosomal translocation that generates an oncogenic fusion consisting of transcription factor acute myeloid leukemia-1 (*AML1*) and co-repressor eighty-twenty-one (*ETO*; 18-19), and the t(15;17) translocation the generates an oncogenic fusion consisting of the promyelocytic leukemia gene (*PML*) and the retinoic acid receptor alpha gene (*RAR α* ; 19).

Leukemia pathogenesis differs between disease types, with each involving different contributions from each class. For instance, a conjoint effort between class I and class II mutations is required to obtain full-blown AML. CML pathogenesis, on the other hand, is attributable to the proliferative and survival advantage conferred by class I mutations, while normal hematopoietic cell maturation and differentiation are retained (20).

1.4. Leukemia therapy: the Gleevec® era

Because both class I and II mutations are causative alterations in hematopoietic transformation, each mutation, in principle, represents a potential target for anti-leukemia therapy. However, therapeutic agents against class I mutations have proved much more successful. Compared to molecules involved in cell signaling, class II mutations have historically been considered “undruggable”, in part because they don’t possess enzymatic activity and thus are more difficult to chemically inhibit. For several decades, the use of retinoic acid to induce hematopoietic differentiation in PML-RAR α -associated acute promyelocytic leukemia (APL) patients has served as the only example of effective treatment directed to an oncogenic transcription factor (19). Recent efforts have focused on targeting the post-translational modifications of transcription factors that regulate their function, as well as inhibiting formation of oncogenic transcriptional complexes, though such agents are still in their infancy (21-22). In contrast, agents targeting class I mutations have proven widely effective in the treatment of leukemia during the past decade. The most seminal example came in 2001 when imatinib (Gleevec®), a specific tyrosine kinase inhibitor (TKI) of BCR-ABL, c-KIT, and platelet-derived growth factor receptor (PDGFR), became the first targeted therapy approved for CML. Imatinib is a selective and potent tyrosine kinase inhibitor that competes with adenosine triphosphate (ATP) for its binding site in the catalytic cleft of ABL kinase. When bound, imatinib blocks ATP from binding, thus preventing phosphorylation

and activation of downstream leukemogenic signaling, consequently leading to decreased leukemia cell proliferation and/or cell death (23-28).

1.5. Clinical challenges in the Gleevec® era

Imatinib was heralded the “magic bullet” to cure cancer by TIME magazine (29), and revolutionized cancer treatment as whole. Its initial success prompted a comprehensive shift in cancer therapeutics from cytotoxic therapies to molecularly targeted therapies, spurring the development of additional small molecule TKIs targeting a wide array of leukemogenic and oncogenic tyrosine kinases (LTKs and OTKs; 30-31). However, it was later shown that many patients treated with imatinib and other TKIs eventually develop resistance or fail to respond. In particular, it was found that many CML patients treated with imatinib rapidly developed point mutations in the ATP binding pocket of BCR-ABL that prevented imatinib from binding. Gorre et al. demonstrated that six out of nine imatinib-resistant CML patients possessed a single-nucleotide substitution in the *ABL1* gene, resulting in a threonine to isoleucine substitution at amino acid 315 (T315I). Modeling of wild-type ABL kinase with imatinib predicted that although the substitution of isoleucine would still permit ATP binding, it would prevent imatinib binding by causing steric hindrance, as well as by eliminating a critical oxygen molecule needed for hydrogen bonding between imatinib and ABL (32-33). Numerous additional mutations have been subsequently characterized throughout the *ABL1* sequence, and the total number of reported point mutations continues to grow (34-37). This prompted the

development of second-generation BCR-ABL kinase inhibitors that would attempt to overcome drug resistance. Dasatinib (38-39) and nilotinib (40), two second-generation BCR-ABL inhibitors, proved to be effective against most imatinib-resistant mutations, but neither is effective against the T315I mutation. As of 2010, several third-generation leads were under development, including one compound, ponatinib, that has been shown to be effective against the T315I mutation (41). However, ponatinib is currently one of the most expensive drugs in medicine at \$138,000 per year, which precludes it from being a viable treatment option for most patients (42).

Finally, it is worth noting that all of the TKIs currently approved for clinical use are “multi-kinase inhibitors”, and thus are not specific for the causative OTK. For example, first-, second-, and third-generation BCR-ABL kinase inhibitors exhibit inhibitory effects toward other tyrosine kinases including c-KIT, PDGFR, and SRC family kinases. Since all approved tyrosine kinase inhibitors are designed to specifically attack the ATP binding site, achieving selectivity for one particular tyrosine kinase has proven difficult due to the high degree of ATP binding site conservation between tyrosine kinases. Each TKI therefore targets multiple tyrosine kinases, at least one of which may be non-causative, making treatment likely to cause more side effects, as well as to increase the possibility of drug resistance (43).

1.6. Leukemia therapy in the post-Gleevec® era

Identifying common downstream effectors of discrete LTKs. Notwithstanding these therapeutic impediments, the introduction of BCR-ABL kinase inhibitors to the clinic has undoubtedly changed the landscape of leukemia therapy during the past decade. It is important to bear in mind, however, that CML remains the only leukemia that has benefited from such pathway-directed therapy; AML, ALL, and CLL are still treated primarily with conventional chemotherapy. This underscores the enduring need to identify features that, while unique to leukemic cells compared to their normal counterparts, are common amongst a broader cohort of leukemia patients, spanning disease types and subtypes, thus potentiating the advent of targeted pan-leukemia therapy (Figure 1.1.6). Selective targeting of specific alterations that represent common phenomena in leukemia as a whole would indeed help to overcome numerous hurdles that current therapeutic strategies have yet to conquer. In particular, elucidating key downstream pathways that may be commonly important for leukemias that are transformed by different LTKs would offer the potential for pan-leukemia therapeutic targets that may be more selectively inhibited than tyrosine kinases. This would help to circumvent drug resistance and reduce adverse outcomes associated with TKI treatment (43-44).

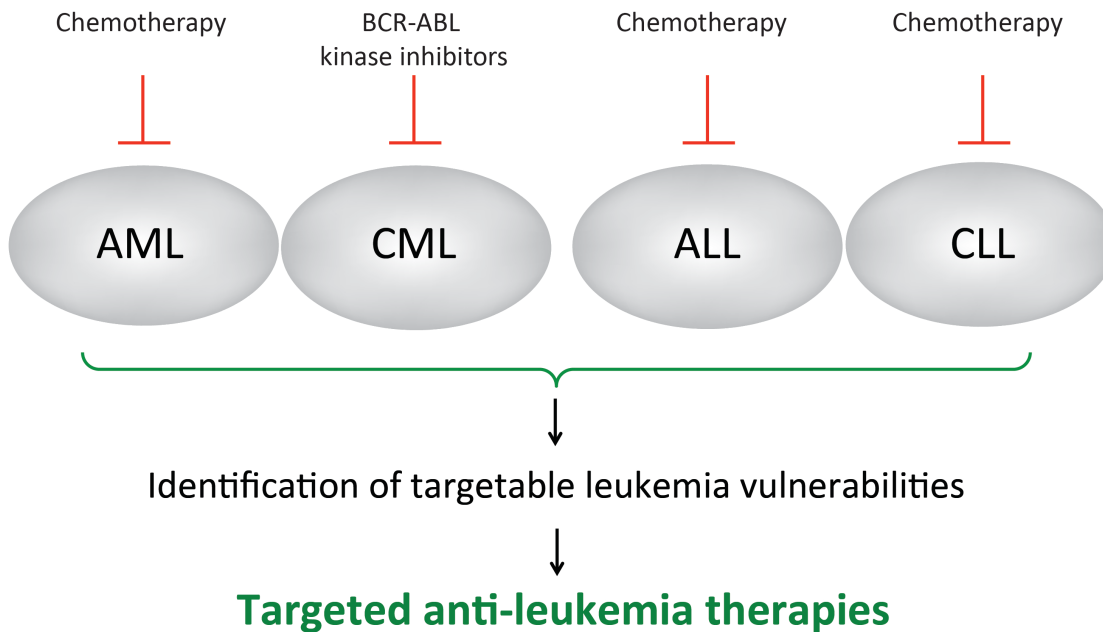


Figure 1.1.6. Current cornerstone treatments for leukemia depend on disease type. Treatment strategies for leukemia differ depending on the disease type. CML is currently the only leukemia type in which targeted therapy is available as a first-line treatment strategy. AML, ALL, and CLL still rely primarily upon conventional treatment strategies. This underscores the importance of identifying vulnerabilities that are common amongst a broader cohort of leukemia disease types in order to develop commonly applicable targeted therapies.

Leukemia cell metabolism. While identifying specific genetic abnormalities and aberrant signaling pathways in leukemia cells has considerably furthered our understanding of leukemia biology and informed the development of targeted therapies, it represents a relatively narrow vantage point with regard to the vast assortment of alterations present in leukemia cells versus their normal counterparts. It is thus quite auspicious that a recent resurgence of interest in tumor metabolism, a concept pioneered by German physiologist Otto Warburg nearly a century ago, has led to a number of discoveries concerning specific alterations to cellular metabolism in cancer cells, some of which are requisite for malignant transformation (45). It has been shown that the metabolic signatures of cancer cells are remarkably different from those of normal cells, a phenomenon first identified as “the Warburg effect”. The Warburg effect describes Otto Warburg’s observation that cancer cells produce energy primarily by glycolysis in the cytosol rather than by oxidative phosphorylation in mitochondria as in most normal cells. While normal cells switch to glycolysis for energy production in the absence of oxygen, cancer cells use glycolysis even when oxygen is present (aerobic glycolysis). Leukemia cells, for example, are highly glycolytic despite residing in the bloodstream where oxygen is plentiful. Warburg hypothesized that this altered metabolism arose from mitochondrial defects that inhibited their ability to effectively oxidize glucose carbon to CO₂ (46).

Despite his prescient observations regarding the distinctiveness of tumor metabolism and the suggestion that such alterations could represent targetable

vulnerabilities in cancer cells, nearly 80 years passed before Warburg's hypothesis was revisited. While recent discoveries have served to reinforce many of Warburg's initial postulations, the notion that the metabolic properties of cancer cells are a result of damaged mitochondria has since been refuted. Instead, it has been found that these alterations are in fact a result of oncogene-driven metabolic reprogramming required to support cancer cell proliferation and survival. This helps illuminate why cancer cells would "choose" glycolysis, a relatively inefficient mode of energy production, over the much more efficient oxidative phosphorylation - glycolysis is quicker, and readily provides energy in the form of ATP required by rapidly proliferating cancer cells (47-48).

In addition to the expeditious production of energy, aerobic glycolysis also facilitates rapid cell division by providing metabolic intermediates that can be shunted into diverging pathways, where they serve as precursors for anabolic biosynthesis of macromolecules. These include nucleotides, amino acids and fatty acids, to produce RNA/DNA, proteins and lipids, respectively, which are necessary for rapid cell division (46-48). Moreover, glycolytic intermediates can also be diverted into pathways that produce reduced nicotinamide adenine dinucleotide phosphate (NADPH), which not only fuels macromolecular biosynthesis of lipids, but also functions as an antioxidant to quench the reactive oxygen species (ROS) produced during rapid proliferation of cancer cells, which is imperative for maintenance of cellular redox homeostasis.

Targeting leukemia cell metabolism. The molecular characterization of the metabolic differences between cancer cells and normal cells has provoked exploration of the therapeutic opportunities these differences might provide. Drug development in this vein has sought to exploit metabolic vulnerabilities in cancer cells much as the so-called “oncogene revolution” (45) sought to exploit the genetic vulnerabilities that in leukemia became known as class I and class II mutations. Leukemia cell metabolism was propelled to the forefront of the still nascent cancer cell metabolism field in 2008 following systematic whole genome sequencing of two AML patients. Sequencing results revealed mutations in metabolic enzyme isocitrate dehydrogenase 1 (IDH1), a mutation found in 10% of AML patients (49). Mutations in isocitrate dehydrogenase 2 (IDH2) were subsequently identified in AML as well, and both mutations have since been identified in other hematological neoplasms (50). The identification of IDH mutations prompted the development of IDH mutant inhibitors, which thus far have shown promising efficacy in inducing hematopoietic cell differentiation of primary AML patient blast cells in culture (51).

However, even before the discovery of IDH mutations in leukemia, targeting leukemia metabolism was a concept already in practice. The use of the enzyme L-asparaginase to treat ALL represents a far more rudimentary example of how the distinctive metabolism of leukemia cells has been exploited for therapy. In contrast to normal hematopoietic cells, ALL cells are unable to synthesize the non-essential amino acid asparagine and thus depend on circulating asparagine. L-asparaginase catalyzes the conversion of asparagine to aspartic acid, thereby depriving the

leukemic cell of the circulating asparagine it requires to survive, leading to cell death (52-53). However, L-asparaginase is still a non-targeted chemotherapy drug, and its systemic administration leads to severe side effects, including pancreatitis, hepatic dysfunction, nephrotoxicity, and central nervous system dysfunction (54).

While such efforts to target leukemia cell metabolism have been promising and effective, sizable obstacles remain. Sequencing the AML genome indeed represented an exponential leap forward in the identification of novel anti-leukemia targets including IDH, and consequently shed light on leukemia cell metabolism as a viable avenue for therapy. However, many metabolic enzymes that may contribute to leukemogenesis are not mutated, and thus would have eluded the list of hits generated by sequencing results. Moreover, in the case of IDH inhibitors, only 10-20% of AML patients harbor IDH mutations, leaving the vast majority of AML cases and other leukemias untouched by this advance. This again highlights the need to identify vulnerabilities more common to the leukemic cell for the development of pan-leukemia therapies.

1.7. Identifying pan-leukemia therapeutic targets

This work focuses on the identification and characterization of novel anti-leukemia therapies from the distinct but interconnected viewpoints of leukemogenic signal transduction and leukemia cell metabolism.

p90 ribosomal S6 kinase 2 (RSK2). Given the aforesaid obstacles regarding currently available TKI therapy, we began by exploring alternative targets for therapy in tyrosine kinase-induced leukemias. We previously performed phospho-proteomics studies that identified serine/threonine kinase RSK2 as a substrate of oncogenic fibroblast growth factor 3 (FGFR3), and further determined that RSK2 is a critical downstream effector of FGFR3-induced hematopoietic malignancies (55). We proceeded to examine the role of RSK2 in FLT3-ITD-induced AML and BCR-ABL-induced CML, and found that targeting RSK2 revealed key differences in the signaling properties of FLT3-ITD and BCR-ABL in AML and CML, respectively. We determined anti-RSK2 therapy to be a promising therapeutic strategy for FLT3-ITD positive AML, but not BCR-ABL positive CML (56).

Phosphoglycerate mutase 1 (PGAM1). Interestingly, our phospho-proteomics studies also revealed numerous metabolic enzymes as being tyrosine phosphorylated by diverse leukemogenic tyrosine kinases. We found that indeed, the activity of several key metabolic enzymes including pyruvate kinase M2 (PKM2; 57), lactate dehydrogenase A (LDHA; 58), pyruvate dehydrogenase kinase 1 (PDHK1; 59), and PGAM1 (60) is regulated by LTK-mediated tyrosine phosphorylation. Among these, we found expression and activity of glycolytic enzyme PGAM1 to be upregulated in diverse leukemia disease types, and thus developed a selective PGAM1 targeting strategy that effectively inhibited cell viability in a broad spectrum of both leukemia cell lines and patient samples with minimal off-target toxicity (61).

6-phosphogluconate dehydrogenase (6PGD). Our PGAM1 studies exposed the potential of an additional pan-leukemia metabolic target, 6PGD in the oxidative pentose phosphate pathway (PPP). Though not tyrosine phosphorylated by LTKs, 6PGD activity was found to be significantly upregulated in diverse leukemia cell lines and patient samples. Thus, we similarly developed a selective strategy to target 6PGD that effectively inhibited cell viability in a wide range of leukemia cell lines and patient samples *in vitro*, and attenuated leukemia cell-derived tumor growth *in vivo*, with minimal off-target toxicity.

Combinatorial targeting of 6PGD. In examining the potential side effects induced by anti-6PGD therapy, we encountered the clinical observation that genetic deficiency of 6PGD (62) as well as glucose-6-phosphate dehydrogenase (G6PD; 63), the first enzyme in the oxidative PPP, exists in human patients. Individuals with 6PGD or G6PD deficiency are typically asymptomatic, with complications arising only upon exposure to certain chemicals, including aspirin and anti-malarial drugs, which can induce hemolytic anemia (64). We thus sought to translate this concept into anti-leukemia therapy, and reasoned that treatment with our 6PGD inhibitors or G6PD inhibitors combined with anti-malarial drugs may induce synergistic leukemia cell death. Indeed, we found that combining our novel 6PGD inhibitors Physcion or S3 with anti-malarial drug dihydroartemisinin (DHA) synergistically inhibited viability in leukemia cell lines, and significantly inhibited viability of primary cells from leukemia patients with different disease types. Moreover, in a K562 leukemia cell xenograft model, we found that S3 + DHA significantly

attenuated tumor growth *in vivo*. Importantly, we found that our novel combination treatment caused no evidence of red blood cell (RBC) destruction, nor did it perturb the integrity of the hematopoietic system as a whole.

Here we identify several pan-leukemia targets against which we successfully developed and characterized small molecule inhibitors to be used in novel anti-leukemia treatment strategies. While our compounds demonstrate significant inhibitory efficacy against leukemia cells, they are well tolerated by normal human blood cells isolated from healthy donors, as well as at the whole organism level in mice, thus minimizing the potential for adverse side effects in human patients.

Chapter 2: Targeting p90 ribosomal S6 kinase 2 in myeloid leukemia

2.1. Introduction

RSK2 is a serine/threonine kinase that belongs to a family containing 4 members, RSK1 through 4, all of which are downstream substrates of ERK. RSK family members are highly homologous (80-85% amino acid identity between isoforms) and are uniquely characterized by the presence of two distinct kinase domains, both of which are catalytically functional (65-70). The C-terminal kinase (CTK) domain is responsible for auto-phosphorylation at Ser386 in the linker region, which is required for RSK activation, while the N-terminal kinase (NTK) domain phosphorylates RSK substrates (66), which include anti-apoptotic proteins, cell cycle regulatory proteins, and transcription factors that regulate expression of genes involved in cell growth and motility (66, 68, 71). We recently reported that tyrosine phosphorylation of RSK2 facilitates inactive ERK binding to RSK2 in the initial activation step, and disrupts an autoinhibitory region of RSK2 to achieve full activation (55, 72-73).

RSK2 phosphorylates multiple signaling effectors that contain RRXS/T or RXXRXXS/T motifs (74), including transcriptional regulators such as cAMP-response element-binding protein (CREB; 75), c-Fos (76-77), NFATc4 (78), NFAT3 (79), ATF4 (80) and Nur77 (81). Phosphorylation and subsequent activation of these transcription factors is important for regulation of gene expression. RSK2 also phosphorylates

histone H3, which contributes to chromatin remodeling during mitosis and transcriptional activation (82). In addition, RSK2 promotes cell survival by phosphorylating and inhibiting pro-apoptotic protein factors including BAD (83), Bim (84) and death associated protein kinase (DAPK; 85). Moreover, RSK2 promotes proliferation by phosphorylating GSK3 β (86), NHE-1 (87), and p27^{kip1} (88). RSK2 thus appears to serve as a key regulator of pro-proliferative and pro-survival signaling.

Defects in the human RSK2 gene are associated with Coffin-Lowry syndrome (CLS), a syndromic form of X-linked mental retardation (71, 89). Although there is no evidence to suggest that RSK2 is mutated in human cancers, RSK2 signaling has been shown to play a key role in the pathogenesis and disease progression of numerous human malignancies in addition to FGFR3-induced hematopoietic malignancies (55), including metastatic head and neck cancer (90), fibroblast growth factor receptor 1 (FGFR1)-expressing prostate cancer (91-92) and osteosarcoma (93). Together, these observations suggest that RSK2 may be an attractive anti-cancer target.

In this work, we examine on the role of RSK2 in hematopoietic malignancies induced by diverse LTKs, with a particular focus on BCR-ABL and FLT3-ITD, the two most commonly mutated tyrosine kinases in human leukemia. The pathogenic role of BCR-ABL and FLT3 has made them important therapeutic targets for treatment of

CML and AML respectively. However, the detailed signaling properties of these leukemogenic tyrosine kinases in hematopoietic transformation remain unclear.

Here, we demonstrate that RSK2 is dispensable in BCR-ABL-induced myeloproliferative neoplasm (MPN), but is required for FLT3-ITD-induced hematopoietic transformation, where it is likely involved in pathogenesis and lineage determination. Our findings suggest that the role of RSK2 in hematopoietic transformation may depend on distinct upstream oncogenic signals mediated by different leukemogenic tyrosine kinases.

2.2. Materials and Methods

Cell culture. Ba/F3 cells were cultured in RPMI 1640 medium supplemented with 10% fetal bovine serum (FBS) and 1.0 ng/mL interleukin-3 (IL-3) (R & D Systems). Ba/F3 cells expressing various leukemogenic tyrosine kinases were cultured in RPMI 1640 with 10% FBS and 1 mg/ml of G418 (Invitrogen). Leukemia cell lines including EOL-1, HEL, KARPAS, K562, Molm14, Mv(4;11), Mo91, and FGFR3 positive multiple myeloma cell line OPM1 were cultured in RPMI 1640 medium supplemented with 10% FBS and penicillin/streptomycin. ANBL6 cells were cultured in RPMI 1640 medium supplemented with 10% FBS and interleukin-6 (IL-6) (R & D Systems).

Immunoprecipitation and Western blot. Cells ($\sim 1 \times 10^7$) were lysed and cell extracts were clarified by centrifugation and used for immunoprecipitation or immunoblotting as described (94). Phospho-Tyr antibody pY99, c-ABL, FLT3, RSK1, and RSK2 antibodies were from Santa Cruz Biotechnology, phospho-RSK (Ser380) antibody was from Cell Signaling Technology (CST). Antibody against β -actin was from Sigma.

Mice. Blab/C RSK2 knock out (RSK2 KO) mice were developed as described previously (95). Murine BMT assays were performed as described previously (96). In brief, retroviral supernatants were generated by transient co-transfection of 293T cells with the MSCV2.2-Gateway-IRES-GFP-BCR-ABL (97) or FLT3-ITD/51

(98) constructs and packaging construct using Superfect (Qiagen). The viral titer was estimated by infecting Ba/F3 cells with serial dilutions of viral supernatant and percentage of GFP-positive cells was determined by flow cytometry 48 hours post infection. Viral titers of constructs used for each round of murine BMT were 24.56×10^4 /ml, 32.55×10^4 /ml, and 14.56×10^4 /ml for BCR-ABL, 11.57×10^4 /ml, 43.27×10^4 /ml, and 20.03×10^4 /ml for FLT3-ITD. The wild type (WT) and RSK2 KO donor mice used for each bone marrow transplant experiment were littermates of the same age. 4-6 week-old WT or RSK2 KO Balb/C donor mice were treated with 150 mg/kg of 5-Fluorouracil (5-FU, Sigma) 6 days prior to harvest of bone marrow cells. Two days before the BMT, the bone marrow cells were collected from the femurs and tibias of the donor mice. The same batch of retroviral supernatant with the same titer was used to infect WT or RSK2 KO Balb/C donor bone marrow cells by spin infection in RPMI 1640 media containing recombinant murine IL-3 (rmIL-3; 6 ng/ml; R&D Systems), recombinant murine stem cell factor (rmSCF; 10 ng/ml; R&D Systems), recombinant human IL-6 (10 ng/ml; R&D System) and 10% FBS. 1×10^6 cells in 0.5 mL HBSS were injected into the lateral tail veins of lethally irradiated (2×450 cGy) syngeneic Balb/C recipient mice. Animals were carefully monitored under the auspices of institutionally approved protocols for the humane care of animals. Diseased BMT mice were examined each day, and sacrificed at first signs of morbidity, including scruffy coat, lethargy, weight loss, leukocytosis, and splenomegaly palpable beyond the midline. White blood cell (WBC) counts and weights of organs including spleen and liver were recorded at time of necropsy.

Histopathology and flow cytometric immunophenotyping. Histopathologic analyses were performed as described previously (99). Prior to flow cytometric analysis, cell samples of single-cell suspensions were washed in the staining buffer (PBS with 0.1% NaN₃ and 0.1% bovine serum albumin) and stained for 20 minutes on ice with combinations of labeled monoclonal antibodies recognizing Gr-1/Mac-1 and CD4/CD8 (BD Biosciences). After washing, the cells were resuspended in staining buffer containing 0.5 mg/ml 7-amino-actinomycin D (BD Biosciences) to allow discrimination of nonviable cells and flow cytometric analysis was done on a FACSCalibur cytometer (BD Biosciences). At least 10,000 events were acquired, and the data was analyzed using CellQuest software (Version 3.3). The results are presented as dot plots of viable cells selected on the basis of scatter and 7-amino-actinomycin D staining.

Cell viability assay and apoptosis assay. For cell viability assays, 1×10^5 cells were cultured in 24-well plates with increasing concentrations of fmk. The relative cell viability at each experimental time point up to 72 hours was determined using a Celltiter96AQueous One solution proliferation kit (Promega). For apoptosis assays, 1×10^6 cells were treated with increasing concentrations of fmk for up to 48 hours. Cells were collected and stained using FITC-conjugated annexin V labeling reagent and propidium iodide (PI) (BD Pharmingen) as per the recommendations of the manufacturers, followed by FACS analysis for apoptotic cell population.

Primary tissue samples from CML and AML patients. The primary patient samples were analyzed as previously described (100). Briefly, mononuclear cells (MNCs) were isolated from blood samples of CML^{Ph+} and AML patients. 1×10^6 /ml cells were cultured in RPMI 1640 medium supplemented with 10% FBS and penicillin/streptomycin and incubated with increasing concentrations of fmk for up to 72 hours. Cell viability assay and apoptosis assay were performed as described above. All clinical samples were obtained with informed consent with approval by the Emory University Institutional Review Board.

2.3. Results

RSK2 is activated in diverse human leukemia cells transformed by different leukemogenic tyrosine kinases including BCR-ABL and FLT3-ITD.

To better understand whether RSK2 is a common signaling pathway that promotes cell proliferation and survival in hematopoietic transformation induced by different LTKs, we first examined RSK2 activation as assessed by phosphorylation levels of S386 in diverse human hematopoietic cancer cell lines, including EOL-1 that expresses FIP1L1-PDGFR α fusion tyrosine kinase and is associated with idiopathic hypereosinophilic syndrome (HES), HEL that expresses the constitutively active JAK2 V617F mutant and is associated with MPN, KARPAS that expresses NPM-ALK fusion tyrosine kinase and is associated with t(2;5)(p23;q35) advanced-stage anaplastic large-cell lymphoma (ALCL), K562 that expresses BCR-ABL fusion tyrosine kinase and is associated with t(9,22) Ph⁺ CML, Molm14 that expresses the constitutively active FLT3-ITD mutant and is associated with AML, and Mo91 that expresses TEL-TrkC fusion tyrosine kinase is associated with t(12;15)(p13;q25) AML. Also included are OPM1, a t(4;14) positive FGFR3-expressing human myeloma cell line as a positive control (55), and ANBL6 cells, a t(4;14) negative human myeloma cell line with no known transforming tyrosine kinases as a negative control (55). As shown in Figure 1.2, RSK2 is activated in leukemia cells expressing FIP1L1-PDGFR α (EOL-1), JAK2 V617F mutant (HEL), BCR-ABL (K562), and FLT3-ITD (Molm14), but not in cells expressing NPM-ALK (KARPAS) or TEL-TrkC (Mo91). RSK2 activation was assessed by phosphorylation levels of RSK2 at S386. This result

suggests that RSK2 signaling may represent a common proliferative and prosurvival pathway in leukemia cells transformed by different leukemogenic tyrosine kinases that are associated with various myeloid malignancy subtypes. From here, we chose to focus on the two most commonly mutated tyrosine kinases in human leukemia, BCR-ABL and FLT3-ITD, both of which are recognized as significant prognostic indicators in CML and AML, respectively.

Immunoblotting results show that RSK2 is activated and phosphorylated at S386 in BCR-ABL positive human leukemia K562 cells. Inhibition of BCR-ABL by a small molecule tyrosine kinase inhibitor imatinib resulted in decreased S386 phosphorylation levels of RSK2 in K562 cells (Figure 1.2 and Figure 2.2). In addition, RSK2 is activated in FLT3-ITD positive human leukemia Mv(4;11) and Molm14 cells. We first targeted FLT3-ITD in these cells by using TKI258 (4-amino-5-fluor-3-[5-(4-methylpiperazin-1-yl)-1H-benzimidazol-2-yl]quinolin-2(1H)-one, formerly known as CHIR258), which is an ATP-competitive inhibitor with activities against class III and IV receptor kinases including FGFR, vascular endothelial growth factor receptor (VEGFR), PDGFR, FLT3, and KIT (101-102). Targeting FLT3-ITD by TKI258 led to markedly reduced S386 phosphorylation levels of RSK2 in these cells (Figure 1.2C and Figure 2.2). In addition, inhibition of FLT3-ITD by two alternative FLT3 inhibitors, CEP701 and MLN518, also resulted in decreased RSK2 activation (Figure 3.2). These data suggest that leukemogenic tyrosine kinases BCR-ABL and FLT3-ITD activate RSK2 in transformed leukemia cells.

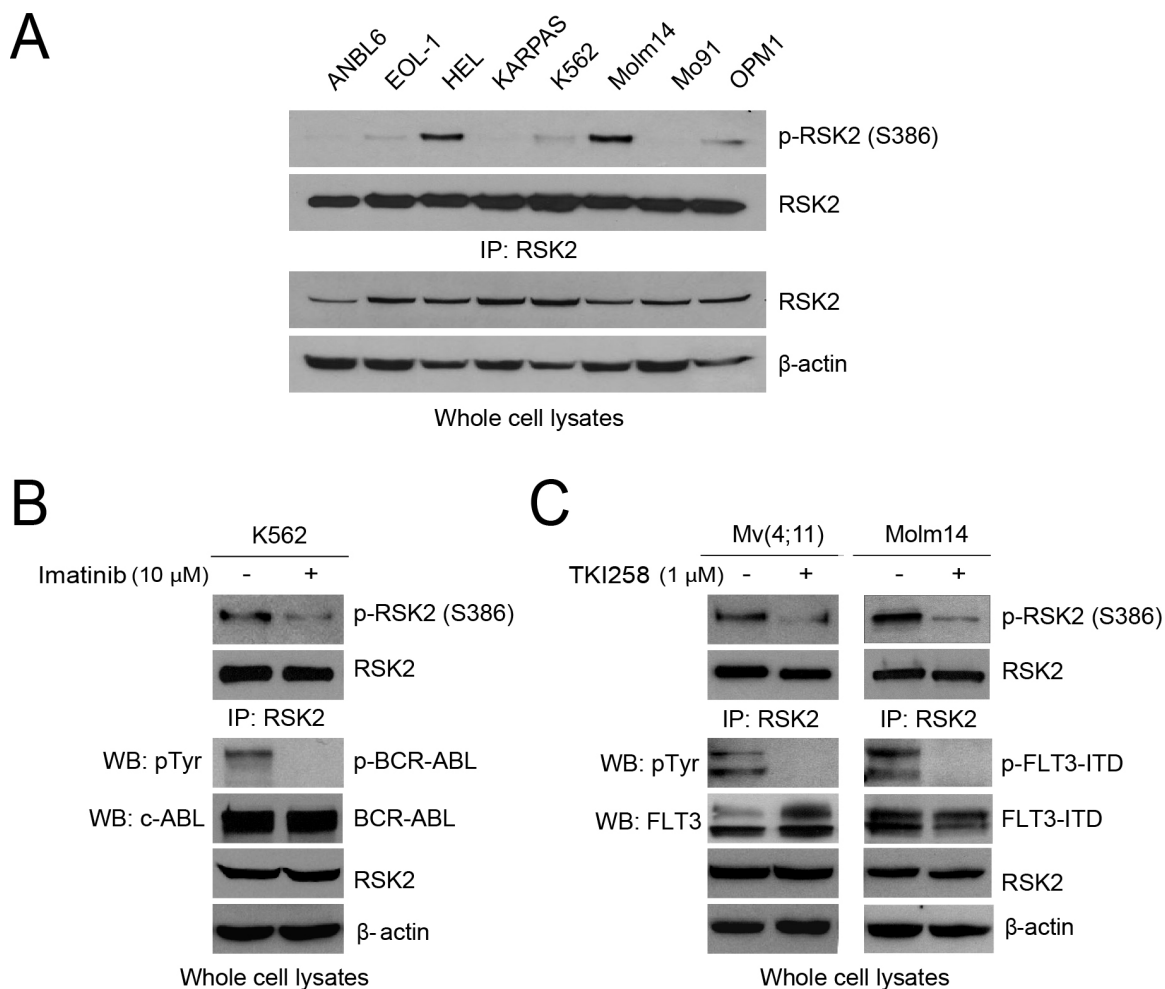


Figure 1.2. RSK2 is activated in diverse human leukemia cells transformed by different leukemogenic tyrosine kinases including BCR-ABL and FLT3-ITD. (A) Immunoblotting detects S386 phosphorylation of RSK2 in various hematopoietic cancer cell lines expressing diverse leukemogenic tyrosine kinases, including EOL-1 (FIP1L1-PDGFR α), HEL (JAK2V617F), KARPAS (NPM-ALK), K562 (BCR-ABL), Molm14 (FLT3-ITD), Mo91 (TEL-TrkC), OPM1 (FGFR3 K560E). ANBL6 is a human myeloma cell line without tyrosine kinase dysregulation and included as a negative control. (B-D) Immunoblotting shows that targeting BCR-ABL by imatinib in K562 cells (B) and FLT3-ITD by TKI258 in Mv(4;11) cells and Molm14 cells (C) decreases phosphorylation of RSK2 S386.

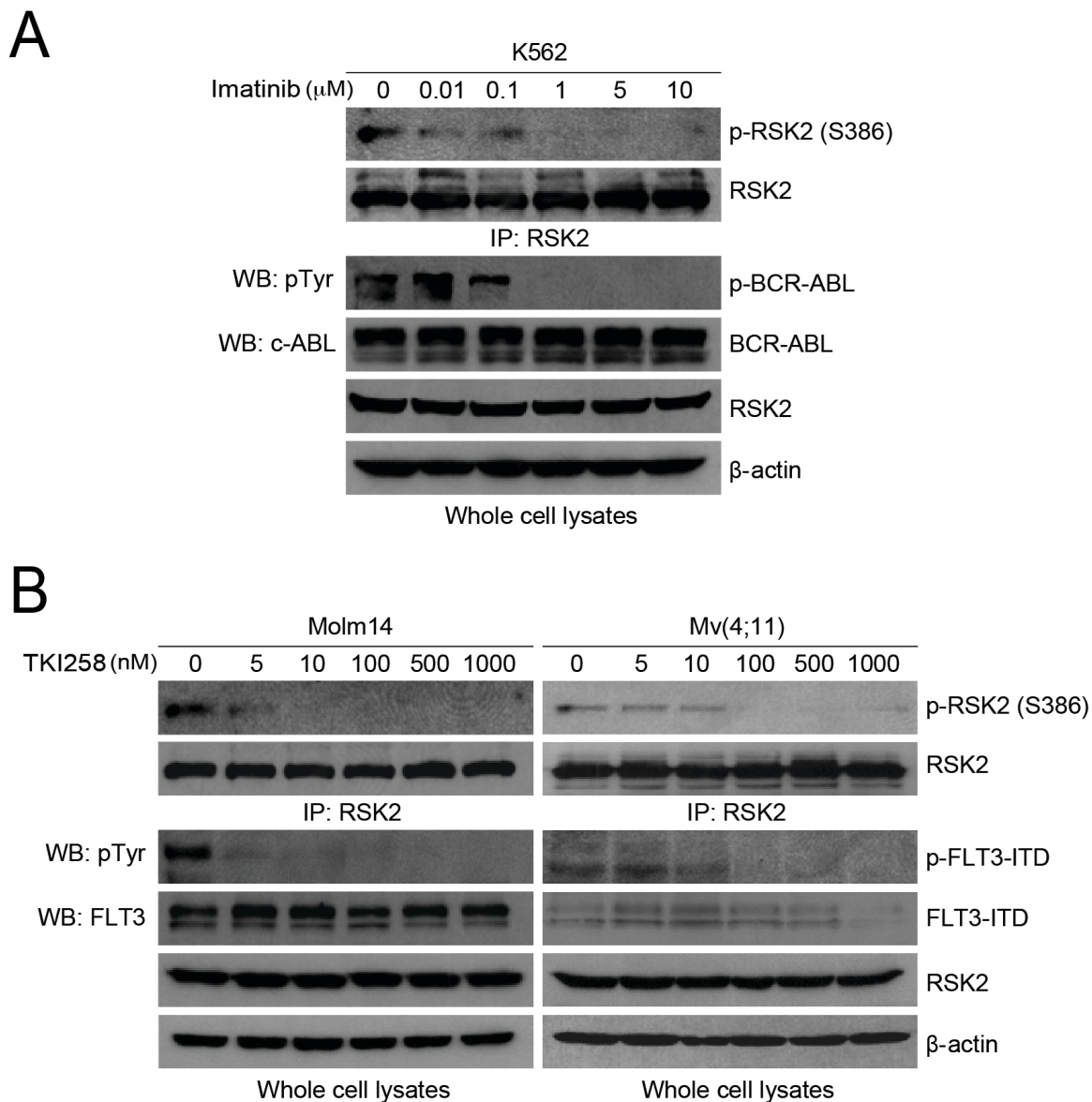


Figure 2.2. Targeting BCR-ABL by imatinib in K562 cells and FLT3-ITD by TKI258 in Molm14 and Mv(4;11) cells attenuates RSK2 activation in a dose dependent manner. (A) K562 cells, (B) Molm14, and Mv(4;11) cells were treated with distinct tyrosine kinase inhibitors at indicated concentrations for 4 hours prior to immunoblotting.

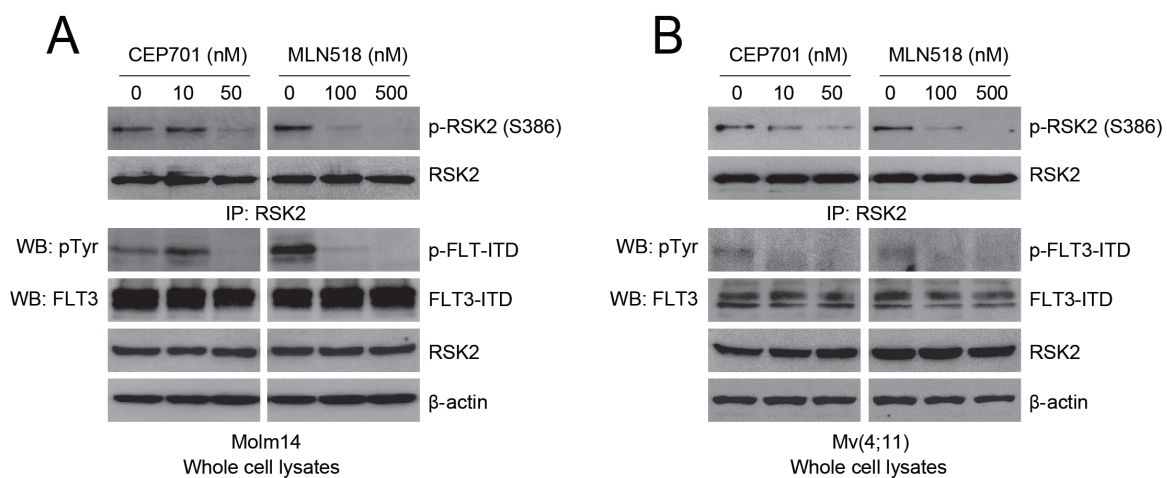


Figure 3.2. Targeting FLT3-ITD by CEP701 and MLN518 results in decreased RSK2 activation in FLT3-ITD positive human leukemia cell lines. (A) Molm14 and (B) Mv(4;11) cells were treated with distinct inhibitors at indicated concentrations for 4 hours prior to immunoblotting.

Genetic deficiency of RSK2 does not affect BCR-ABL-induced myeloproliferative neoplasm in a murine bone marrow transplant (BMT) assay.

To further decipher the role of RSK2 in BCR-ABL- or FLT3-ITD-induced hematopoietic transformation, we performed a murine BMT assay to examine whether RSK2 is required for the *in vivo* transforming activity of BCR-ABL or FLT3-ITD in primary hematopoietic cells. BCR-ABL or FLT3-ITD were retrovirally transduced into donor bone marrow cells from either wild type Balb/C mice or mice that are genetically deficient of RSK2 (RSK2 KO; 95). The transduced cells were subsequently injected into lethally irradiated syngeneic wild type Balb/C recipient mice. Our pilot bone marrow transplantation experiments demonstrated that RSK2 KO bone marrow cells are comparable to WT bone marrow cells in regard to retroviral infection efficiency, homing efficiency in the BMT recipient mice, and capacity to reconstitute the hematopoietic properties in lethally irradiated recipient mice (Figure 4.2).

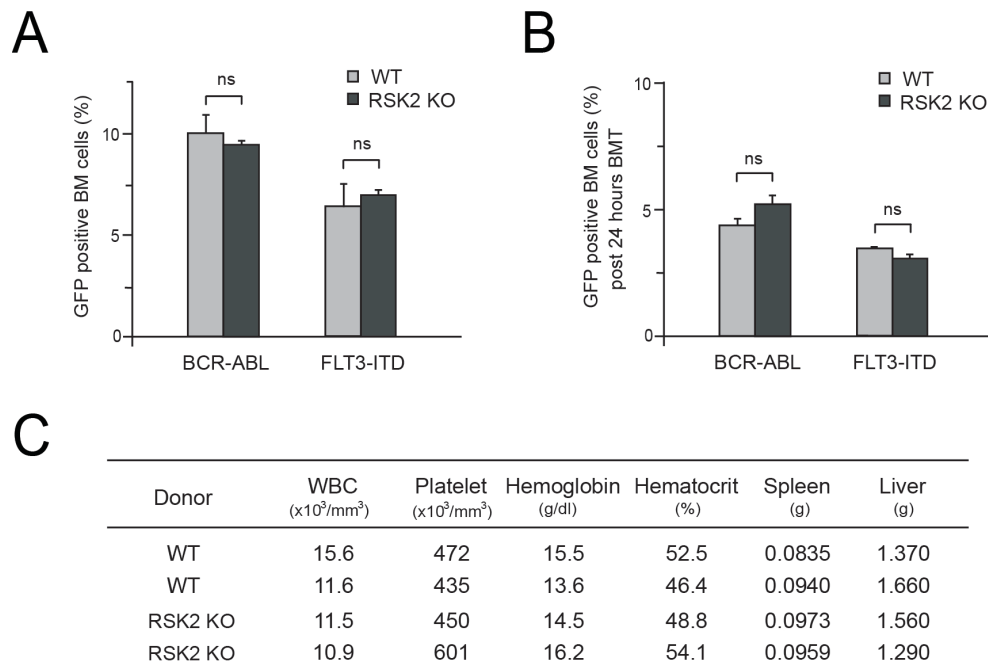


Figure 4.2. Genetic deficiency of RSK2 in donor bone marrow cells does not affect retroviral infection efficiency or hematopoietic reconstitution capability. (A) Bone marrow cells from 6-week old RSK2 KO and WT mice were isolated and transduced with retroviral supernatant carrying the MSCV2.2-Gateway-IRES-GFP-BCR/ABL or FLT3-ITD constructs. Retroviral infection efficiency was determined by the percentage of GFP positive cells in total cells after 24 hours. (B) WT and RSK2 KO bone marrow cells expressing BCR-ABL or FLT3-ITD demonstrated similar initial transplant efficiency in the BMT recipient mice. 0.5×10^6 infected cells from (A) were injected into each recipient mouse. Twenty-four hours after injection, bone marrow cells were harvested from recipients and GFP positive population was determined by FACS. (C) Wild type and RSK2 KO bone marrow cells similarly reconstituted the hematopoietic properties of lethally irradiated recipient mice. 0.5×10^6 WT or RSK2 KO bone marrow cells were injected into lethally irradiated (2×450 cGy) mice. Sixty days after BMT, the reconstitution ability was determined by organ weights and complete blood counts (CBC), which includes WBC, platelet counts, and hemoglobin/hematocrit levels. Two control mice receiving the same dose of irradiation but not bone marrow transplantation were dying and sacrificed at 14 and 16 days post irradiation, respectively, indicating that the irradiation dose was lethal. *p* values were determined by two-tailed Student's *t* test (ns, not significant).

As shown in Figure 5.2B, mice receiving either WT or RSK2 KO bone marrow cells transduced by BCR-ABL developed a fatal myeloproliferative neoplasm with no significant difference in survival latency ($p=0.388$). The disease phenotype in both WT and RSK2 KO BMT mice was similarly characterized by marked splenomegaly and a peripheral blood (PB) leukocytosis comprised predominantly of mature granulocytes, with no significant difference in WBC and spleen weights (Figure 5.1C). These results indicate a comparable myeloproliferative neoplasm state in both WT and RSK2 KO BMT mice. This notion was further confirmed by flow cytometric analysis, which showed similar numbers of mature neutrophils that were positive for late myeloid markers Gr-1 and Mac-1 in spleen and bone marrow samples of representative mice transplanted with BCR-ABL-transformed RSK2 KO bone marrow (BM) cells, compared with BCR-ABL-expressing wild type BM transplanted animals (Figure 5.2D).

In consonance with these observations, histopathologic examination of tissue samples from representative BCR-ABL-expressing WT BM transplanted mice demonstrated a perturbation of normal splenic architecture with loss of white pulp and expansion of red pulp by a prominent population of maturing myeloid forms, markedly hypercellular bone marrow with a predominance of mature myeloid forms and frequent number of admixed histiocytes and macrophages, and extensive myeloid cell infiltration in the liver (Figure 5.2E). Similar histologic evidence of myeloproliferation was also evident in the spleen, bone marrow, and liver from representative BCR-ABL-expressing RSK2 KO BM transplanted mice with a

comparable extent and degree of a myeloproliferative neoplasm. These data together suggest that RSK2 is dispensable for BCR-ABL-induced myeloproliferative neoplasm in mice.

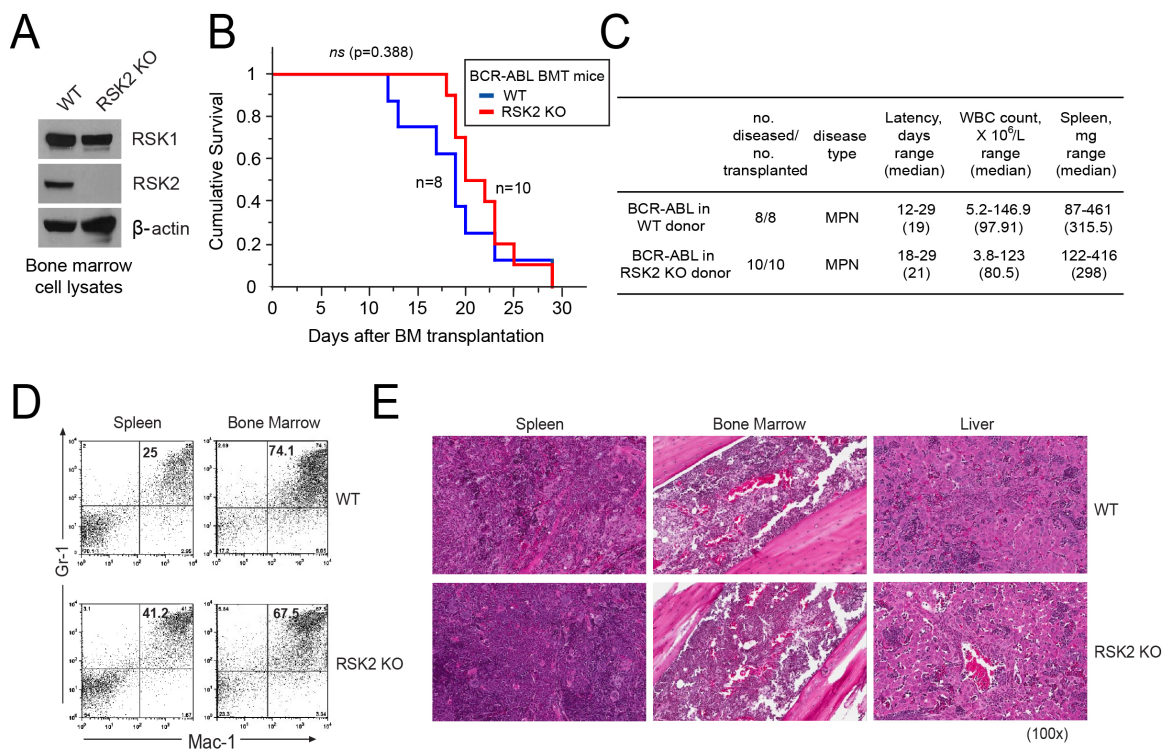


Figure 5.2. Genetic deficiency of RSK2 does not affect BCR-ABL-induced myeloproliferative neoplasm in a murine bone marrow transplant (BMT) assay. (A) Immunoblotting shows protein expression of RSK1 and RSK2 in bone marrow (BM) cells from Balb/C wild type (WT) and RSK2-deficient (RSK2 KO) mice. (B) Kaplan-Meier survival plot of mice receiving either WT or RSK2 KO bone marrow cells retrovirally transduced by BCR-ABL. All BMT mice in the WT group (n=8) and RSK2 KO group (n=10) developed an aggressive and rapidly fatal myeloproliferative neoplasm with a comparable latency. The statistical significance for survival was assessed by log-rank. (C) Analyses of mice transplanted with either WT or RSK2 KO BM cells expressing BCR-ABL. (D) Flow cytometry analysis demonstrates an expansion of Gr-1/Mac-1 double positive mature myeloid cells in spleen (left) and bone marrow (right) consistent with a myeloproliferative neoplasm in representative BMT mice receiving either WT or RSK2 KO BM cells expressing BCR-ABL, with comparable percentages that are supportive of similar disease burdens. (E) Tissue sections of spleen (left), bone marrow (middle) and liver (right) demonstrate evidence of a marked myeloproliferative neoplasm with an expansion of maturing myeloid cells observed in representative BMT mice receiving either WT or RSK2 KO BM cells expressing BCR-ABL. Magnifications are as indicated (H&E).

FLT3-ITD induces a T-cell acute lymphoblastic leukemia (T-ALL) in BMT mice receiving RSK2 KO BM cells, phenotypically distinct from the myeloproliferative neoplasm induced by FLT3-ITD using WT BM cells.

Next we sought to explore the role of RSK2 in FLT3-ITD-induced hematopoietic transformation *in vivo*. As shown in Figure 6.2A, mice transplanted with FLT3-ITD expressing WT bone marrow cells from Balb/C mice developed a myeloproliferative neoplasm with a median latency of 82 days. In contrast, mice transplanted with RSK2 KO BM cells expressing FLT3-ITD showed a significant delay in disease latency (Median latency=106 days; Figure 6.2A). Moreover, 6 out of 10 mice in this group developed T-ALL characterized by thymic enlargement with a much longer latency, while the remaining 4 mice in this group did not develop any discernable disease by the experimental endpoint (180 days). Those mice with T-ALL had significantly lower WBC and spleen weight compared to BMT mice receiving WT bone marrow cells expressing FLT3-ITD (Figure 6.2B).

Flow cytometry-based immunophenotypical analysis confirmed that the majority of leukemic cells in the spleen and bone marrow of representative FLT3-ITD WT BMT mice were Gr-1/Mac-1 double positive neutrophils, while such myeloid expansion was absent from the spleen and bone marrow of FLT3-ITD RSK2 KO BMT mice (Figure 6.2C, *upper panels*). Instead, CD4/CD8 double positive T cell expansion in spleen and thymus consistent with a T-ALL disease was detected in the representative FLT3-ITD RSK2 KO BMT mice (Figure 6.2C, *lower panels*).

Histopathologic examination of spleen, bone marrow, and liver tissue samples from FLT3-ITD WT BMT mice demonstrated evidence of a marked myeloproliferative neoplasm with an expansion of maturing myeloid cells, characterized by effacement of splenic architecture with expansion of red pulp by a prominent population of maturing myeloid elements, hypercellularity comprised primarily of mature myeloid elements in bone marrow, and extramedullary hematopoiesis with predominantly maturing myeloid elements in liver (Figure 6.2D). In contrast, the tissue samples from mice receiving RSK2 KO BM cells transformed by FLT3-ITD revealed extensive cell infiltration in spleen, bone marrow, and liver consistent with T-ALL (Figure 6.2D). This was essentially characterized by splenic red pulp expansion with infiltration of immature lymphoid blasts with some admixed maturing erythroid elements, marked hypercellularity in bone marrow with prominent infiltration of immature lymphoid blasts, infiltration of immature lymphoid blasts in liver, and effacement of normal thymic architecture by diffuse infiltration of immature lymphoid blasts.

Thus, these data together suggest that RSK2 is required for FLT3-ITD-induced myeloproliferative neoplasm in mice.

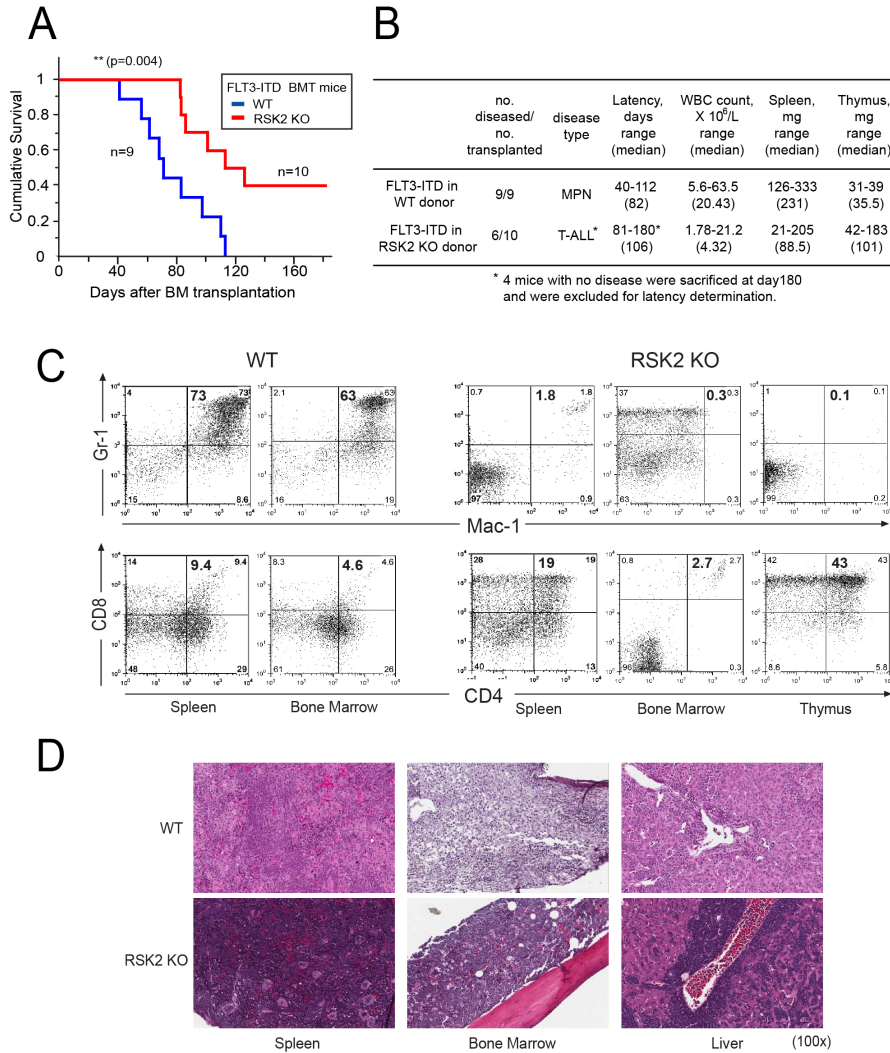


Figure 6.2. FLT3-ITD induced T-ALL in BMT mice using RSK2 KO BM cells, phenotypically distinct from the myeloproliferative neoplasm induced by FLT3-ITD using WT BM cells. (A) Kaplan-Meier survival plot of mice receiving either WT or RSK2 KO bone marrow cells retrovirally transduced by FLT3-ITD. All BMT mice in the WT group (n=9) developed an aggressive and fatal myeloproliferative neoplasm. In contrast, 6 out of 10 mice in the group receiving RSK2 KO BM cells transformed by FLT3-ITD developed T-ALL characterized by thymic enlargement, with a significantly longer latency, while 4 mice in this group did not develop any discernable disease by the experimental endpoint (180 days). The statistical significance for survival was assessed by log-rank. (B) Analyses of mice transplanted with either WT or RSK2 KO BM cells expressing FLT3-ITD. (C) Flow cytometry analysis demonstrates an expansion of Gr-1/Mac-1 double positive mature myeloid cells in spleen and bone marrow consistent with a myeloproliferative neoplasm in a representative BMT mouse receiving WT BM cells expressing FLT3-ITD (upper left), whereas such myeloid expansion was absent in the representative FLT3-ITD mouse receiving RSK2 KO BM cells (upper right). Instead, an expansion of CD4/CD8 double positive T cells in spleen and thymus consistent with T-ALL was detected in the representative FLT3-ITD BMT mouse receiving RSK2 KO BM cells (lower right), compared to the FLT3-ITD mouse receiving WT BM cells (lower left). (D) Tissue sections of spleen, bone marrow, and liver demonstrate evidence of a marked myeloproliferative neoplasm with an expansion of maturing myeloid cells observed in the representative FLT3-ITD BMT mouse receiving WT cells, and a T-ALL disease in the FLT3 mouse receiving RSK2 KO BM cells. Magnifications are as indicated (H&E).

Targeting RSK2 by a small molecule RSK inhibitor fmk attenuates cell viability and induces apoptosis in FLT3-ITD, but not BCR-ABL expressing murine Ba/F3 cells and human leukemia cells.

Next we tested whether RSK2 is a critical signaling effector in FLT3-ITD but not BCR-ABL-mediated hematopoietic transformation. We used a specific RSK inhibitor, fmk, which is a fluoromethylketone molecule that was designed to specifically exploit two selectivity filters of RSK and has been shown to potently inactivate the CTD auto-kinase activity of RSK (103). We found that fmk treatment effectively inhibited RSK2 activation, as assessed by phosphorylation levels of RSK2 S386, in Ba/F3 cells stably expressing BCR-ABL or FLT3-ITD (Figure 7.2A), as well as in human leukemia cells including BCR-ABL-expressing K562 cells and FLT3-expressing Molm14 cells and Mv(4;11) cells (Figure 7.2B). We then performed a dose-response analysis of Ba/F3 cells stably expressing BCR-ABL or FLT3-ITD (Figure 7.2C). Ba/F3 cells depend on IL-3 to proliferate, while expression of active, leukemogenic tyrosine kinases such as BCR-ABL and FLT3-ITD confers IL-3-independent proliferation to Ba/F3 cells. Treatment of fmk did not affect cell viability (Figure 7.2C, *left*) or induce apoptotic cell death (Figure 7.2C, *right*) in control parental Ba/F3 cells, Ba/F3 cells with FLT3-ITD in the presence of IL-3, or cells transformed by BCR-ABL in the absence of IL-3. In contrast, fmk treatment effectively inhibited growth of the FLT3-ITD expressing Ba/F3 cells in the absence of IL-3 with a cellular IC₅₀ of 4.19 μ M, and also induced apoptosis in a dose dependent manner (Figure 7.2C, *left* and *right*, respectively).

We next performed fmk treatment experiments using human leukemia cells expressing either BCR-ABL or FLT3-ITD. Consistent with the result of the BMT assays and fmk treatment experiments using Ba/F3 cells, inhibition of RSK2 by fmk treatment did not affect cell viability nor induce apoptosis in K562 cells (Figure 7.2D). In contrast, treatment with fmk inhibited RSK2 in FLT3-expressing human leukemia Molm14 cells and Mv(4;11) cells (Figure 7.2B), which resulted in decreased cell viability in Molm14 and Mv(4;11) cells with cellular IC_{50} values of 7.19 μ M and 12.94 μ M, respectively, and induced significant apoptosis in these cells (Figure 7.2E-F). Furthermore, as shown in Figure 7.2G-H and 8.2, siRNA-mediated targeted down regulation of RSK2 (Figure 7.2G), but not RSK1 (Figure 8.2), significantly induced apoptosis (Figure 7.2H, *left*) and attenuated cell viability (Figure 7.2H, *right*) in FLT3-ITD expressing human leukemia Molm14 and Mv(4;11) cells, but not K562 cells expressing BCR-ABL. These data further support our hypothesis that RSK2 plays a critical role in cell proliferation and survival in FLT3-ITD but not BCR-ABL transformed leukemia cells.

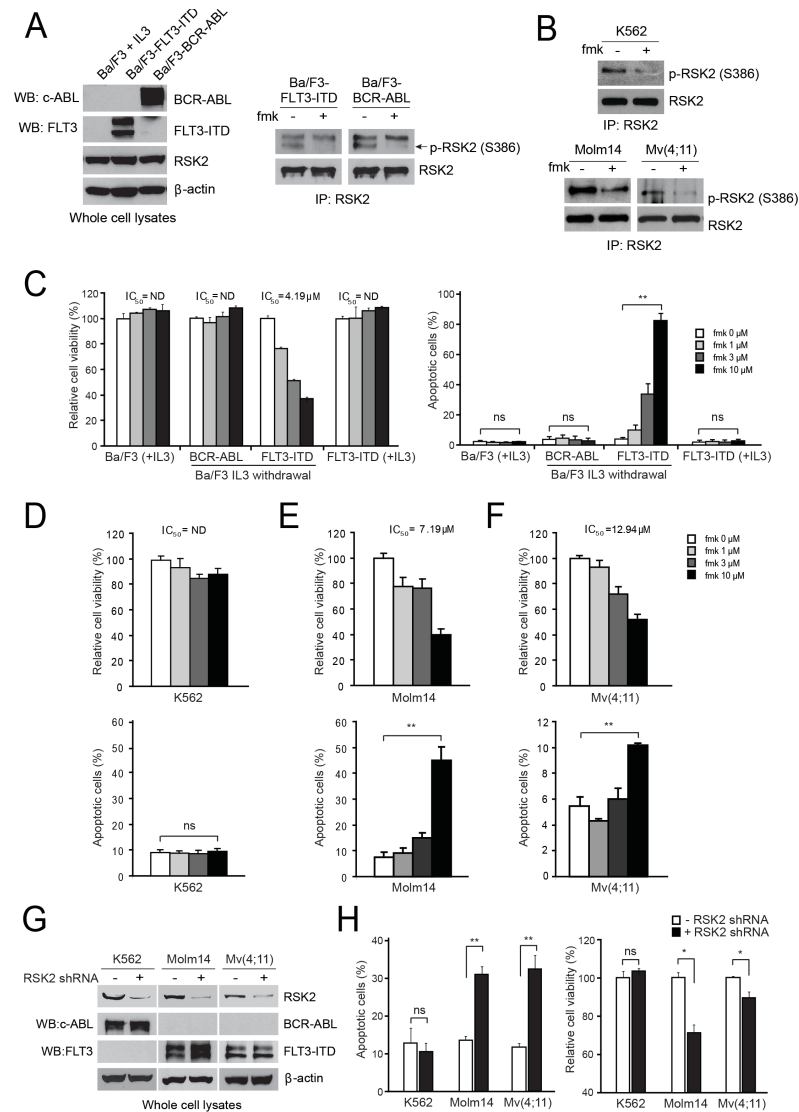


Figure 7.2. Targeting RSK2 by fmk attenuates cell viability and induces apoptosis in FLT3-ITD, but not BCR-ABL expressing Ba/F3 cells and human leukemia cells. (A) Left: Immunoblotting results show stable expression of BCR-ABL and FLT3-ITD in Ba/F3 cells. Right: 3 μ M of Fmk treatment inhibits RSK2 in Ba/F3 expressing BCR-ABL or FLT3-ITD. (B) 3 μ M of Fmk treatment inhibits RSK2 in BCR-ABL positive K562 (upper) and FLT3-ITD positive Molm14 and Mv(4;11) human leukemia cells (lower). (C) Treatment with increasing concentrations of fmk resulted in decreased cell viability (left) and increased apoptosis (right) in FLT3-ITD positive Ba/F3 cells in the absence of IL3 (-IL3), but not in cells expressing BCR-ABL (-IL3), control Ba/F3 cells cultured in the presence of IL3 (+IL3), or FLT3-ITD positive cells in the presence of IL3 (+IL3). (D-F) Targeting RSK2 by fmk does not affect cell viability nor induce apoptosis in K562 cells expressing BCR-ABL (D), but results in decreased cell viability and increased apoptosis in FLT3-ITD-expressing Molm14 (E) and Mv(4;11) cells (F). (G-H) RNAi-mediated targeted down-regulation of RSK2 (G) significantly induced apoptosis (H; left) and attenuated cell viability (H; right) in FLT3-ITD expressing Molm14 and Mv(4;11) human leukemia cell lines, but not in K562 cells expressing BCR-ABL. Cells were transiently infected with lentivirus harboring an empty pLKO.1 vector or shRNA specific to RSK2 for 24 hours. The apoptotic population was characterized as the fraction of Annexin V positive cells of total treated cells. The relative cell viability was determined by MTT based assay. p values were determined by two-tailed Student's *t* test (*0.01<p<0.05; **p<0.01; ns, not significant).

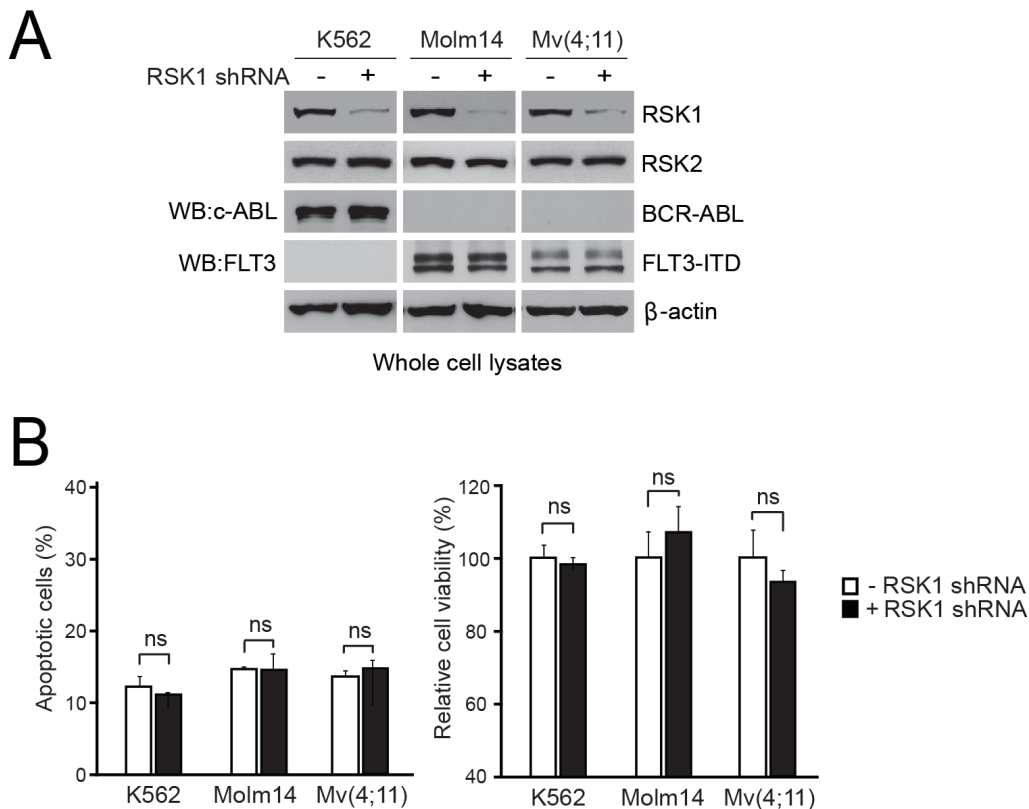


Figure 8.2. RNAi-mediated targeted down-regulation of RSK1 failed to significantly induce apoptosis or attenuate cell viability in BCR-ABL or FLT3-ITD expressing human leukemia cell lines. (A) K562, Molm14, and Mv(4;11) cells were transiently infected with lentivirus harboring an empty pLKO.1 vector or shRNA specific to RSK1 for 24 hours. (B; left) The apoptotic population was characterized as the fraction of Annexin V positive cells of total treated cells. (B; right) The relative cell viability was determined by MTT based assay. p values were determined by two-tailed Student's *t* test (ns, not significant).

Fmk treatment induces significant apoptosis in FLT3-ITD but not BCR-ABL-expressing primary human leukemia cells.

Moreover, we observed that fmk significantly attenuated cell viability (Figure 9.2A) and induced apoptosis (Figure 9.2B) in primary FLT3-ITD-positive leukemia cells from AML patients, but not in primary BCR-ABL-expressing leukemia cells from two Ph⁺ leukemia patients, nor in primary leukemia cells from two FLT3-ITD negative AML patients (Figure 9.2C). These data provide “proof of principle” that demonstrate the therapeutic potential of targeting RSK2 by fmk in FLT3-ITD-positive AML.

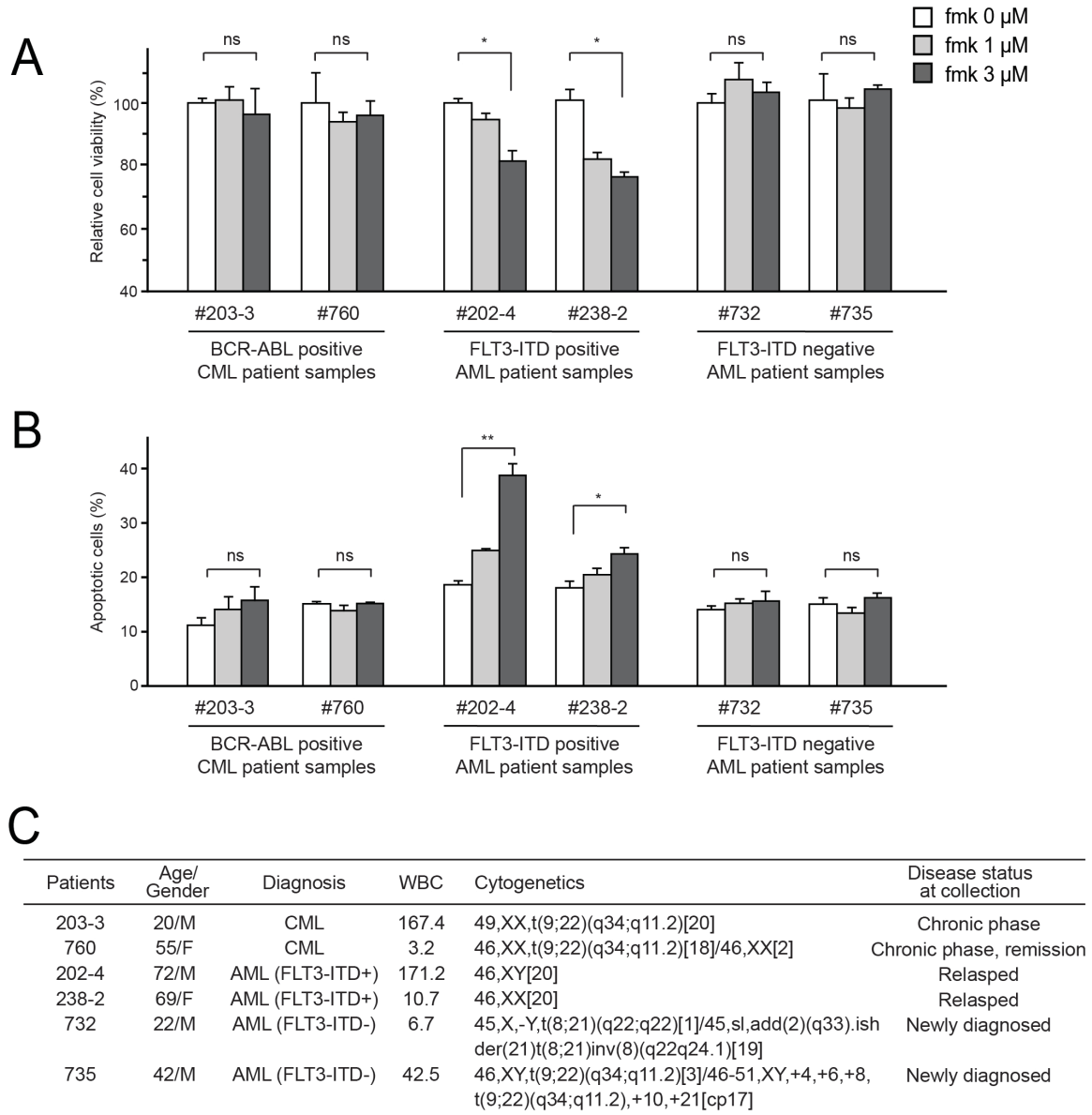


Figure 9.2. Fmk treatment induces significant apoptosis in FLT3-ITD but not BCR-ABL-expressing primary human leukemia cells. Inhibition of RSK2 by treatment with fmk does not affect cell viability nor induce apoptosis (left, A and B, respectively) in primary BCR-ABL-positive leukemia cells from two CML patients, and primary FLT3-ITD-negative leukemia cells from two AML patients (right, A and B, respectively), whereas fmk treatment results in decreased cell viability and increased apoptosis in primary FLT3-ITD-positive leukemia cells from two AML patients. Apoptotic population was determined as the percentage of annexin V positive cells of total treated cells. (C) Clinical information for the leukemia patients. p values were determined by two-tailed Student's *t* test (*0.01 < p < 0.05; **p < 0.01; ns, not significant).

2.4. Discussion

Our data suggest that although both BCR-ABL and FLT3-ITD activate RSK2 in leukemia cells, RSK2 is differentially required for hematopoietic transformation induced by BCR-ABL and FLT3-ITD. Genetic deficiency of RSK2 did not affect the pathogenesis or disease progression of BCR-ABL-induced myeloproliferative neoplasm in a murine BMT model, and inhibition of RSK2 by small molecule inhibitor fmk did not effectively attenuate cell proliferation or induce apoptosis in murine Ba/F3 cells and human leukemia K562 cells expressing BCR-ABL, nor in primary leukemia cells from BCR-ABL positive CML patients. In contrast, FLT3-ITD failed to induce myeloproliferative neoplasm in BMT mice receiving RSK2 KO bone marrow cells, and instead induced T-ALL. In consonance with these results, targeting RSK2 by fmk resulted in decreased cell viability and increased apoptosis in FLT3-ITD positive Ba/F3 cells and human leukemia Molm14 and Mv(4;11) cells, as well as in primary leukemia cells from FLT3-ITD positive AML patients. These findings suggest that RSK2 is dispensable for BCR-ABL induced hematopoietic transformation, but is likely required for pathogenesis and myeloid lineage determination in FLT3-ITD induced hematopoietic transformation, and that RSK2 plays a key role in cell proliferation and survival of FLT3-ITD transformed myeloid cells (Figure 10.2).

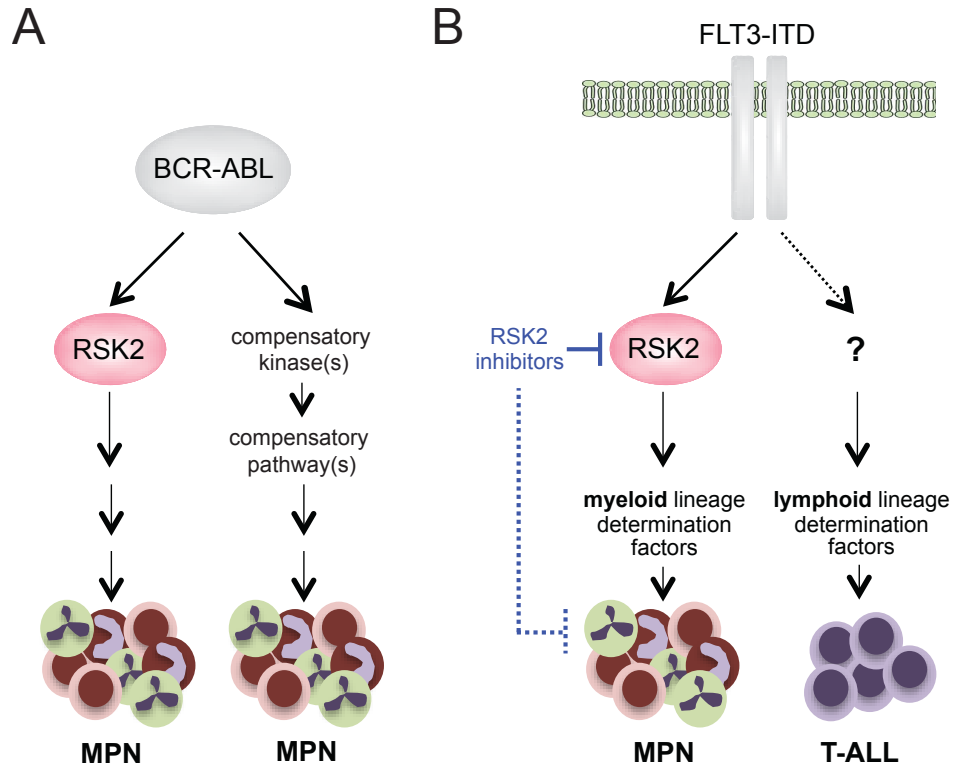


Figure 10.2. Proposed model: role of RSK2 in BCR-ABL and FLT3-ITD-induced MPN. Both BCR-ABL (A) and FLT3-ITD (B) signal through RSK2 to induce myeloproliferative neoplasm. However, BCR-ABL may circumvent the loss of RSK2 by signaling through compensatory pathways in order to achieve myeloid transformation. On the other hand, FLT3-ITD appears to absolutely require RSK2 in order to achieve myeloid transformation, as the loss of RSK2 leads instead to lymphoid transformation and the development of T-ALL with a complete absence of myeloid disease. This indicates that RSK2 may play a role in myeloid lineage determination in FLT3-ITD induced hematopoietic disease, and when inhibited, FLT3-ITD is forced to signal through lymphoid transforming pathways instead, leading to T-ALL in place of MPN. RSK2 may thus represent a promising therapeutic target in the treatment of FLT3-ITD-induced AML.

We previously reported that in a murine BMT assay, RSK2 plays an important role in leukemogenic TEL-FGFR3-induced myeloproliferative neoplasm (73). TEL-FGFR3 is a constitutively activated fusion tyrosine kinase that is associated with t(4;12)(p16;p13) AML (104). Genetic deficiency of RSK2 resulted in a significantly delayed and attenuated myeloproliferative syndrome induced by TEL-FGFR3 as compared with wild type cells, suggesting that RSK2 may be required in TEL-FGFR3-induced pathogenesis and disease progression, but not lineage determination in hematopoietic transformation. Together these findings suggest that, although all three leukemogenic tyrosine kinases are involved in hematopoietic transformation and induce a similar myeloproliferative neoplasm characterized by expansion of Gr-1⁺/Mac-1⁺ neutrophils in a murine BMT assay, the role of RSK2 in hematopoietic transformation might depend on discrete upstream oncogenic signals mediated by different leukemogenic tyrosine kinases.

Previous studies reported that RSK2 KO mice have decreased bone mass due to the critical role of RSK2 in osteoblast differentiation (80, 105). However, RSK2 KO mice have a normal lifespan and no histologic or metabolic evidence of internal organ dysfunction (80, 95, 105). Lin et al demonstrated that RSK2 is dispensable for normal lymphoid development and RSK2 KO animals had normal numbers of Gr-1⁺ and Mac-1⁺ cells in the spleen (95). Therefore, the change in disease phenotype and attenuation of disease burden seen in FLT3-ITD and TEL-FGFR3-induced disease using RSK2-deficient bone marrow cells in BMT mice, respectively, is likely due to impairment of RSK2-mediated signal transduction rather than abnormalities in the

target cell populations. It is possible that, although RSK2 may not be required for normal myelopoiesis, these three leukemogenic tyrosine kinases activate distinct signaling pathways to induce hematopoietic transformation. While BCR-ABL appears not to require RSK2 signaling, the role of RSK2 in FLT3-ITD-induced hematopoietic transformation is more critical and is likely associated with disease initiation, lineage determination and disease progression. As for TEL-FGFR3, RSK2 appears to be primarily involved in the proliferation of TEL-FGFR3-transformed myeloid cells rather than the initiation of TEL-FGFR3-dependent myeloid transformation. Further studies are warranted to explore the differential involvement of RSK2 in FLT3-ITD and TEL-FGFR3 dependent transformation of hematopoietic stem cells and/or myeloid progenitors.

Our studies cumulatively implicate a differential requirement for RSK2 in FLT3-ITD positive AML and T-ALL. It was previously reported that BMT mice receiving bone marrow cells expressing FLT3-ITD developed myeloproliferative disease, whereas mice transplanted with bone marrow cells transformed by FLT3-TKD mutants harboring mutations in tyrosine kinase domain (TKD) developed a lymphoid disorder (14). Interestingly, FLT3-TKD mutants have differential signaling properties compared to FLT3-ITD. FLT3-ITD activates STAT5 and inhibits protein expression of C/EBP α and PU.1 (106-107), while FLT3-TKD does not. However, the activation levels of STAT5 and protein expression levels of C/EBP α and PU.1 are not affected by RSK2 knockdown (KD) in Molm14 cells expressing FLT3-ITD, or in Ba/F3 cells stably expressing FLT3-ITD (data not shown). These results suggest that

the RSK2 signaling pathway is involved in FLT3-ITD-induced hematopoietic transformation independent of STAT5, C/EBP α and PU.1. Future studies would thus involve further elucidation of the signaling mechanisms underlying RSK2-mediated lineage dependent transformation by FLT3-ITD.

In addition, it appears that the other RSK family members such as RSK1 that are expressed in the RSK2 KO BM cells could not functionally compensate the genetic deficiency of RSK2 to maintain myeloproliferative neoplastic initiation and development in BMT mice receiving FLT3-ITD transformed RSK2 KO BM cells. Moreover, targeting RSK2 by fmk effectively induced apoptosis in FLT3-ITD positive human leukemia cell lines and primary leukemia cells from AML patients. Thus, RSK2 may represent an alternative therapeutic target in treatment of FLT3-ITD positive AML, but not T-ALL. We recently demonstrated that fmk induced significant apoptosis in human t(4;14) primary myeloma cells from a multiple myeloma patient, but not in primary myeloma cells from a t(4;14) negative myeloma patient (55). These data demonstrate that RSK inhibitors such as fmk may have minimal non-specific cytotoxicity in human cells. In consonance with this finding, Dumont et al demonstrated that triple knockout of RSK1, 2, and 3 does not affect mouse viability (108), further suggesting that targeting RSK may represent a promising therapeutic strategy to treat FLT3-ITD positive AML without serious side effects in whole organism homeostasis.

Chapter 3: Targeting leukemia metabolism as a novel therapeutic strategy

3.1. Signaling and targeting of phosphoglycerate mutase 1 in human cancers

3.1.1. Introduction

The Warburg effect describes the phenomenon that cancer cells produce energy predominantly by glycolysis in the cytosol even when oxygen is plentiful, rather than by the oxidation of pyruvate in the mitochondria as normal cells do (46). Cancer cells thus take in greater amounts of glucose than their normal counterparts, using this glucose as a carbon source for anabolic biosynthesis of macromolecules. These include nucleotides, amino acids and fatty acids, to produce RNA/DNA, proteins and lipids, respectively, which are necessary to sustain the rapid rate at which cancer cells proliferate (46). Interestingly, leukemia cells display a similar metabolic shift in energy metabolism from oxidative phosphorylation to glycolysis, (109-110), despite residing in the bloodstream where oxygen is readily available.

During glycolysis, glycolytic intermediates can be diverted into the oxidative phase of the PPP at the point of glucose-6-phosphate (G-6-P). The oxidative PPP contributes to macromolecular biosynthesis by producing reducing potential in the form of NADPH and/or ribose-5-phosphate (R-5-P), the building blocks for nucleotide synthesis. NADPH is the most essential metabolite produced by the PPP, functioning not only to fuel macromolecular biosynthesis of lipids, but also to serve

as an antioxidant, scavenging the ROS produced during rapid proliferation of cancer cells. Glycolysis and glutaminolysis supply the carbon input required for the TCA cycle to function as a biosynthetic 'hub' and permit the production of other macromolecules including amino acids and fatty acids (45). Thus, cancer cells appear to coordinate glycolysis and anabolic biosynthesis to provide an overall metabolic advantage to cancer cell proliferation and disease development. However, the detailed mechanisms underlying this coordination remain largely unknown.

We found that glycolytic enzyme PGAM1, which catalyzes the conversion of 3-phosphoglycerate (3-PG) to 2-phosphoglycerate (2-PG) during glycolysis, promotes cancer cell proliferation and tumor growth through coordination of glycolysis and anabolic biosynthesis. PGAM1 regulates a unique step in glycolysis, and most of the glycolytic intermediates that are used as precursors for anabolic biosynthesis are upstream of this step. In many cancers, including hepatocellular carcinoma and colorectal cancer, PGAM1 activity is increased compared to that in the normal tissues (111-112). Moreover, PGAM1 gene expression is believed to be upregulated due to loss of *TP53* in cancer cells, as *TP53* negatively regulates PGAM1 gene expression (113-115). In this work, we first demonstrate a novel mechanism that explains how PGAM1 regulates the oxidative PPP, at least in part by controlling the metabolite levels of its substrate 3-PG and product 2-PG, which exert regulatory functions on key metabolic enzymes including 6PGD and 3-phosphoglycerate dehydrogenase (PHGDH), respectively. Moreover, we identified and developed a small molecule PGAM1 inhibitor, PGMI-004A, which demonstrates promising

efficacy and minimal non-specific toxicity in inhibition of cell proliferative and tumor development potential of human cancer cells *in vitro* and *in vivo*, respectively, as well as in treatment of human primary leukemia cells isolated from tissue samples from human leukemia patients. These translational studies provide “proof-of-principle” to suggest that PGAM1 is an attractive anti-leukemia target.

3.1.2 Materials and Methods

Drug screening: *In vitro* PGAM1 and enolase assays. We performed an *in vitro* PGAM1 assay as primary screening. In brief, we prepared PGAM1 enzyme mix containing 100 mM Tris-HCl, 100 mM KCl, 5 mM MgCl₂, 1 mM ADP, 0.2 mM nicotinamide adenine dinucleotide (NADH), 5 mg/ml recombinant PGAM1, 0.5 units/ml enolase, 0.5 units/ml recombinant pyruvate kinase M1, and 0.1 units/ml recombinant LDH. 3-PG was added last at the final concentration of 2 mM to initiate the reaction. The decrease in autofluorescence (ex:340 nm, em:460 nm) from oxidation of NADH was measured as PGAM1 activity. We also performed an *in vitro* enolase assay as secondary screening. In brief, we prepared enolase enzyme mix containing 100 mM Tris-HCl, 100 mM KCl, 5 mM MgCl₂, 1 mM ADP, 0.2 mM NADH, 0.5 units/ml enolase, 0.5 units/ml recombinant pyruvate kinase M1, and 0.1 units/ml recombinant LDH. 2-PG was added last at the final concentration of 2 mM to initiate the reaction. The decrease in autofluorescence (ex:340 nm, em:460 nm) from oxidation of NADH was measured as enolase activity.

Cell proliferation and viability assays. For leukemia cell proliferation assay, 10×10^4 cells were seeded in non-tissue culture coated 6-well plate and incubated at 37 °C for indicated times. Cell numbers were counted by trypan blue exclusion under a microscope (x40) at indicated times and the percentage of cell proliferation was determined by comparing PGAM1 KD cells to pLKO.1 vector expressing cells. For cell viability assays of leukemia cells, 10×10^4 cells were seeded in non-culture

coated 6-well plate and incubated with PGMI-004A at 37 °C for indicated times. Cell viability was determined by counting drug-treated cells compared to dimethyl sulfoxide (DMSO)-treated control cells with trypan blue exclusion under a microscope (x40) and by using CellTiter96Aqueous One solution proliferation kit (Promega).

Xenograft studies. Approval of use of mice and designed experiments was given by the Institutional Animal Care and Use Committee of Emory University. Nude mice (Athymic Nude-Foxn1^{nu}, female 6–8-week-old, Harlan) were subcutaneously injected with 10×10^6 H1299 cells harboring empty vector on the left flank, and cells with stable KD of endogenous hPGAM1 on the right flank, respectively. The tumors were harvested and weighed at the experimental endpoint, and the masses of tumors (g) derived from cells with and without stable KD of endogenous hPGAM1 in both flanks of each mouse were compared. Statistical analyses were performed by comparison in relation to the control group with a two-tailed paired Student's *t* test. For drug evaluation of PGMI-004A using xenograft mice, the drug was administered by daily intraperitoneal injection at a dose of 100 mg/kg from 6 days after subcutaneous injection of H1299 cells on right flank of each mouse. Tumor growth was recorded by measurement of two perpendicular diameters of the tumors over a 3-week course using the formula $4\pi/3 \times (\text{width}/2)^2 \times (\text{length}/2)$. The tumors were harvested and weighed at the experimental endpoint. The masses of tumors (g) treated with vehicle control (DMSO:PEG400:PBS at a ratio of 4:3:3) and PGMI-004A were compared and the *p* values were determined by a two-tailed Student's *t* test.

Primary tissue samples from human patients with leukemia and healthy donors. Approval of use of human specimens was given by the Institutional Review Board of Emory University School of Medicine. All clinical samples were obtained with informed consent with approval by the Emory University Institutional Review Board. Clinical information for the patients was obtained from the pathological files at Emory University Hospital under the guidelines and with approval from the Institutional Review Board of Emory University School of Medicine and according to the Health Insurance Portability and Accountability Act. Only samples from patients that were not previously treated with chemotherapy or radiation therapy were used. Mononuclear cells (MNCs) were isolated from PB and bone marrow samples from human leukemia patients or PB samples from healthy donors using lymphocyte separation medium (Cellgro). Cells were cultured in RPMI 1640 medium supplemented with 10% FBS and penicillin/streptomycin and incubated with increasing concentrations of PGMI-004A for up to 72 or 120 hours.

3.1.3. Results

PGAM1 controls intracellular 3-PG and 2-PG levels and is important for cancer cell glycolysis, anabolic biosynthesis, proliferation, and tumor growth.

To better understand how cancer cells coordinate glycolysis and anabolic biosynthesis, we first examined the effects of targeted downregulation of the glycolytic enzyme PGAM1. Global Metabolic Profiling (Metabolon) using cell lysates samples of parental H1299 cells and cells with stable KD of PGAM1 revealed that PGAM1 KD causes altered intracellular concentrations of 118 biochemicals, including PGAM1 substrate 3-PG, which was significantly increased, and PGAM1 product 2-PG, which was significantly decreased in PGAM1 KD compared to control cells.

We next examined the role of PGAM1 in cancer cell metabolism. We found that, compared to vector control cells, stable KD of PGAM1 results in a decreased glycolytic rate and lactate production, as well as reduced glucose-dependent biosynthesis of RNA and lipids, accompanied by reduced NADPH/NADP⁺ ratio. Because the PPP produces NADPH and R-5-P to contribute to macromolecular biosynthesis, we next examined whether PGAM1 contributes to PPP flux. Indeed, we found that oxidative PPP flux is reduced in PGAM1 KD compared to control vector cells. Interestingly, attenuation of PGAM1 in cancer cells does not affect glucose uptake rate, intracellular ATP levels, or O₂ consumption rate in either the presence or absence of ATP synthase inhibitor oligomycin. These results suggest

that downregulation of PGAM1 attenuates glycolysis, PPP and biosynthesis, but does not significantly affect glucose uptake or intracellular ATP levels (data courtesy of Taro Hitosugi; not shown).

In addition, we found that stable KD of PGAM1 results in decreased cell proliferation in diverse human cancer and leukemia cells (Figure 1.3.1A). Moreover, we performed a xenograft experiment in which nude mice were subcutaneously injected with control H1299 cells harboring an empty vector on the left flank and PGAM1 KD H1299 cells on the right flank (Figure 1.3.1B; left). The mice were monitored for tumor growth over 6 weeks. The masses of tumors derived from PGAM1 knock- down H1299 cells were significantly reduced compared to those of tumors formed by vector control cells (Figure 1.3.1B; right).

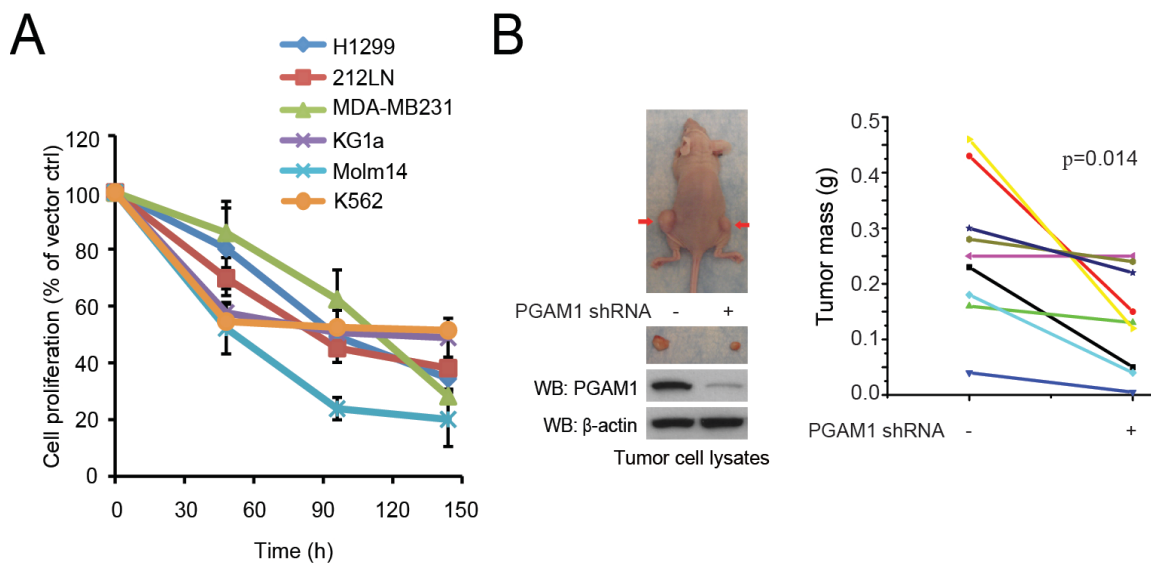


Figure 1.3.1. PGAM1 is important for cancer cell proliferation and tumor growth. (A) Cell proliferation rates were determined by cell counting in diverse human cancer (H1299, 212LN, and MDA-MB231) and leukemia (KG1a, Molm14, and K562) cells with stable KD of PGAM1, which were normalized to the corresponding control cells harboring an empty vector. (B) Stable KD of PGAM1 by shRNA attenuates tumor growth potential of H1299 cells in xenograft nude mice. Left: Dissected tumors (indicated by red arrows) in a representative nude mouse and expression of PGAM1 in tumor lysates are shown. Right: PGAM1 KD cells show significantly reduced tumor formation in xenograft nude mice compared to cells harboring empty vector control. The error bars represent mean values \pm SD from three replicates of each sample. *p* values were determined by a two-tailed paired Student's *t* test.

PGAM1 KD results in elevated levels of 3-PG, which binds to and inhibits 6PGD by competing with its substrate, 6-PG.

We next explored the molecular mechanism by which PGAM1 regulates the PPP. To determine if the abnormally high levels of 3-PG in PGAM1 KD cells inhibit oxidative PPP flux, we examined the effect of 3-PG on G6PD, the first and most important enzyme of the oxidative PPP, which produces NADPH, and 6PGD, which also produces NADPH while converting 6-phosphogluconate (6-PG) into ribulose-5-phosphate (Ru-5-P). We performed in vitro 6PGD and G6PD assays in the presence of increasing concentrations of 3-PG, and found that treatment with 3-PG concentrations analogous to those in PGAM1 KD H1299 cells results in decreased enzyme activity of 6PGD, but not G6PD. These results suggest that abnormally high levels of 3-PG, as in PGAM1 KD cells, may selectively and directly inhibit 6PGD but not G6PD.

Thermal melt shift assays, kinetics studies, and structural analysis together revealed that 3-PG directly binds to 6PGD and inhibits 6PGD enzyme activity by competing with its cognate substrate 6-PG, representing a molecular mechanism to explain how PGAM1, as a glycolytic enzyme, contributes to the regulation of the oxidative PPP and consequently anabolic biosynthesis (data courtesy of Taro Hitosugi; not shown).

Rescue of reduced 2-PG levels in PGAM1 KD cells results in decreased 3-PG levels by activating 3-PG dehydrogenase.

To examine the effect of decreased 2-PG levels on cancer cell metabolism, we treated PGAM1 KD cancer cells with a cell permeable agent, methyl-2-PG, which converts to 2-PG in cells. We observed that methyl-2-PG treatment rescues the reduced lactate production but has no significant effect on intracellular ATP levels in H1299 cells with stable KD of PGAM1 compared to control vector cells. This result suggests that rescuing cellular 2-PG levels reverses the inhibitory effect of PGAM1 KD on glycolysis and allows downstream glycolytic reactions to resume and ultimately produce lactate. Surprisingly, we also found that methyl-2-PG treatment rescues the decreased oxidative PPP flux and biosynthesis of RNA and lipids, as well as partially restores the reduced cell proliferation in various PGAM1 KD cancer cells compared to the corresponding control vector cells. These data suggest that the increased 2-PG levels in PGAM1 KD cells provide a feedback mechanism to rescue the abrogated PPP and anabolic biosynthesis upstream of PGAM1. We tested this hypothesis by examining the effect of rescued 2-PG levels on 3-PG concentrations in PGAM1 KD cells. We found that treatment with methyl-2-PG results in decreased 3-PG concentrations in diverse PGAM1 KD cells to levels that are comparable to the 3-PG concentrations in the corresponding vector control cells. These results further suggest that PGAM1 controls 2-PG levels in cancer cells, which contributes to PGAM1-dependent coordination of glycolysis and anabolic biosynthesis by adjusting 3-PG levels.

We next determined the molecular mechanism underlying 2-PG-dependent feedback regulation of intracellular 3-PG levels. Besides conversion to 2-PG catalyzed by PGAM1 in glycolysis, 3-PG also serves as a precursor for serine synthesis and can be converted to 3-phosphohydroxypyruvate (pPyr) by 3-PG dehydrogenase (PHGDH). We found that treatment with 2-PG concentrations equivalent to those determined in control H1299 cells or methyl-2-PG treated PGAM1 KD cells results in higher PHGDH enzyme activity. In contrast, 2-PG concentrations that correspond to those determined in PGAM1 KD cell did not significantly affect PHGDH activity. Together, these studies reveal a feedback mechanism by which cellular 2-PG levels contribute to control of 3-PG levels in cells through regulation of PHGDH.

In addition, we found that stable KD of PGAM1 results in significantly decreased serine biosynthesis, while treatment with methyl-2-PG rescues the phenotype. Moreover, shRNA-mediated KD of PHGDH does not affect rescued 2-PG levels in PGAM1 KD cells upon treatment with methyl-2-PG, while PHGDH KD abolishes the methyl-2-PG-dependent decrease of the elevated 3-PG levels in H1299 PGAM1 KD cells. These data support our hypothesis that PGAM1 controls 2-PG levels to regulate PHGDH, which consequently regulates 3-PG levels by diverting 3-PG in serine biosynthesis. Furthermore, KD of PHGDH in PGAM1 stable KD cells reverses the methyl-2-PG treatment dependent rescue of oxidative PPP flux as well as biosynthesis of serine, lipids, and RNA. These data together suggest that, besides being a glycolytic metabolite, 2-PG may also signal through PHGDH to provide

regulation of PPP flux and anabolic biosynthesis, at least in part by regulating 3-PG levels (data courtesy of Taro Hitosugi; not shown).

PGAM1 enzyme activity strikes a balance between 3-PG and 2-PG levels, which coordinates glycolysis and biosynthesis to promote cancer cell proliferation.

To study the role of PGAM1 enzyme activity in cancer metabolism and tumor development, we screened and developed a small molecule inhibitor of PGAM1. Currently the only reported PGAM1 inhibitor is MJE3, which specifically inhibits PGAM1 activity exclusively in intact cells, probably by targeting the active site of PGAM1 with certain modifications *in vivo* (116-117). We designed a screening strategy using coupled PGAM1 and enolase assays and identified three lead small molecule compounds, including alizarin, as PGAM1 inhibitors from a library of 2,000 US Food and Drug Administration (FDA)-approved small molecule compounds (Figure 2.3.1A). We focused on 1,2-dihydroxyanthraquinone, commonly known as alizarin ($C_{14}H_8O_4$) (Figure 2.3.1B, top), which is an organic compound that is historically important as a prominent dye, originally derived from the roots of plants of the Madder genus. Treatment with alizarin results in decreased proliferation of human leukemia KG1a cells in a dose-dependent manner (Figures 2.3.1C and 2.3.1D).

We next identified alizarin red S (Figure 2.3.1B, middle) as a more potent PGAM1 inhibitor from a group of alizarin derivatives. We designed a group of alizarin red S derivatives by adding hydrophobic groups through a sulfonamide bond (Figure

2.3.1E). Among these compounds, we focused on PGAM1 inhibitor 004A (PGMI-004A) (Figure 2.3.1B, bottom), which, although less potent than red S in vitro, demonstrates enhanced potency to inhibit PGAM1 in leukemia KG1a cells compared to its parental compounds (2.3.1F). This may be due to the fact that PGMI-004A is more hydrophobic than alizarin and alizarin red S, which confers better cell permeability.

PGMI-004A inhibits PGAM1 with an IC_{50} of 13.1 μ M (Figure 2.3.1G) and the K_d value of the PGMI-004A-PGAM1 interaction was determined to be $7.2 \pm 0.7 \mu$ M from a fluorescence-based binding assay (Figure 2.3.1H). In a competitive binding assay where PGMI-004A was incubated with recombinant PGAM1 protein in the presence of different concentrations of PGAM1 substrate 3-PG, we found that increasing concentrations of 3-PG caused an increase in the fluorescence intensity from PGMI-004A-unbound form of PGAM1 in the presence of different concentrations of PGMI-004A, but not in the absence of PGMI-004A (Figure 2.3.1I). This suggests that PGMI-004A may allosterically modulate the enzyme activity of PGAM1. The K_i value was determined to be $3.91 \pm 2.50 \mu$ M using Dixon plot analysis (Figure 2.3.1J).

In addition, we performed a thermal melt shift assay to examine the interaction of protein (PGAM1) and ligand (PGMI-004A). Incubation of increasing concentrations of PGMI-004A raises PGAM1 melting temperature (T_m) in a dose-dependent manner, suggesting that PGMI-004A directly binds to the protein (Figure 2.3.1K). The K_d value for protein-ligand interaction was calculated to be $9.4 \pm 2.0 \mu$ M.

Together, these results suggest that PGMI-004A directly binds to PGAM1 and inhibits its enzyme activity.

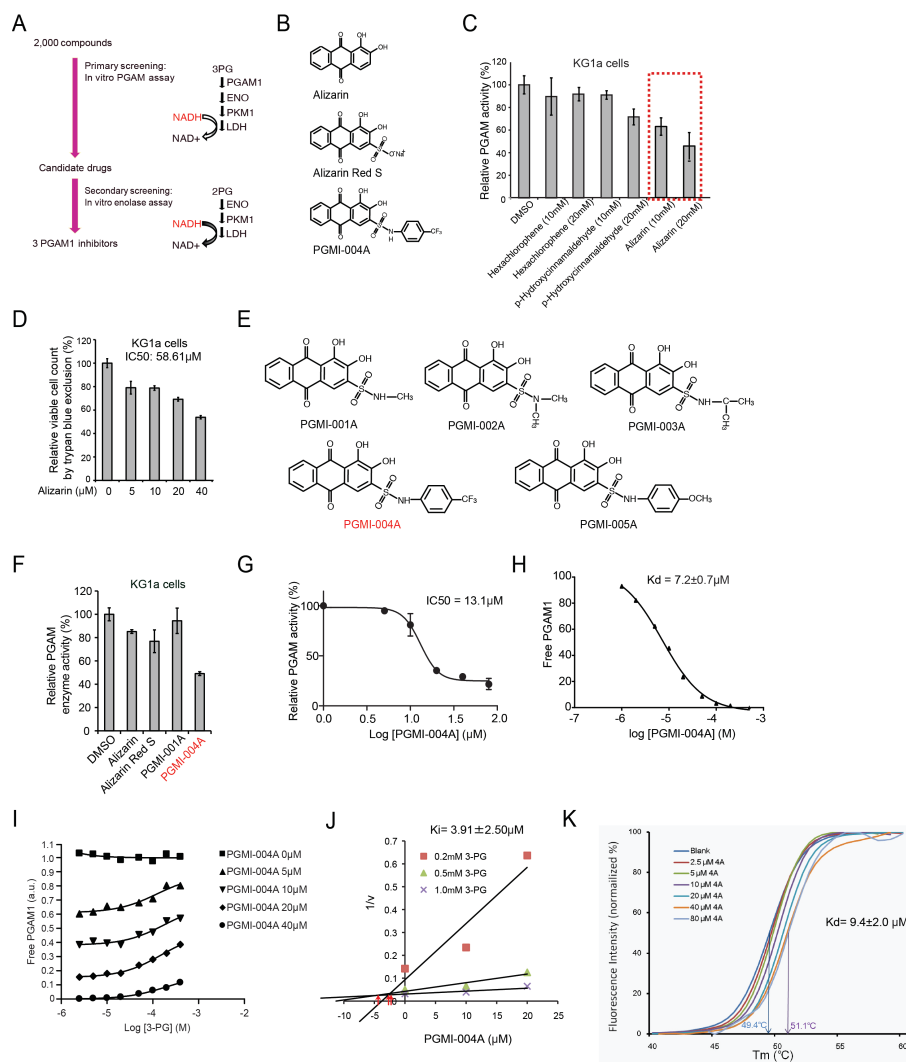


Figure 2.3.1. Identification and characterization of a small molecule PGAM1 inhibitor, PGMI-004A. (A) Schematic representation of the primary and secondary screening strategies to identify lead compounds as PGAM1 inhibitors. (B) Structure of alizarin and its derivatives alizarin red S and PGAM1 inhibitor (PGMI)-004A. (C) Inhibitory potency of different lead compounds including Alizarin, hexachlorophene and p-hydroxycinnamaldehyde in human leukemia KG1a cells. Cells were treated with individual compounds for 4h. (D) Cell viability of KG1a cells in the presence of increasing concentrations of Alizarin (72h). Cell viability was determined by trypan blue exclusion. (E) Chemical structures of specially designed derivatives of alizarin Red S, including PGMI- 001A to 5A. (F) PGMI-004A demonstrates more potent activity in regard to PGAM1 inhibition in KG1a cells compared to controls including alizarin, alizarin Red S and PGMI-001A (2h). (G) PGMI-004A inhibits PGAM1 with an IC₅₀ of 13.1 μM, which was determined by incubating purified human PGAM1 proteins with increasing concentrations of PGMI-004A. The error bars represent mean values ± SD from three replicates of each sample. (H) K_d value was determined as 7.2 ± 0.7 μM by incubating purified human PGAM1 proteins with increasing concentrations of PGMI-004A. The fluorescence intensity (Ex: 280 nm, Em: 350 nm) from tryptophan was measured. (I) Competitive binding assay of PGMI-004A with recombinant PGAM1 protein in the presence of increasing concentrations of PGAM1 substrate 3-PG. Increased free PGAM1 was determined by an increase in fluorescence intensity. (J) Dixon plot analysis of PGAM1 enzyme assay in the presence of different concentrations of PGMI-004A and 3-PG. (K) Thermal shift melting curves of PGAM1 and PGMI-004A. Thermal shift assay was performed to examine the protein (PGAM1) and “ligand” (inhibitor PGMI- 004A) interaction.

We found that inhibition of PGAM1 activity by PGMI-004A treatment results in decreased 2-PG and increased 3-PG levels in H1299 cells, which could be rescued by treatment with methyl-2-PG. Moreover, treatment with PGMI-004A results in significantly reduced lactate production that was rescued by methyl-2-PG treatment, but has no significant effect on intracellular ATP levels. In consonance with these observations, the rescued lactate production due to methyl-2-PG treatment was abolished when enolase was knocked down or inhibited by specific inhibitor NaF in PGMI-004A treated cells. These results also suggest that rescued 2-PG derived from methyl-2-PG is metabolized by cells to restore the decreased glycolysis due to PGAM1 inhibition in cancer cells. We also found that PGMI-004A treatment results in decreased oxidative PPP flux and NADPH/NADP⁺ ratio, as well as reduced biosynthesis of lipids and RNA and cell proliferation in H1299 cells. These phenotypes are similar to those observed in PGAM1 KD cells, which could be significantly rescued by treatment with methyl-2-PG, suggesting that PGMI-004A targets PGAM1 to inhibit cancer cell metabolism and proliferation (data not shown).

In addition, we observed that PGMI-004A treatment results in decreased cell proliferation of diverse leukemia cells (Figure 3.3.1A,B), but not control human dermal fibroblasts (HDF), human foreskin fibroblasts (HFF), human HaCaT keratinocyte cells and human melanocyte PIG1 cells (Figure 3.3.1C-F), suggesting minimal non-specific toxicity of PGMI-004A in normal, proliferating human cells.

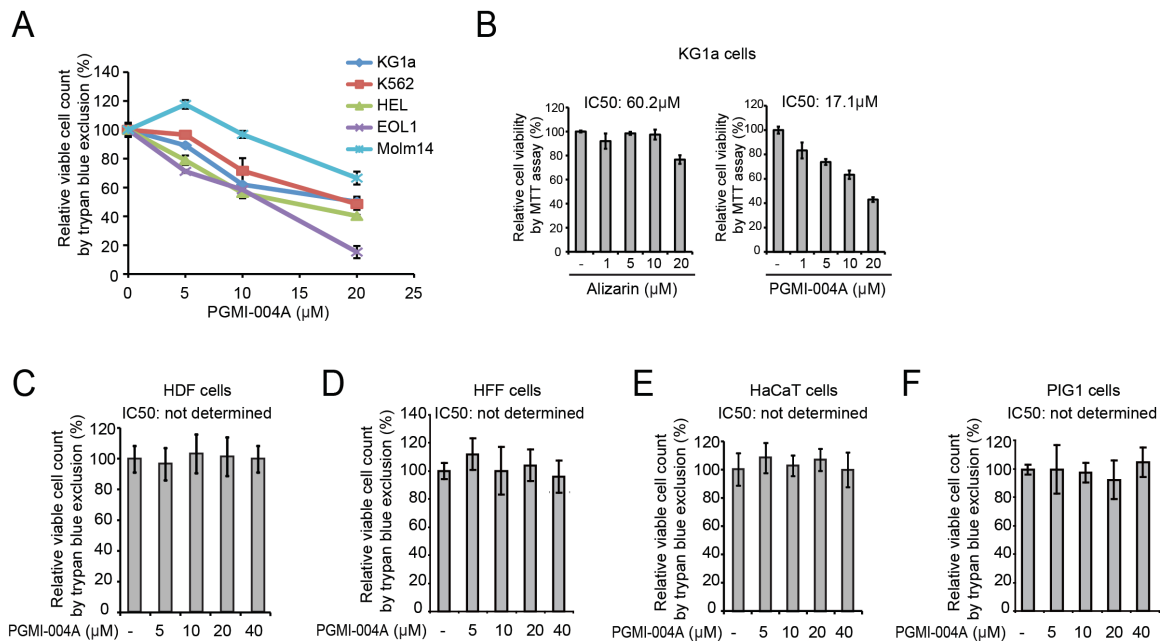


Figure 3.3.1. Inhibition of PGAM1 by PGMI-004A decreases viability of diverse leukemia cells but not normal, proliferating human cells. (A-B) Cell viability of diverse human leukemia cells (C-F) and control HDF, HFF, HaCaT, and PIG1 cells in the presence of increasing concentrations of PGMI-004A. Cell viability was determined by trypan blue exclusion or MTT assay. The error bars represent mean values \pm SD from three replicates of each sample. IC₅₀ values were determined; NR=not reached.

Targeting PGAM1 by PGMI-004A treatment inhibits cancer cell proliferation and tumor growth and alters 3-PG and 2-PG levels in primary leukemia cells from patients, leading to attenuated leukemia cell proliferation.

We next performed an *in vivo* drug treatment experiment. Initial toxicity studies by chronic injection of PGMI-004A to nude mice for 4 weeks revealed that 100 mg/kg/day administered intraperitoneally is a well-tolerated dose. In addition, continuous treatment with PGMI-004A (100 mg/kg/day) for 7 days did not result in significant alteration in body weight, complete blood cell counts, or hematopoietic properties of nude mice (Figure 4.3.1A). Histopathologic analyses revealed that no notable differences between the vehicle-treated and PGMI-004A-treated groups were evident (Figures 4.3.1B).

A

Test Name	Normal range	DMSO (mean)	100 mg/kg/day PGMI-004A (mean)
WBC (x 10 ³ /μL)	2.6-10.1	7.85 ± 5.44	7.95 ± 1.45
LYM (x 10 ³ /μL)	1.3-8.4	5.00 ± 2.68	5.65 ± 1.40
MONO (x 10 ³ /μL)	0-0.3	0.60 ± 0.70	0.75 ± 0.58
GRAN (x 10 ³ /μL)	0.4-2	2.25 ± 2.05	1.55 ± 0.58
HCT (%)	32.8-48	29.45 ± 17.04	45.05 ± 5.69
MCV (fl)	42.3-55.9	55.10 ± 3.25	55.35 ± 4.70
RDW _a (%)	0-99.9	37.35 ± 0.91	37.05 ± 2.38
HGB (g/dl)	10-16.1	10.10 ± 5.79	12.8 ± 2.08
MCHC (g/dl)	29.5-35.1	34.55 ± 0.35	28.80 ± 4.04
RBC (x 10 ⁶ /μL)	6.5-10.1	5.46 ± 3.41	8.13 ± 1.40
MCH (pg)	13.7-18.1	19.05 ± 1.34	15.85 ± 1.17
PLT (x 10 ³ /μL)	250-1540	363.00 ± 128.69	450.50 ± 237.30
MPV (fl)	0-99.9	7.70 ± 1.27	6.10 ± 0.15

B

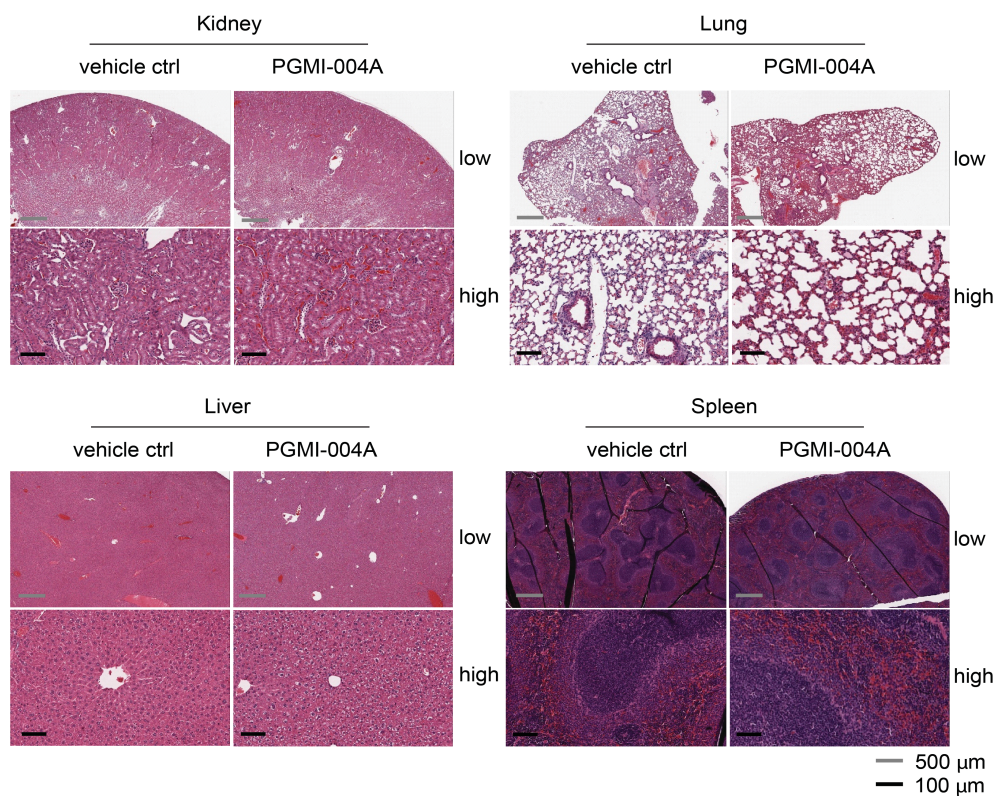


Figure 4.3.1. Chronic PGMI-004A treatment causes no off-target toxicity in nude mice. (A) Athymic nude mouse hematology. Nude mice (n=3) were treated with either vehicle control or PGMI-004A for 7 days. CBC analysis shows no significant difference in the hematopoietic properties between the two groups of mice. (B) Histological morphology of hematoxylin-eosin stained tissue sections of representative nude mice in PGMI-004A or vehicle control-treated groups. Nude mice were treated daily with PGMI-004A (100 mg/kg/day) intraperitoneally for 7 days. PB samples were collected and applied for analysis of hematological properties (A). The vital organs were collected for histopathological analysis. Histopathologic tissue sections (kidney, lung, liver and spleen) from representative nude mice stained with hematoxylin-eosin did not reveal significant differences between the vehicle and PGMI-004A treated groups. Images were analyzed and captured using ImageScope software (Aperio Technologies Inc.) without any additional or subsequent image processing (high power images are 20x; low power images are either 4.0x, 4.2x, or 4.4x). Scale bars are indicated.

We performed xenograft experiments by injecting H1299 cells into nude mice as described (57). Six days post-injection, mice were divided into two groups (n = 8/group) and treated with either PGMI-004A (100 mg/kg/day) or vehicle for 21 days. We found that PGMI-004A treatment results in significantly decreased tumor growth and size in treated mice compared with mice receiving vehicle control (Figures 5.3.1A-D). Moreover, treatment with PGMI-004A effectively inhibits PGAM1 enzyme activity in tumors *in vivo* in resected tumors from xenograft nude mice (Figure 5.3.1E). These combined data suggest that targeting PGAM1 by PGMI-004A inhibits PGAM1 *in vivo*, and that this inhibition causes specific toxicity to tumor cells.

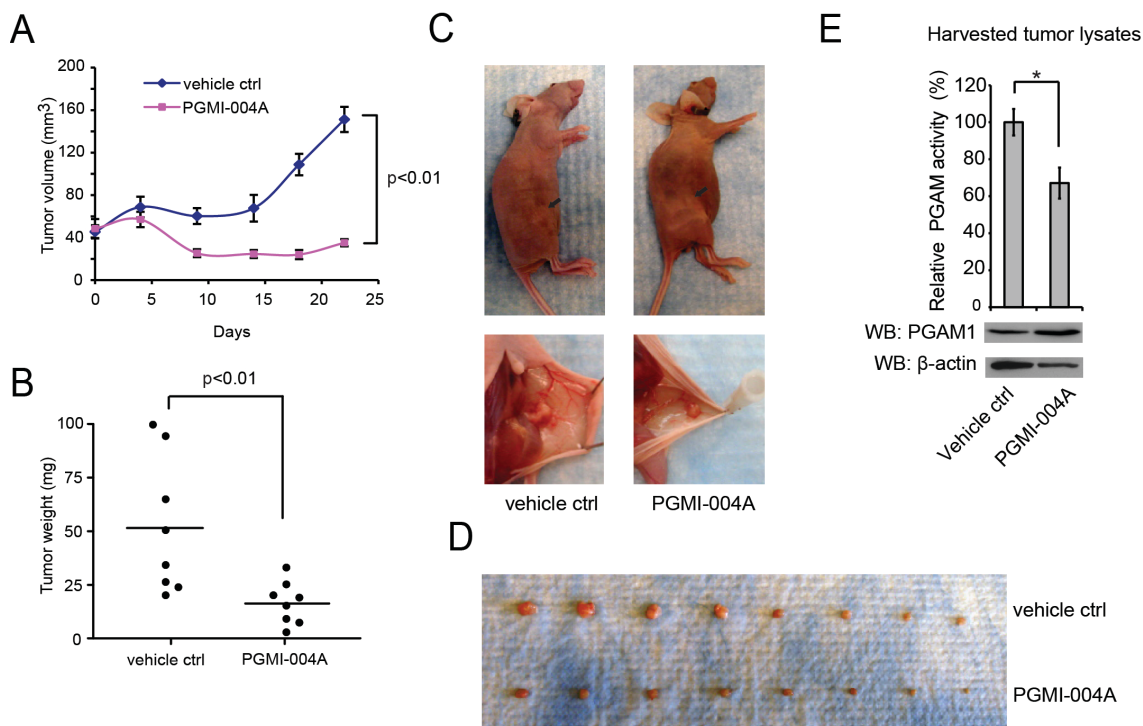


Figure 5.3.1. PGMI-004A treatment results in attenuated tumor growth in xenograft nude mice *in vivo*. (A and B) Tumor growth (A) and tumor size (B) in xenograft nude mice injected with H1299 cells were compared between the group of mice treated with PGMI-004A and the control group treated with vehicle control. P values were determined by a two-tailed Student's *t* test. (C) Dissected tumors (indicated by arrows) in representative nude mice treated with vehicle control or PGMI-004A are shown. (D) Tumors from two groups of xenograft nude mice treated with either vehicle control or PGMI-004A are shown. (E) Treatment with PGMI-004A effectively inhibits PGAM1 enzyme activity *in vivo* in resected tumors from xenograft nude mice. p values were determined by two-tailed Student's *t* test (*0.01 < p < 0.05).

We found that PGAM1 protein expression and enzyme activity levels are commonly upregulated in primary leukemia cells from diverse patients with AML, CML, or B-cell ALL (B-ALL; n = 12) compared to control PB cells from healthy donors (n = 4) (Figure 6.3.1A), suggesting that PGAM1 is an attractive anti-leukemia target. We next found that, consistent with our observations in cancer cell lines, inhibiting PGAM1 by PGMI-004A treatment results in increased 3-PG and decreased 2-PG levels in primary leukemia cells from a representative patient with AML (data not shown). PGMI-004A treatment also results in decreased cell viability and reduced PGAM1 activity and lactate production in the samples from seven (one CML and six AML) out of eight patients with leukemia (representatives shown in Figure 6.3.1B). Moreover, methyl-2-PG treatment rescues the decreased cell viability and lactate production in primary leukemia cells from representative patients with AML (data not shown). In addition, PGMI-004A treatment did not affect cell viability of mononucleocytes in PB samples from two healthy human donors (Figure 6.3.1C) and CD34+ cells isolated from bone marrow samples from four healthy donors (Figures 6.3.1D), suggesting promising anticancer potential of PGMI-004A with minimal toxicity to human blood cells. These combined results of translational studies suggest that PGAM1 is a promising therapeutic target in the treatment of human malignancies, including both myeloid and lymphoid leukemias.

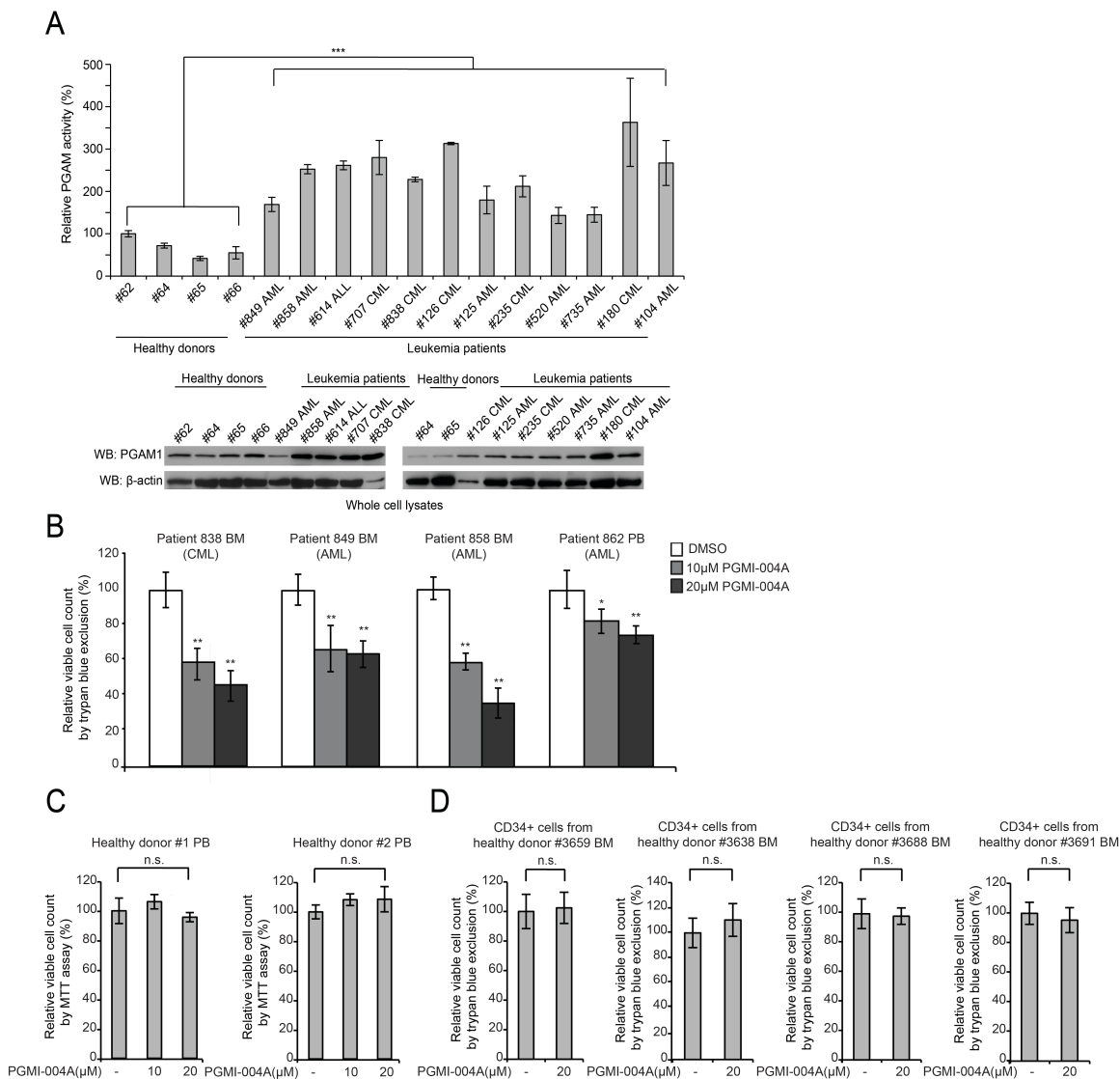


Figure 6.3.1. PGMI-004A treatment results in reduced cell proliferation of primary leukemia cells from patients, but not hematopoietic cells from healthy human donors. (A) PGAM1 protein expression (lower) and enzyme activity (upper) levels were examined using primary leukemia cells from diverse human patients with AML, CML, or B-ALL and compared to control PB cells from healthy donors. (B) Effect of PGMI-004A treatment on cell viability on human primary leukemia cells from a representative patients with CML and AML. (C and D) PGMI-004A shows no toxicity in treatment (120 hr) of PB cells (C) and CD34+ cells isolated from bone marrow samples (D) from representative healthy human donors. The error bars represent mean values \pm SD from three replicates of each sample. p values were determined by two-tailed Student's *t* test (* $0.01 < p < 0.05$; ** $0.001 < p < 0.01$; *** $p < 0.001$; ns, not significant).

3.1.4 Discussion

Our findings suggest that upregulation of PGAM1 by increased gene expression in cancer cells provides a metabolic advantage to cancer cell proliferation and tumor growth; PGAM1 coordinates glycolysis and anabolic biosynthesis, at least in part by controlling intracellular levels of its substrate 3-PG and product 2-PG. Our results revealed a molecular mechanism by which 3-PG inhibits 6PGD by directly binding to the active site of 6PGD and competing with its substrate 6-PG. Attenuation of PGAM1 results in abnormal accumulation of 3-PG, which in turn inhibits 6PGD and consequently the oxidative PPP and anabolic biosynthesis. Moreover, our findings suggest that PGAM1 controls the intracellular levels of its substrate 3-PG not only directly through substrate consumption, but also indirectly by controlling levels of its product 2-PG. Physiologic concentrations of 2-PG promote the enzyme activity of PHGDH, which converts 3-PG to pPYR, reducing the cellular 3-PG levels.

Upon attenuation of PGAM1, 2-PG is decreased to levels below the physiologic concentrations, leading to decreased PHGDH activity, which facilitates 3-PG accumulation. This represents a regulatory mechanism by which 2-PG activates PHGDH to provide feedback control of 3-PG levels. Thus, we suggest that PGAM1 activity is upregulated in cancer cells to promote glycolysis and keep the intracellular 3-PG levels low, which in turn permits high levels of the PPP and biosynthesis to facilitate rapid cell division and tumor growth (Figure 7.3.1). This is consistent with previous report that expression of TP53 suppresses oxidative PPP in

cancer cells (118). In addition, PGAM1 may also be responsible for maintaining the physiological levels of 2-PG to sustain PHGDH activity, which diverts 3-PG from glycolysis to serine synthesis and contributes to maintaining relatively low levels of 3-PG in cancer cells.

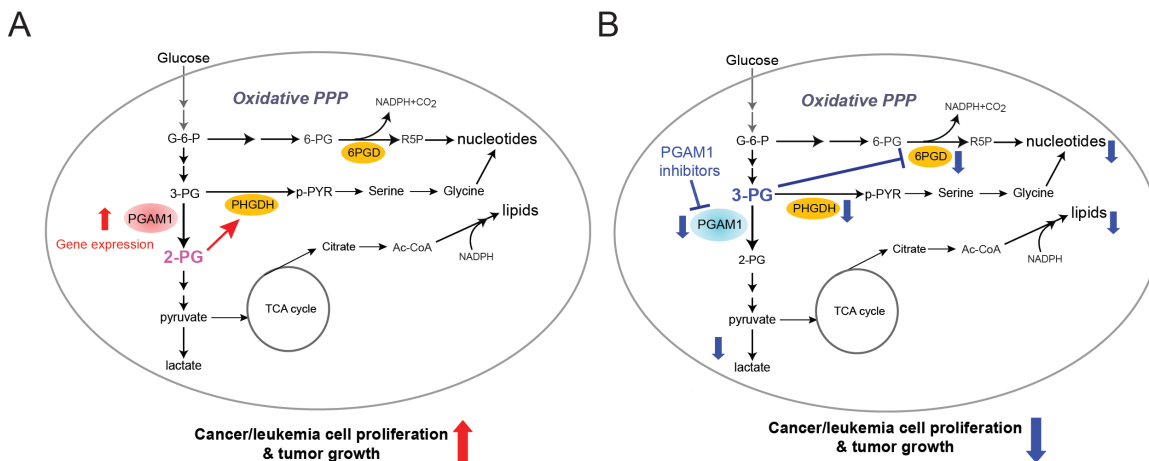


Figure 7.3.1. Proposed model: role of PGAM1 in cancer cell metabolism. (A) PGAM1 activity is upregulated in cancer cells to promote glycolysis and keep the intracellular 3-PG levels low, which in turn permits high levels of the PPP and biosynthesis to fulfill the request of rapidly growing tumors. PGAM1 also maintains the physiologic levels of 2-PG to sustain PHGDH activity, which diverts 3-PG from glycolysis to serine synthesis and contributes to maintaining relatively low levels of 3-PG in cancer cells. These effects in concert provide a metabolic advantage to cancer cell proliferation and tumor growth. (B) When PGAM1 is inhibited by shRNA or small molecule PGAM1 inhibitor PGMI-004A, 3-PG levels are elevated, which in turn inhibit 6PGD and consequently the oxidative PPP and anabolic biosynthesis. At the same time, 2-PG is decreased to levels below the physiologic concentrations, leading to decreased PHGDH activity, which facilitates 3-PG accumulation. Such metabolic changes result in attenuated cell proliferation and tumor development.

Inhibition of PGAM1 by shRNA or treatment with a small molecule inhibitor PGMI-004A results in altered glycolysis and anabolic biosynthesis, and reduced cancer cell proliferation and tumor growth. Interestingly, targeting PGAM1 does not significantly affect intracellular ATP levels. Decreased ATP production due to attenuated glycolysis in PGAM1 KD cells may be compensated by alternative mechanisms other than mitochondrial oxidative phosphorylation, or perhaps the ATP consumption in PGAM1 KD cells is decreased accordingly. Methyl-2-PG treatment rescues most of the aforementioned phenotypes. Rescued 2-PG levels in cells with attenuated PGAM1 reversed decreased lactate production by rescuing the glycolytic process downstream of PGAM1, as well as reduced oxidative PPP flux and biosynthesis of RNA and lipids, at least in part by decreasing elevated 3-PG levels. However, methyl-2-PG treatment only partially rescues the attenuated cell proliferation in PGAM1 KD cells or cells treated with PGMI-004A. This result suggests that PGAM1 may contribute to cell proliferation in both 2-PG-dependent and -independent manners.

The current understanding of the connection between glycolysis and PPP/biosynthesis is based on a model in which glycolytic intermediates can be diverted into PPP and biosynthesis pathways as precursors. Our results show that the concentrations of glycolytic metabolites such as 3-PG and 2-PG can directly affect the catalytic activity of enzymes involved in PPP and biosynthesis, which represents an additional link between glycolysis, PPP, and biosynthesis. Metabolites have been suggested to function as signaling molecules in the past. Examples

include AMP, which is an allosteric activator for adenine monophosphate-activated protein kinase (AMPK), a kinase that senses intracellular energy levels (ATP/AMP ratio) (119), and glutamine, which activates leucine uptake, leading to mTOR activation (120). We found that the cellular levels of 3-PG and 2-PG, two key intermediates in glycolysis, have additional regulatory impact on metabolic enzymes to affect cell metabolism and consequently proliferation, which provides an example to suggest that glycolytic metabolites could also serve as signaling molecules to control cell metabolism and cellular responses. Moreover, our findings also describe a feedback mechanism by which the product levels (2-PG) of a metabolic enzyme (PGAM1) can regulate its substrate levels (3-PG) by affecting an alternative enzyme (PHGDH) that is involved in production of this substrate. Thus, this study showcases the complexity of cellular metabolism, demonstrating that control of the intracellular levels of a particular metabolite may involve diverse enzymes in different metabolic reactions, such that the balance of the intracellular levels of various metabolites may exert regulatory functions on enzymes in different pathways to control cellular metabolism. Such a mechanism can be explored for anti-cancer therapies.

Previous reports describe that targeting PGAM1 by a PGAM1-derived inhibitory peptide or PGAM inhibitor MJE3 attenuates cancer cell proliferation (116, 121). In consonance with these observations, our studies suggest that protein expression and enzyme activity levels of PGAM1 are important for cancer cell proliferation and tumor growth. Our compound PGMI-004A exhibits promising efficacy in the

treatment of xenograft nude mice *in vivo* with minimal toxicity, as well as in diverse human cancer cells and primary leukemia cells from human patients *in vitro* with no obvious off-target effect and minimal toxicity to normal human hematopoietic cells. These translational studies provide “proof of principle” to suggest anti-PGAM1 as a promising therapy in clinical treatment of tumors that heavily rely on the Warburg effect, including both lymphoid and myeloid leukemias. However, it is important to note that the potential toxicity of PGAM inhibitors *in vivo* to normal post-mitotic, metabolically active organs such as brain, liver, skeletal muscle, and heart, all of which are glycolytic, remains undetermined. This warrants further detailed toxicity and pharmacokinetics studies to improve the proposed anti-PGAM1 therapy in leukemia treatment.

3.2. Signaling and targeting of 6-phosphogluconate dehydrogenase in human leukemia

3.2.1. Introduction

As previously discussed, cancer cells display exquisite coordination of bioenergetic and anabolic biosynthetic pathways to promote cell proliferation and tumor growth. Our PGAM1 studies revealed that an integral component of this coordination involves the control of intracellular metabolite levels, which can in turn function as signaling molecules to regulate distal metabolic pathways. Our results revealed a molecular mechanism by which 3-PG inhibits 6PGD in the oxidative PPP by directly binding to the active site of 6PGD and competing with its substrate 6-PG. When PGAM1 is attenuated, 3-PG accumulates and functions to inhibit 6PGD and consequently the oxidative PPP and anabolic biosynthesis. These results suggest that 6PGD may also represent an attractive, and perhaps more direct anti-cancer target.

6PGD is the third enzyme in the oxidative PPP, which catalyzes the decarboxylating reduction of 6-PG to Ru-5-P and concomitantly produces NADPH. 6PGD functions as a homodimer in which each monomer acts independently (122). NADPH is the most crucial metabolite produced in the oxidative PPP by both 6PGD and the first enzyme in the oxidative PPP, G6PD. Increased 6PGD activity has been reported in many cancers, including colorectal cancers (123), cervical intraepithelial neoplasia (124-

125) and thyroid tumors (126). In addition, 6PGD activity has been documented as a reliable prognostic biomarker in primary breast cancer (127). However, how 6PGD is activated in human cancers and whether 6PGD activity is important for cancer pathogenesis and tumor development remain unknown.

In this work, we found that acetylation at K76 and K294 enhances 6PGD activation and is commonly observed in diverse human cancer cells. Moreover, we show that in addition to its crucial role in providing building blocks for nucleotide biosynthesis and NADPH to quench ROS, 6PGD controls intracellular concentrations of its product Ru-5-P to inhibit liver kinase B1 (LKB1)-AMPK signaling and subsequently activate lipogenesis, providing novel crosstalk between metabolic pathways and cell signaling networks. Furthermore, we demonstrate that both protein expression and lysine acetylation levels of 6PGD are important for cancer cell proliferation and tumor growth. Thus, we identified and developed selective small molecule 6PGD inhibitors, Physcion and its derivative S3, which demonstrate promising efficacy and minimal non-specific toxicity in inhibition of cell proliferative and tumor development potential of human cancer cells *in vitro* and *in vivo*, respectively, as well as in treatment of human primary leukemia cells from leukemia patients. These translational and pre-clinical studies provide “proof-of-principle” to suggest that 6PGD is an attractive anti-leukemia target.

3.2.2. Materials and methods

Reagents. Stable KD of endogenous h6PGD was achieved using lentiviral vector harboring shRNA construct (Open Biosystems; 5'-CCGGGTGGATGATTTTCATCGAGAACTCGAGTTTCTCGATGAAATCATCCACTTTTT -3'). The shRNA is designed to target the 3' non-coding region of h6PGD-A mRNA and shows no effect on the plasmid directed expression of 6PGD cDNA in cells. 6PGD rescue H1299 cell lines were generated as previously described (57-61) using Flag-tagged human 6PGD WT, K76R, K294R, K76/294R, K76Q, K294Q and K76/294Q in retroviral vector pLHCX (Clontech). Antibodies against pan K-Ac, 6PGD K76-Ac, and 6PGD K294-Ac were from Cell Signaling Technology (CST); antibody against 6PGD was from Novus; antibody against β -actin was from Sigma; predilute Ki67 antibody was from Invitrogen. Trichostatin A (TSA), Nicotinamide (NAM), and N-Acetyl-L-cysteine (NAC) were purchased from Sigma. Phycion was purchased from Santa Cruz Biotechnology. 1-hydroxy-8-methoxy-anthraquinone (S3) was purchased Sigma. Compound C was purchased from EMD Millipore.

Cell culture. H1299, A549, H322, H157, HEL, KG1a, Molm14, Mo91, EOL1, and K562 cells were cultured in RPMI 1640 medium with 10% FBS. 293T, MDA-MB231, MCF7, HFF, and HaCaT cells were cultured in Dulbecco Modified Eagle Medium (DMEM) with 10% FBS. 212LN and Tu212 cells were cultured in DMEM/F12 medium with 10% FBS. HDF cells were cultured in FibroLife medium. PIG1 cells were cultured in

Medium 254. NAM+TSA treatment was performed by incubating cells with 10 mM NAM and 5 μ M TSA for 16 hours.

Purification of r6PGD. (His)₆-tagged 6PGD proteins were purified by sonication of high expressing BL21(DE3)pLysS cells obtained from a 250 mL culture subjected to IPTG-induction for 14 hours. Cell lysates were resulted by centrifugations and loaded onto a Ni-NTA column in 20mM imidazole. After washing twice, the protein was eluted with 250 mM imidazole. Proteins were desalted on a PD-10 column and the purification efficiency was examined by Coomassie staining and western blotting.

G6PD and 6PGD assays. G6PD activity was determined by the NADPH production rate from G6PD and 6PGD, then subtracting that of 6PGD, since a product of G6PD, 6-phosphogluconolactone, is rapidly hydrolyzed to a substrate of 6PGD, 6-phosphogluconate, in cells. To obtain the combined dehydrogenase activity, substrates for both dehydrogenase enzymes were added to a cuvette. In another cuvette, substrates for the second enzyme, 6PGD, were added to obtain the activity of this enzyme. Substrate concentrations were as follows: 0.2 mM glucose 6-phosphate, 0.2 mM 6-phosphogluconate, and 0.1 mM NADP⁺. 10 μ g of cell lysates or 1 μ g of recombinant protein was added to a cuvette containing buffer (50 mM Tris/1 mM MgCl₂, pH 8.1) and the reaction was then initiated by NADP⁺. The increase in 341 nm absorbance (OD₃₄₀) as a measure of NADPH production was

measured every 20 seconds for 10 minutes on a DU800 Spectrophotometer (Beckman Coulter).

Cell proliferation and viability assays. Cell proliferation assays were performed by seeding 5×10^4 cells in a 6-well plate and culturing the cells at 37°C in normoxia (5% CO₂ and 95% air). Twenty-four hours after seeding, cells that were used for further culture under hypoxia were cultured at 37°C in a sealed hypoxia chamber filled with 1% O₂, 5% CO₂, and 94% N₂. Cell proliferation was determined by cell numbers recorded at 48 and 96 hours after being seeded, and normalized to that of each of the cell lines at the starting time (T=0 hr). For cell viability assays, 5×10^6 cells were seeded in 6-well plates and incubated with increasing concentrations of Physcion or S3 at 37°C for indicated times. Relative cell viability at each experimental time point up to 72 hours was determined using either CellTiter96Aqueous One solution proliferation kit (Promega), or by trypan blue exclusion using a TC10 Automated Cell Counter (BioRad).

Apoptosis assay. 1×10^5 cells were treated with increasing concentrations of Physcion or S3 for up to 48 hours, then collected and stained using FITC-conjugated annexin V labeling reagent (BD Pharmingen) and PI (Sigma) followed by FACS analysis for apoptotic cell population.

Drug screening: *In vitro* 6PGD assays. We performed *in vitro* 6PGD enzyme assay to screen 2000 biologically active compounds (The Spectrum Collection;

MicroSource). In brief, 0.2 mM 6-phosphogluconate was added to assay buffer containing 50 mM Tris (pH 8.1), 1 mM MgCl₂, 0.1 mM NADP⁺, 0.5 μg r6PGD, and 10 μM drug. The increase in absorbance at 341 nm was measured using a SpectraMax Plus spectrophotometer (Molecular Devices)

Drug binding assay. 1 μg r6PGD was incubated with different concentrations of Physcion or S3 (0-80μM), and Tryptophan fluorescence (ex: 280nm, em: 350nm) from r6PGD was measured in 100 mM Tris-HCl buffer. Relative fluorescence intensity without any treatment is presented as 100%.

Xenograft studies. Approval of use of mice and designed experiments was given by the Institutional Animal Care and Use Committee of Emory University. Nude mice (nu/nu, male 4–6-week-old, Harlan Laboratories) were subcutaneously injected with 20 x 10⁶ H1299 cells or 5 x 10⁶ K562 cells harboring empty vector on the left flank, and cells with stable KD of endogenous h6PGD on the right flank, or with 20 x 10⁶ H1299 cells stably expressing h6PGD WT and K76R or K294R with stable KD of endogenous h6PGD on the *left* and *right* flanks, respectively. Tumor growth was recorded by measurement of two perpendicular diameters using the formula $4\pi/3 \times (\text{width}/2)^2 \times (\text{length}/2)$. The tumors were harvested and weighed at the experimental endpoint, and the masses of tumors (g) derived from cells with and without stable KD of endogenous h6PGD, or from cells expressing h6PGD WT and K76R or K294R mutant were compared. Statistical analyses have been done by comparison in relation to the control group with a two-tailed paired Student's *t* test.

For drug evaluation of S3 using xenograft mice, the drug was administered by daily intraperitoneal injection at a dose of 20 mg/kg from 10 days after subcutaneous injection of 20×10^6 H1299 cells on *right* flank of each mouse, or 3 days after subcutaneous injection of 7×10^6 K562 cells on the *right* flank of each mouse. Tumor growth was recorded by measurement of two perpendicular diameters using the formula $4\pi/3 \times (\text{width}/2)^2 \times (\text{length}/2)$. The tumors were harvested and weighed at the experimental endpoint, and the masses of tumors (g) treated with vehicle control (DMSO) and S3 were compared by a two-tailed unpaired Student's *t* test.

Histopathology and complete blood counts. For histopathological analysis, sections of mouse tissue were stained with hematoxylin and eosin and slides were digitally scanned at 20X magnification using a ScanScope XT from Aperio Technologies Inc. Images were analyzed and captured using ImageScope software (Aperio Technologies Inc) without any additional or subsequent image processing. For complete blood counts, blood was collected retro-orbitally and immediately applied to a HemaVet 950FS (Drew Scientific) for generation of complete hematology profile.

Immunohistochemical staining. Resected tumors from xenograft mice were fixed in 10% buffered formalin, embedded in paraffin and mounted on slides. After deparaffinization and rehydration, mouse tumor sections were incubated in 3% hydrogen peroxide to suppress endogenous peroxidase activity. Antigen retrieval was achieved by microwaving the sections in 10 mM Sodium citrate (pH 6.0).

Sections were then blocked by incubation in 2.5% horse serum. Human predilute Ki67 antibody (Invitrogen) was applied for 1 hour at room temperature. Detection was achieved with the Avidin-Biotin Complex System (Vector Laboratories). Slides were stained with 3,3'-diaminobenzidine, washed, counterstained with hematoxylin, dehydrated, treated with xylene, and mounted.

Primary tissue samples from patients with leukemia and healthy donors.

Approval of use of human specimens was given by the Institutional Review Board of Emory University School of Medicine. All clinical samples were obtained with informed consent with approval by the Emory University Institutional Review Board. Clinical information for the patients was obtained from the pathologic files at Emory University Hospital under the guidelines and with approval from the Institutional Review Board of Emory University School of Medicine and according to the Health Insurance Portability and Accountability Act. Only samples from patients that were not previously treated with chemotherapy or radiation therapy were used. Mononuclear cells were isolated from PB and bone marrow samples from patients with leukemia or from healthy donors using lymphocyte separation medium (Cellgro). Cells were cultured in RPMI 1640 medium supplemented with 10% FBS and penicillin/streptomycin and incubated with increasing concentrations of Physcion or S3 for up to 72 hours.

3.2.3. Results

K76 and K294 acetylation activate 6PGD via distinct mechanisms.

Previous studies in our lab have demonstrated that post-translational modifications regulate the activity of many metabolic enzymes, including PKM2 (57), LDHA (58), PDHK1 (59), and PGAM1 (60). Because our proteomics-based study identified 6PGD as acetylated at a group of lysine residues in human cancer cells, we began by examining the effect of lysine acetylation on 6PGD activity. We found that treatment of diverse human cancer cells with two compounds that lead to global lysine acetylation increase in cells, Sirtuin deacetylase (SIRT) inhibitor NAM and histone deacetylase (HDAC) inhibitor TSA, resulted in increased lysine acetylation levels and enzyme activity of 6PGD. These results suggest that lysine acetylation commonly activates 6PGD in human cancer cells.

We next performed mutational analysis and generated diverse acetyl-deficient (K→R) mutants of 6PGD to replace each of the seven lysine residues of 6PGD that were identified as acetylated in human cancer cells. We identified K76 and K294 as major acetylation sites responsible for regulating 6PGD enzyme activity, and determined that each activates 6PGD via distinct mechanisms. Through structural analysis followed by confirmatory studies, we found that K76 and K294 acetylation contribute to 6PGD activation by promoting cofactor NADP⁺ binding and the formation of active 6PGD homodimers, respectively.

Moreover, we performed 6PGD enzyme assay-based shRNA screening studies to identify putative upstream acetyltransferases and deacetylases of 6PGD, and identified dihydrolipoamide S-acetyltransferase (DLAT) as responsible for acetylating 6PGD at K76, and acetyl-CoA acetyltransferase 2 (ACAT2) as responsible for acetylating 6PGD at K294, while HDAC4 was found to deacetylate both lysine sites (data courtesy of Changliang Shan; not shown).

Lysine acetylation of 6PGD is common in human cancer cells.

We next examined whether lysine acetylation of 6PGD can be commonly detected in cancer cells, and found that indeed, K76 and K294 acetylation levels were upregulated in the majority of human cancer cell lines tested. Leukemia cells including HEL, KG1a, Molm14, Mo91, EOL1 and K562 (Figure 1.3.2A), and solid tumor cells including A549 and H1299 lung cancer, MDA-MB-231 breast and Tu212 head and neck cancer (Figure 1.3.2B). all demonstrated increased levels of 6PGD lysine acetylation compared to normal proliferating human cells including HaCaT keratinocyte cells and human foreskin fibroblasts (HFF), whereas MCF-7 breast cancer and 212LN head and neck cancer cells (Figure 1.3.2B) have similar lysine acetylation levels of 6PGD compared to control HaCaT and HFF cells.

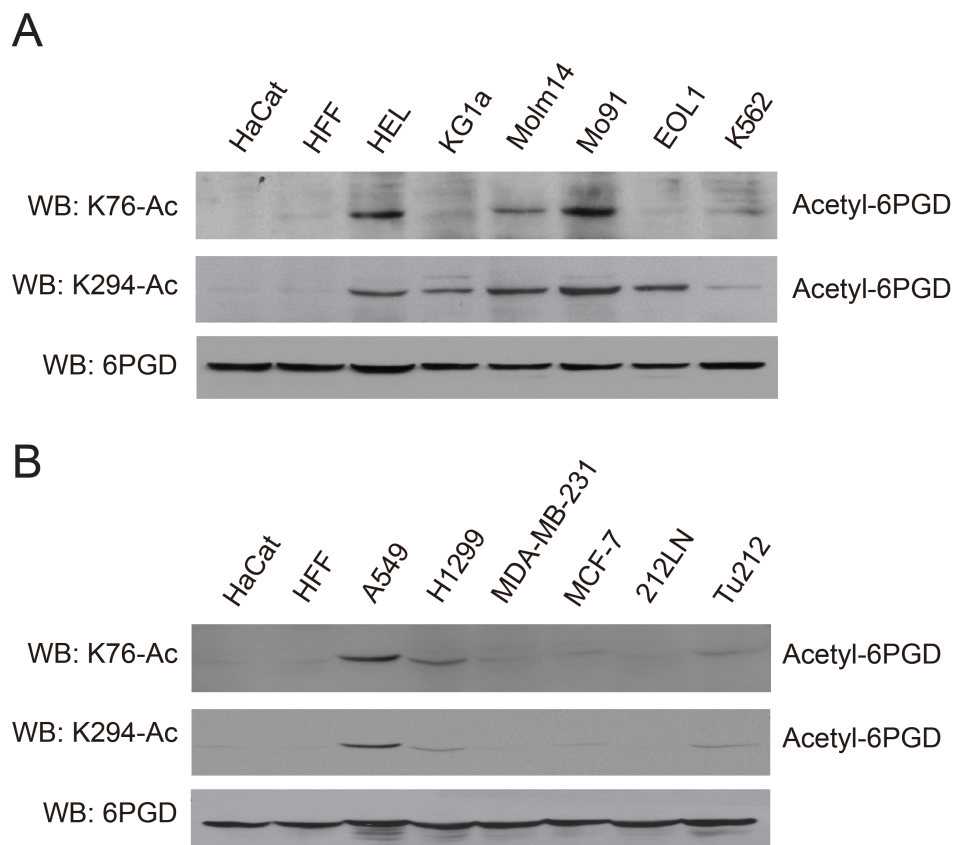


Figure 1.3.2. 6PGD is lysine acetylated in diverse human leukemia and solid tumor cell lines. Western blot results showing acetylation levels of K76 and K294 using specific acetyl-6PGD antibodies, K76-Ac and K294-Ac, respectively, in diverse human leukemia (A) and solid tumor (B) cell lines. Normal proliferating human HaCaT keratinocyte cells and HFF cells were included as controls.

To examine whether K76 and K294 acetylation-dependent activation of 6PGD is important for cancer cell proliferation, we first generated and examined a group of human tumor/leukemia cells with stable KD of 6PGD. We found that 6PGD KD results in decreased cell proliferation, while rescue expression of FLAG-6PGD WT, but not acetyl-deficient K76R, K294R or K76/294R mutants, rescued the decreased 6PGD enzyme activity and cell proliferation in 6PGD KD cells. These results suggest that acetylation at either K76 or K294 of 6PGD itself is sufficient and important for the enhanced 6PGD activity that provides a proliferative advantage to cancer cells. We also found that inhibition of 6PGD by shRNA or disruption of lysine acetylation in cancer cells results in reduced oxidative PPP flux, decreased NADPH/NADP⁺ ratio, decreased intracellular level of 6PGD product Ru-5-P and subsequently decreased intracellular levels of R-5-P compared to control parental cells. Together these defects in oxidative PPP result in decreased RNA biosynthesis (data courtesy of Changliang Shan; not shown).

6PGD promotes lipogenesis by controlling intracellular Ru-5-P levels to inhibit LKB1-AMPK signal pathway.

In addition to the predicted defects in the oxidative PPP and RNA biosynthesis upon 6PGD attenuation, we also found that 6PGD KD cells and distinct rescue cells expressing K76R, K294R or K76/294R cells show decreased lipogenesis compared to control vector and WT rescue cells. To explore the potential mechanism responsible for decreased lipogenesis, we examined the effect of 6PGD product Ru-5-P on regulatory components of the lipid synthesis pathway. We found that Ru-5-P

exerts an inhibitory effect on the activity of serine/threonine kinase LKB1. LKB1 achieves activation by forming a heterotrimeric complex with adaptor protein MO25 and pseudokinase STRAD. The LKB1-STRAD-MO25 complex represents a biologically active unit that proceeds to phosphorylate downstream substrates including AMPK. Ru-5-P functions to disrupt the active LKB1-MO25-STRAD complex and thus prevent activation of AMPK. When active, AMPK phosphorylates and inhibits acetyl Co-A carboxylase 1 (ACC1) in the lipid synthesis pathway, thus impeding lipogenesis. When Ru-5-P levels are high as a result of increased 6PGD activity, inhibition of LKB1-AMPK signaling relieves inhibition of ACC1 and consequently permits high lipogenic activity to contribute to rapid cell proliferation and tumor growth. This suggests that 6PGD provides a novel crosstalk between metabolic and signaling pathways to promote lipogenesis by controlling intracellular levels of its product Ru-5-P (data not shown).

Protein and lysine acetylation levels of 6PGD are important for tumor growth.

We next performed a xenograft experiment in which nude mice were injected with control human leukemia K562 cells and 6PGD KD cells on the left and right flanks, respectively, the growth rate (Figure 2.3.2A *left*) and masses (2.3.2A; *right*) of tumors derived from 6PGD KD cells were significantly reduced compared to those of tumors formed by control cells over a ~2-week time period. Similar results were obtained in lung cancer cell xenograft nude mice using parental and stable 6PGD KD H1299 cells over a ~7-week time period. (data not shown). In addition, we performed xenograft experiments in which nude mice were injected with H1299

cells with rescue expression of FLAG-6PGD WT, K76R or K294R. FLAG-6PGD WT rescue cells were injected on the left flank and K76R (Figure 2.3.2B) or K294R (Figure 2.3.2C) rescue cells were injected on the right flank. The mice were monitored for tumor growth over a ~6-week time period. We found that the growth rate and masses of tumors derived from K76R (Figure 2.3.2B *left* and *middle*, respectively) or K294R (Figure 2.3.2C; *left* and *middle*, respectively) rescue H1299 cells were significantly reduced with decreased 6PGD enzyme activity in tumor cells (*right panels*; Figure 2.3.2B-C) compared to those of tumors formed by the control 6PGD WT rescue cells. Together these data demonstrate an important role for 6PGD in tumor growth, and that acetylation at either K76 or K294 of 6PGD itself is sufficient and important for tumor growth, suggesting 6PGD as a novel anti-cancer target.

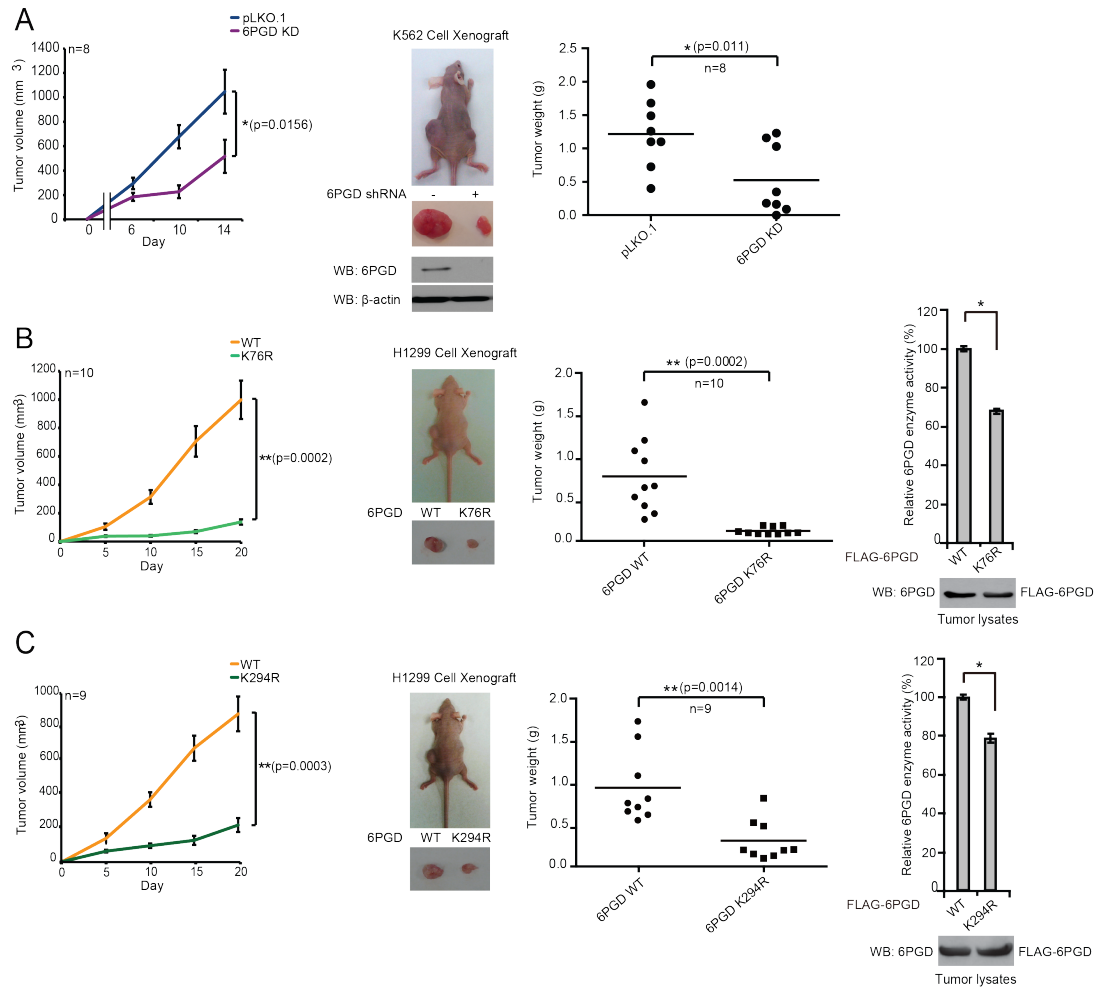


Figure 2.3.2. Protein levels and lysine acetylation of 6PGD are important for tumor growth *in vivo*. (A) *Left*: Tumor growth was compared between xenograft nude mice injected with 6PGD KD (KD) K562 leukemia cells and control vector cells. *Middle*: Dissected tumors in a representative nude mouse and expression of 6PGD in tumor lysates. *Right*: Tumor mass in xenograft nude mice injected with 6PGD KD K562 cells compared to mice injected with the control vector cells. (B-C) Attenuation of 6PGD by rescue expression of K76R mutant (B) or K294R mutant (C) results in decreased tumor growth potential of H1299 cells in xenograft nude mice (*left*). *Middle*: Dissected tumors in a representative nude mouse; tumor mass in xenograft nude mice injected with K76R (B) or K294R (C) cells compared to mice injected with the control vector cells are shown. *Right*: 6PGD enzyme activity in tumor lysates of mice injected with K76R (B) or K294R (C) cells compared to mice injected with WT rescue cells. p values were determined by two-tailed paired Student's *t* test (*0.01 < *p* < 0.05; **0.001 < *p* < 0.01).

Discovery and development of Physcion and its derivative S3 as selective 6PGD inhibitors.

Currently available 6PGD inhibitors including EGCG and 6-aminonicotinamide (6-AN) are not selective; EGCG is a general inhibitor of NADP⁺-dependent enzymes and 6-AN inhibits both G6PD and 6PGD. We designed a screening strategy using an *in vitro* 6PGD assay and identified Physcion (C₁₆H₁₂O₅; 1,8-Dihydroxy-3-methoxy-6-methyl-anthraquinone; Emodin-3-methyl ether) as a potent 6PGD inhibitor from a library of FDA approved 2,000 small molecule compounds (Figure 3.3.2A). We also identified a Physcion derivative S3 (C₁₅H₁₀O₄; 1-Hydroxy-8-methoxy-anthraquinon; Figure 3.3.2A) as an additional 6PGD inhibitor with improved solubility from a group of 10 commercially available Physcion derivatives (data not shown). Physcion effectively inhibits purified 6PGD protein (Figure 3.3.2B (*left*) and 3.3.2C) but not control NADP⁺-dependent metabolic enzymes including G6PD (Figure 3.3.2B (*right*) and 3.3.2C), glutamate dehydrogenase 1 (GLUD1) and IDH1, nor glycolytic enzymes LDHA and PGAM1 (Figure 3.3.2C). Physcion and S3 inhibit 6PGD with IC₅₀ values of approximately 38.0 μM and 15.7 μM, respectively (Figure 3.3.2C) and the K_d values of the Physcion-6PGD and S3-6PGD interaction were determined to be 61.8 μM and 24.8 μM from a tryptophan fluorescence-based binding assay (Figure 3.3.2D). In addition, Physcion treatment inhibits 6PGD enzyme activity (Figure 3.3.2E) and proliferation (Figure 3.3.2F) in K562 leukemia cells, whereas K562 6PGD KD cells are resistant to Physcion treatment (Figure 3.3.2G), suggesting that Physcion as a selective 6PGD inhibitor has no off-target effect when inhibiting cancer cell proliferation.

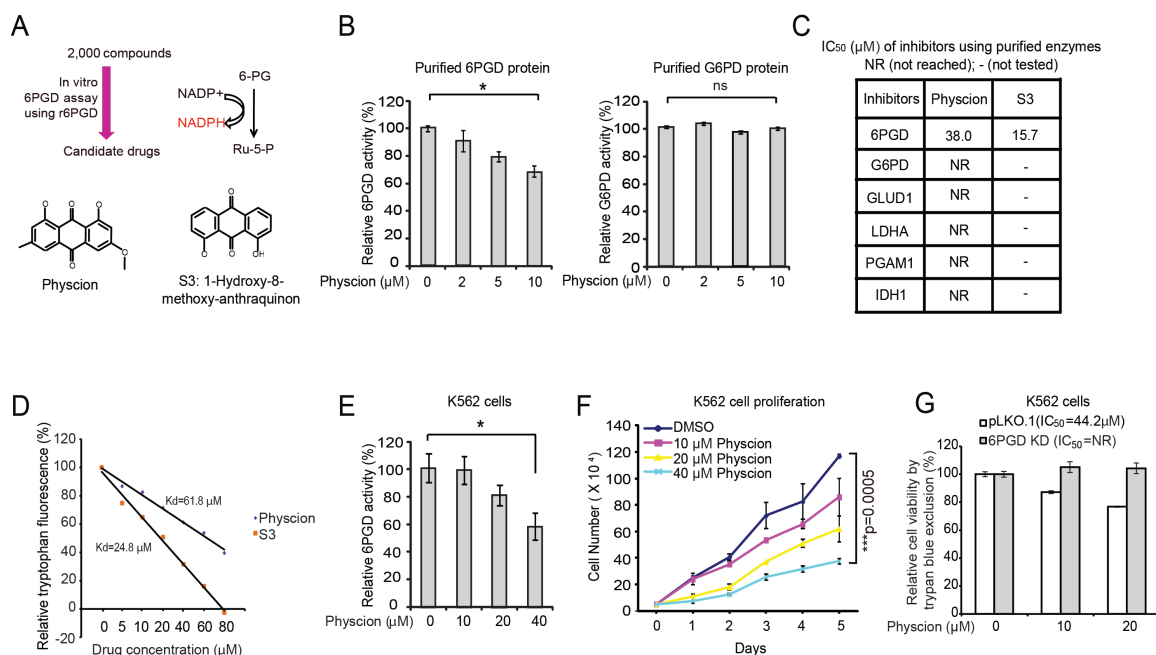


Figure 3.3.2. Physcion and its derivative S3 are selective 6PGD inhibitors. (A) Upper: Schematic representation of screening strategy to identify lead compounds as 6PGD inhibitors. Lower: Structure of Physcion and its derivative S3. (B) Purified 6PGD (left) and G6PD (right) were assayed for 6PGD and G6PD enzyme activity, respectively, in the presence of increasing concentrations of Physcion. (C) IC₅₀ values of Physcion and S3 were determined in diverse enzyme activity assays using different purified metabolic enzymes; NR=not reached. (D) K_d values were determined as 61.8 μM for Physcion and 24.8 μM for S3 by incubating purified human 6PGD proteins with increasing concentrations of Physcion or S3, respectively. The fluorescence intensity (ex: 280nm, em: 350nm) from tryptophan was measured (128). (E) K562 cells treated with increasing concentrations of Physcion were assayed for 6PGD activity, which was normalized to the control cells without drug treatment. (F) Cell proliferation rates of K562 cells in the presence of increasing concentrations of Physcion were determined by cell counting. (G) Cell viability was determined in 6PGD KD K562 cells and control vector cells in the presence of increasing concentrations of Physcion. IC₅₀ values were determined; NR=not reached. The error bars represent mean values ± SD from three replicates of each sample. p values were determined by two-tailed Student's *t* test (*0.01<p<0.05; **p<0.01; ns, not significant).

We further explored the molecular mechanism by which Physcion inhibits 6PGD, we performed a molecular docking study of Physcion based on the crystal structure of 6PGD (PDB code: 3FWN) in complex with its substrate 6-PG. Physcion was initially positioned into the 6-PG binding site and the docking result was optimized by local energy minimization. Physcion fits in a pocket near the binding site of 6-PG surrounded by residues including M15, K76, K261 and H452. Physcion forms hydrophobic interactions with these residues and a hydrogen bond with N103 via its 10-keto group. We then performed mutational studies to show that M15A mutant shows resistance to Physcion or S3 treatment in an *in vitro* 6PGD enzyme activity assay, and expression of M15A confers Physcion- or S3-resistance to H1299 cells. These data also suggest that S3 inhibits 6PGD by a similar molecular mechanism as Physcion, and both Physcion and S3 inhibit cancer cell proliferation by targeting 6PGD with minimal off-target effect (data not shown).

Physcion and S3 inhibit cancer cell proliferation *in vitro* and tumor growth *in vivo*.

We found that both Physcion and S3 treatment results in decreased cell viability of K562 and H1299 cells in a dose dependent manner, but does not significantly affect control proliferating cells including HDF and immortalized human melanocyte PIG1 cells, suggesting minimal toxicity of Physcion in human cells. We next found that both Physcion and S3 treatment in K562 and H1299 cells results in significant apoptosis induction. In diverse metabolic assays, we found that our results in cancer cell lines treated with Physcion and S3 were consistent with the phenomena

observed in cells with attenuated 6PGD, suggesting that Physcion and S3 specifically target 6PGD to inhibit cancer cell viability and proliferation (data not shown).

Since S3 demonstrates improved solubility compared with Physcion, we next performed an *in vivo* drug treatment experiment using S3. Initial toxicity studies by chronic injection of S3 to nude mice for ~4 weeks revealed that 20mg/kg/day administered intraperitoneally is a well-tolerated dose. In addition, continuous treatment with S3 (20mg/kg/day) for 30 days did not result in significant alteration in body weight. Moreover, S3 treatment did not affect the hematopoietic properties of nude mice (Figure 4.3.2A), and histopathological analyses revealed no notable differences between the vehicle-treated and S3-treated groups (Figure 4.3.2B). These results demonstrate that S3 treatment has minimal toxicity *in vivo*.

A

Test Name	Normal range	DMSO (mean)	20 mg/kg/day S3 (mean)
WBC (x 10 ³ /μL)	2.6-10.1	10.9 ± 2.4	7.5 ± 1.6
LYM (x 10 ³ /μL)	1.3-8.4	8.6 ± 2.3	5.9 ± 1.5
MONO (x 10 ³ /μL)	0-0.3	0.7 ± 0.1	0.4 ± 0.2
GRAN (x 10 ³ /μL)	0.4-2	1.7 ± 0.4	1.2 ± 0.3
HCT (%)	32.8-48	49.1 ± 10.3	19.6 ± 9.0
MCV (fl)	42.3-55.9	59.5 ± 5.1	53.1 ± 3.9
RDW _a (%)	0-99.9	40.7 ± 6.1	57.1 ± 18.3
HGB (g/dl)	10-16.1	14.4 ± 2.4	6.9 ± 2.3
MCHC (g/dl)	29.5-35.1	29.7 ± 2.3	36.7 ± 4.4
RBC (x 10 ⁶ /μL)	6.5-10.1	8.2 ± 1.4	5.5 ± 0.3
MCH (pg)	13.7-18.1	17.6 ± 0.6	19.4 ± 1.7
PLT (x 10 ³ /μL)	250-1540	626.0 ± 150.4	263.7 ± 12.0
MPV (fl)	0-99.9	6.5 ± 0.3	14.8 ± 7.1

B

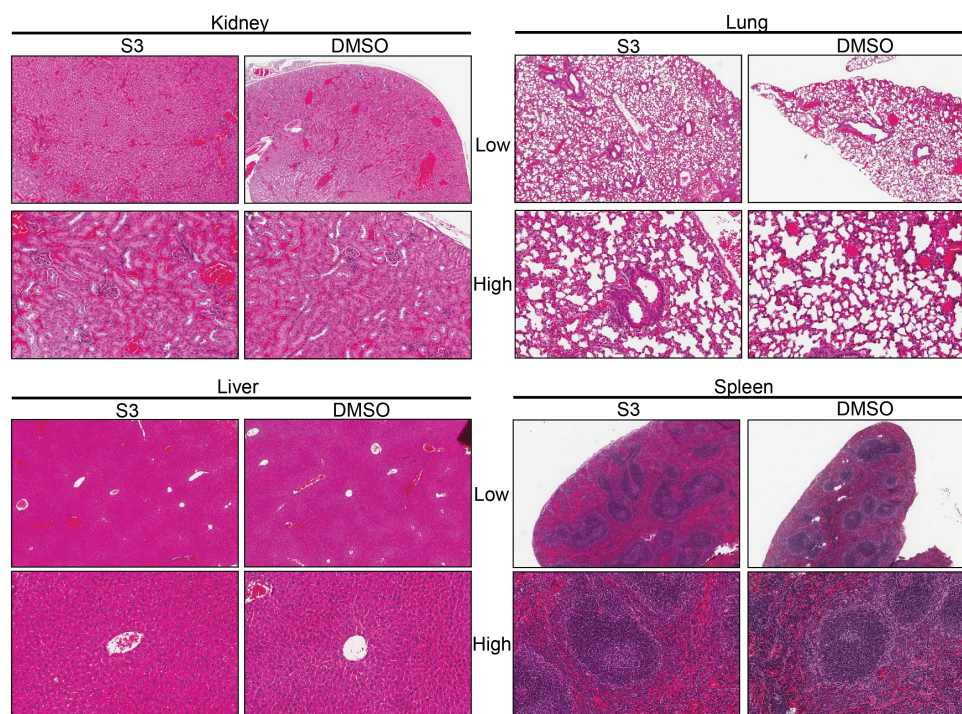


Figure 4.3.2. Chronic S3 treatment causes no off-target toxicity in nude mice (A) Athymic nude mouse hematology. Nude mice (n=3) were treated with either vehicle control or S3 (20 mg/kg/day) for 30 days. CBC analysis shows no significant difference in the hematopoietic properties between the two groups of mice. (B) Histological morphology of hematoxylin-eosin stained tissue sections of representative nude mice in S3 or vehicle control-treated groups. Nude mice were treated daily with S3 (20 mg/kg/day) intraperitoneally for 30 days. PB samples were collected and applied for analysis of hematological properties (A). The vital organs were collected for histopathological analysis. Histopathologic tissue sections (kidney, lung, liver and spleen) from representative nude mice stained with hematoxylin-eosin did not reveal significant differences between the vehicle and S3 treated groups. Images were analyzed and captured using ImageScope software (Aperio Technologies Inc.) without any additional or subsequent image processing (high power images are 20x; low power images are either 4.0x, 4.2x, or 4.4x).

We next performed an *in vivo* drug treatment experiment using xenograft mice by subcutaneously injecting K562 leukemia cells into nude mice. Three days post-injection, mice were divided into two groups and treated with either S3 (20mg/kg/day) or DMSO for 9 days. S3 treatment results in significantly decreased tumor growth (Figure 5.3.2A) and masses (Figure 5.3.2B) in treated mice compared with mice receiving DMSO. Moreover, S3 effectively inhibits 6PGD activity (Figure 5.3.2C) and reduces Ki-67 expression assessed by immunohistochemical (IHC) staining (Figure 5.3.2D) in resected tumors from xenograft nude mice, suggesting that S3 inhibits 6PGD *in vivo*, conferring a specific inhibitory effect on tumor cell proliferation without off-target effect. Similar results were obtained using H1299 cell xenograft nude mice treated with S3 for 11 days, with treatment beginning 20 days post-xenograft injection (data not shown).

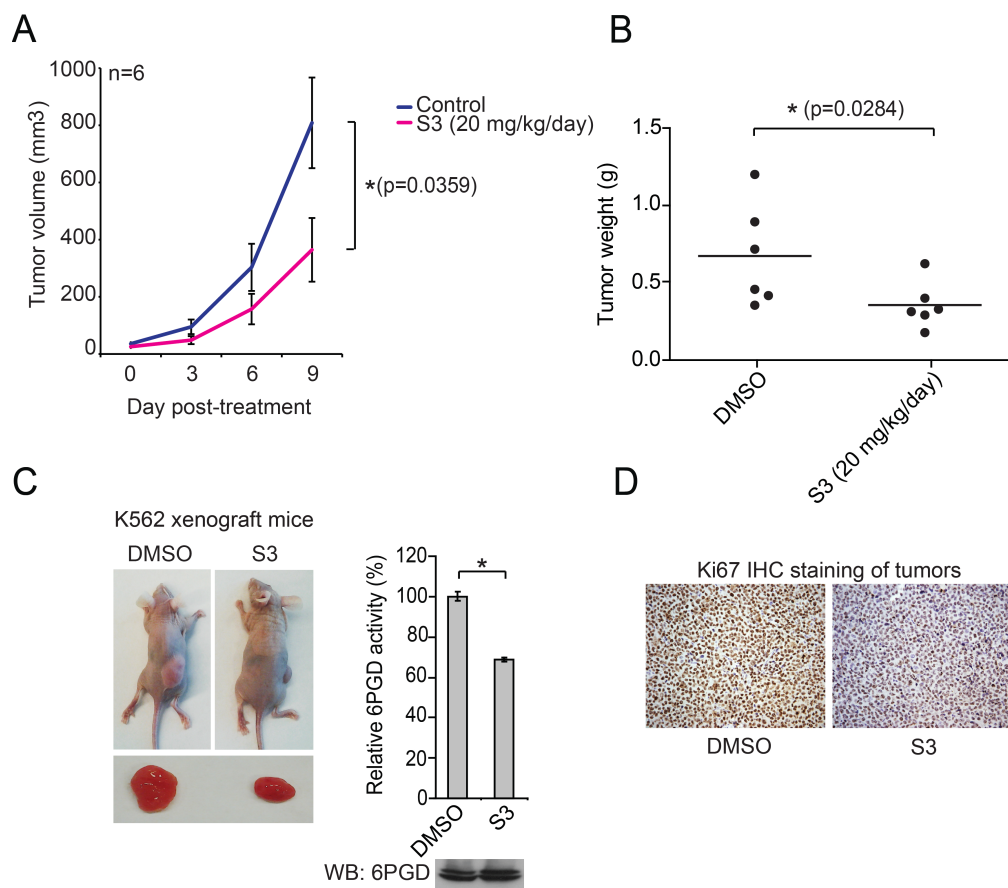


Figure 5.3.2. S3 treatment results in reduced leukemia K562 cell tumor growth *in vivo*. (A-B) Tumor growth (A) and tumor size (B) in xenograft nude mice injected with K562 cells were compared between the group of mice treated with Phycion derivative S3 and the control group treated with vehicle control DMSO. (C) *Left*: Dissected tumors in representative nude mice treated with DMSO control or S3 are shown. *Right*: 6PGD enzyme activity in tumor lysates of K562 xenograft mice treated with DMSO or S3 is shown. (D) Representative images of IHC staining of proliferation marker Ki-67 (brown color) from K562 xenograft mice treated with DMSO or S3 are shown. p values were determined by two-tailed Student's *t* test (*0.01 < p < 0.05).

Enzyme activity and lysine acetylation of 6PGD are upregulated in human leukemias, representing a novel anti-leukemia target.

We next found that 6PGD enzyme activity levels are commonly upregulated in human primary leukemia cells from diverse AML, CML and B-ALL patients (n=15), compared to control PB cells from healthy donors (n=4) (Figure 6.3.2A). However, we did not find significantly increased 6PGD expression levels in human primary leukemia cells compared to control PB (PB) cells from healthy donors. Instead, we observed that K76 and K294 acetylation levels are increased in primary leukemia cells from representative AML patients compared to PB cells from healthy donors (Figure 6.3.2B). Together these data suggest that upregulated 6PGD enzyme activity in human leukemias may be due to increased lysine acetylation of 6PGD.

Moreover, both Physcion and S3 treatment results in decreased 6PGD enzyme activity (Figure 6.3.2C) and cell viability in primary leukemia cells from patients with diverse types and subtypes of leukemia (Figure 6.3.2D-E), including B-ALL, AML, and CML. In contrast, neither Physcion nor S3 treatment affects cell viability of mononucleocytes in PB samples from healthy human donors (Figure 6.3.2F) or CD34+ cells isolated from bone marrow (BM) samples from healthy donors (Figure 6.3.2G), suggesting promising anti-cancer potential of Physcion and S3 with minimal toxicity to human blood cells. The results of these translational studies cumulatively suggest that 6PGD is a promising therapeutic target in treatment of human leukemia.

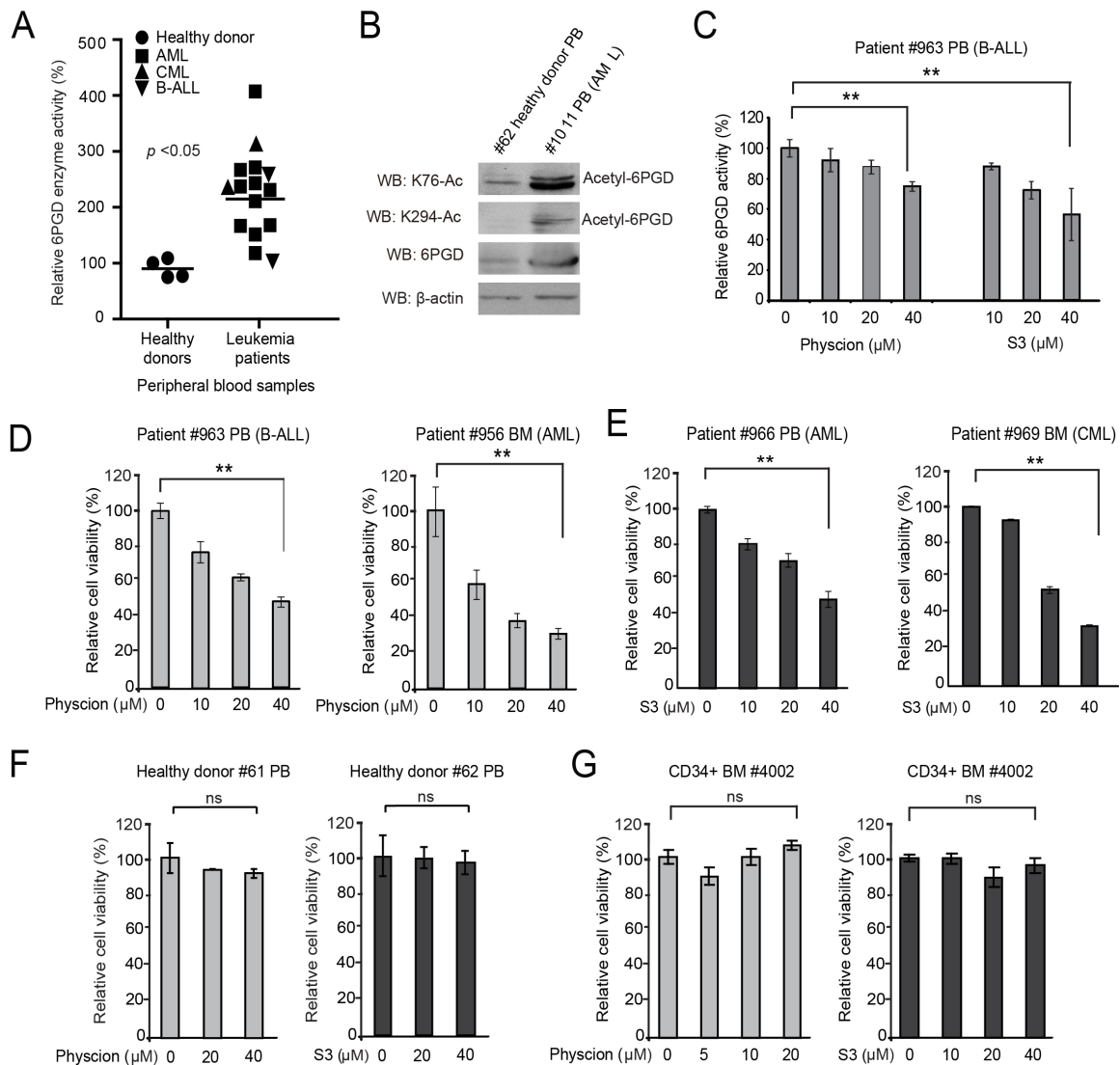


Figure 6.3.2. 6PGD enzyme activity and lysine acetylation levels are commonly upregulated in human primary leukemia cells and Physcion treatment results in reduced cell proliferation of primary leukemia cells from human patients. (A) 6PGD enzyme activity levels were examined using primary leukemia cells from diverse human patients with AML, CML or B-ALL and compared to control PB cells from healthy donors. (B) K76 and K294 acetylation levels of 6PGD in primary leukemia cells from a representative AML patient were examined and compared to control PB cells from a healthy donor. PB=PB. (C) Effects of Physcion and S3 treatment on 6PGD enzyme activity were examined in human primary leukemia cells isolated from a representative B-ALL patient. (D) Effects of Physcion treatment on cell viability of human primary leukemia cells isolated from representative B-ALL and AML patients. (E) Effects of S3 treatment on cell viability of human primary leukemia cells isolated from representative AML and CML patients. (F-G) Neither Physcion nor S3 shows toxicity in treatment (72h) of PB cells (F) and CD34+ cells isolated from bone marrow samples (G) from representative healthy human donors. The error bars represent mean values \pm SD from three replicates of each sample. p values were determined by two-tailed Student's t test (* $0.01 < p < 0.05$; ** $0.001 < p < 0.01$; ns, not significant).

3.2.4. Discussion

Our findings suggest that upregulation of 6PGD by lysine acetylation in cancer cells is common and important for cell proliferation and tumor growth; 6PGD coordinates anabolic biosynthesis and redox homeostasis, at least in part by controlling the intracellular levels of its products Ru-5-P and NADPH (Figure 7.3.2). Our results revealed a novel molecular mechanism by which Ru-5-P inhibits LKB1 by disrupting the active LKB1-MO25-STRAD heterotrimeric complex. In cancer cells, lysine acetylation enhances 6PGD activity to promote oxidative PPP and nucleotide/RNA biosynthesis and keep intracellular Ru-5-P at a physiological level that is sufficient to inhibit LKB1-AMPK signaling, which in turn relieves AMPK-dependent inhibition of ACC1, permitting high levels of lipid biosynthesis to facilitate rapid cell division and tumor growth (Figure 7.3.2A). Attenuation of 6PGD results in decreased Ru-5-P to levels below physiological concentrations, which in turn not only attenuates nucleotide/RNA biosynthesis but also relieves the inhibition of LKB1, leading to activation of AMPK and subsequent inhibition of ACC1 and lipogenesis (Figure 7.3.2B). Moreover, while the current model linking the oxidative PPP to anabolic biosynthesis is based on the production of R-5-P and NADPH produced by the oxidative PPP that are used as precursors in RNA biosynthesis and lipogenesis, respectively, our findings suggest that 6PGD provides an additional and novel link between the oxidative PPP and lipogenesis through Ru-5-P-dependent inhibition of LKB1-AMPK signaling.

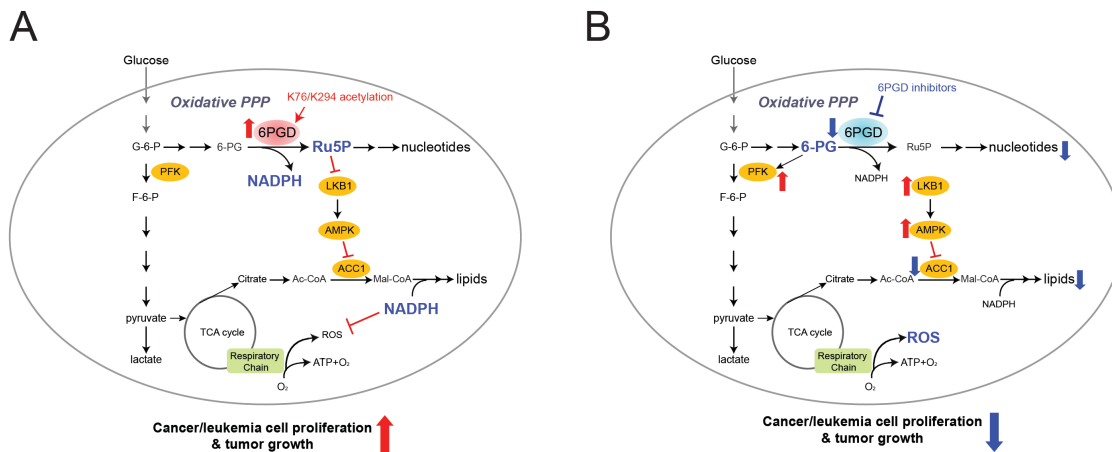


Figure 7.3.2. Proposed model: role of 6PGD in cancer cell metabolism. (A) 6PGD is activated by lysine acetylation in cancer cells to promote oxidative PPP and nucleotide/RNA biosynthesis and keep the intracellular Ru-5-P concentration at a physiological level that is sufficient to inhibit LKB1-AMPK signaling. This in turn relieves AMPK-dependent inhibition of ACC1, permitting high levels of lipid biosynthesis to facilitate rapid cell division and tumor growth. In addition, 6PGD is important for NADPH production, which is crucial in protecting cancer cells from ROS. (B) When 6PGD is inhibited, Ru-5-P is decreased to levels below physiological concentrations, leading to attenuated oxidative PPP flux and RNA/nucleotide biosynthesis, as well as increased activation of LKB1-AMPK pathway, which inhibits ACC1 and subsequently lipogenesis. 6PGD inhibition also leads to decreased NADPH production resulting in levels that are insufficient to combat the increased ROS in cancer cells. These metabolic defects overshadow the increased glycolysis due to activation of PFK by accumulated 6-PD in 6PGD attenuated cells, leading to reduced cancer cell proliferation and tumor growth.

As previously discussed, PGAM1 substrate 3-PG inhibits 6PGD, and inhibition of PGAM1 results in abnormal accumulation of 3-PG, leading to 6PGD inhibition. We found that PGAM1 enzyme activity is not altered in 6PGD KD cells, suggesting that the upregulation of PGAM1 in cancer cells appears to be an upstream event that controls the contribution of 6PGD to metabolic reprogramming in transformed cells. However, 6PGD substrate 6-PG has been shown to activate glycolytic enzyme phosphofructokinase (PFK; 129) upstream of PGAM1, providing feedback control to glycolytic flux. We found that inhibition of 6PGD results in increased 6-PG levels, leading to increased glycolysis and ATP levels. These findings suggest that PGAM1 acts in concert with 6PGD to “fine-tune” metabolic flux through glycolysis and the oxidative PPP. Nevertheless, despite the increased glycolysis and ATP levels, 6PGD inhibition results in reduced cancer cell proliferation and tumor growth, suggesting that other metabolic defects, including diminished capacity for anabolic biosynthesis and disruption of redox homeostasis, eclipse the benefits typically conferred by increased bioenergetics on cancer cell proliferation. Like our PGAM1 studies, these studies provide additional evidence to demonstrate that the balance of the intracellular levels of various metabolites may exert regulatory functions on enzymes in different pathways to control cellular metabolism. Such “metabolite balancing” networks reveal a wealth of potential targets for anti-cancer therapy.

We observed that 6PGD is commonly lysine acetylated in diverse cancer and leukemia cells, and the upregulated 6PGD activity in human primary leukemia cells is also likely due to increased lysine acetylation levels of 6PGD. In consonance with

these observations, our studies suggest that protein expression and acetylation levels of 6PGD are important for cancer cell proliferation and tumor growth. Our novel 6PGD inhibitors Physcion and its derivative S3 are selective and inhibit cell proliferation by targeting 6PGD in diverse human cancer cells and primary leukemia cells from human patients *in vitro* with no obvious off target effect and minimal toxicity to human cells. Moreover, S3 exhibits promising efficacy in a treatment of K562 leukemia cell xenograft nude mice *in vivo* with minimal toxicity. These translational studies suggest inhibition of 6PGD as a promising therapy in clinical treatment of a broad spectrum of human leukemias.

3.3. Development of novel combinatorial anti-leukemia therapies: a lesson from dehydrogenase deficient hemolytic anemia

3.3.1. Introduction

As demonstrated in our 6PGD studies, the oxidative PPP represents a critical mechanism underlying the metabolic coordination of glycolysis, anabolic biosynthesis, and redox homeostasis to promote to cancer cell proliferation and disease development. Both our own 6PGD studies as well as extensive work by others on G6PD have demonstrated that attenuation of metabolic flux through the oxidative PPP shows potent anti-cancer effects.

G6PD, the rate-limiting enzyme for the PPP, converts G-6-P to 6-phosphogluconolactone (6-PGL) and results in the concurrent production of NADPH. Much attention has been paid to the role of G6PD in cancer cell metabolism given its position as the first and rate-limiting enzyme of the oxidative PPP, as well as being one of two enzymes in the oxidative PPP that produces NADPH. G6PD activity is critical for cell proliferation and survival through its role in intracellular redox regulation, and inhibition of G6PD results in attenuated cell growth as well as H₂O₂-mediated cell death, likely due to lack of reducing power in the form of NADPH (133-136). Moreover, Schafer et al. recently demonstrated that matrix-dependent detachment causes a significant increase in G6PD protein level, which confers anoikis-resistance to detached ErbB2 transformed MCF-10A breast cancer cells

(134). In addition, G6PD inhibitors dehydroepiandrosterone (DHEA) and 6-AN have been shown to exhibit anti-tumorigenic effects in diverse cancer cell lines (135-136).

Notably, 6PGD (62) and G6PD deficiency both exist in human patients as X-linked recessive hereditary diseases. G6PD deficiency is the most common human enzyme defect, affecting more than 400 million people worldwide (63). While most individuals with 6PGD or G6PD deficiency are asymptomatic, various clinical manifestations of the disease can occur. For example, exposure to oxidative insults, including infection, medications including aspirin and various antimalarial drugs, and certain foods including fava beans, can lead to non-immune hemolytic anemia. RBCs rely solely upon the PPP for the production of NADPH to use in the reduction of glutathione, which subsequently serves a crucial purpose in protecting the cells from oxidative damage. Attenuation of the PPP due to genetic deficiency of 6PGD or G6PD thus perturbs redox homeostasis in RBCs, and exposure to oxidative stress leads to premature red cell destruction (64). Beyond oxidative damage however, little is understood regarding the molecular mechanisms underlying the chemical induction of hemolytic anemia in these patients.

Inspired by these clinical observations, we hypothesized that combined treatment with our novel, selective 6PGD inhibitors or commercially available G6PD inhibitors and anti-malarial drugs may result in synergistic inhibition of leukemia cell proliferation and survival. We chose to focus on anti-malarial agent DHA due to its

high therapeutic efficacy and safety profile in humans. DHA is a semi-synthetic derivative of artemisinin, a sesquiterpene lactone isolated from the traditional Chinese herb *Artemisia annua* that has been used by Chinese herbalists since 168 B.C (137). DHA is recommended as a first-line anti-malarial drug with low toxicity, and has more recently been shown to possess promising anticancer activities (138-139), although the underlying molecular mechanisms are not well understood.

In this study, we investigate the application of oxidative PPP inhibition combined with DHA treatment as a novel combinatorial therapeutic strategy for leukemia. Our approach establishes an appropriate dosing window that can synergistically inhibit leukemia cell viability without perturbing the viability of isolated RBCs *in vitro* or inducing hemolytic anemia in mice.

3.3.2. Materials and methods

Reagents. Stable KD of endogenous h6PGD was achieved using lentiviral vector harboring shRNA construct (Open Biosystems; 5'-CCGGGTGGATGATTTTCATCGAGAACTCGAGTTTCTCGATGAAATCATCCACTTTTT-3'). The shRNA is designed to target the 3' non-coding region of h6PGD-A mRNA and shows no effect on the plasmid directed expression of 6PGD cDNA in cells. Stable KD of endogenous hG6PD was achieved using lentiviral vector harboring shRNA construct (Open Biosystems; 5'-CCGGCCCTGAAGTGACTGAGACAATCTCGAGATTGTCTCAGTCACTTCAGGGTTTTT-3'). Stable KD of endogenous hAMPK was achieved using lentiviral vector harboring shRNA construct (Open Biosystems; 5'-CCGGGCATAATAAGTCACAGCCAAACTCGAGTTTGGCTGTGACTTATTATGCTTTTT-3'). Antibodies against AMPK and phospho-AMPK were from Cell Signaling Technology (CST); antibody against 6PGD was from Novus; antibody against β -actin was from Sigma; predilute Ki67 antibody was from Invitrogen. Phycion was purchased from Santa Cruz Biotechnology. 1-hydroxy-8-methoxy-anthraquinone (S3) was purchased Sigma. DHEA was purchased from Calbiochem. DHA was purchased from TCI America. A769662 was purchased from LC Laboratories. Compound C was purchased from EMD Millipore.

Cell culture. K562, HEL, KG1a, and Molm14 cells were cultured in RPMI 1640 medium with 10% FBS and penicillin/streptomycin. K562 6PGD stable KD cells

were cultured in the presence of 6 μ g/mL puromycin. K562 G6PD and AMPK stable KD cells were cultured in the presence of 2 μ g/mL puromycin.

G6PD and 6PGD assays. G6PD activity was determined by the NADPH production rate from G6PD and 6PGD, then subtracting that of 6PGD, since a product of G6PD, 6-phosphogluconolactone, is rapidly hydrolyzed to a substrate of 6PGD, 6-phosphogluconate, in cells. To obtain the combined dehydrogenase activity, substrates for both dehydrogenase enzymes were added to a cuvette. In another cuvette, substrates for the second enzyme, 6PGD, were added to obtain the activity of this enzyme. Substrate concentrations were as follows: 0.2 mM glucose 6-phosphate, 0.2 mM 6-phosphogluconate, and 0.1 mM NADP⁺. 10 μ g of cell lysates were added to a cuvette containing buffer (50 mM Tris/1 mM MgCl₂, pH 8.1) and the reaction was then initiated by NADP⁺. The increase in 341 nm absorbance (OD₃₄₀) as a measure of NADPH production was measured every 20 seconds for 10 minutes on a DU800 Spectrophotometer (Beckman Coulter).

Oxidative PPP flux assay using ¹⁴CO₂ Release. Cells were seeded on 6-cm dishes that are placed in a 10-cm dish with 2 sealed pinholes on the top. ¹⁴CO₂ released from cells was collected by completely sealing the 10-cm dish, in which the cells on the 6-cm dish were incubated in 2 mL of medium containing [1-¹⁴C]- or [6-¹⁴C]-glucose, respectively, at a final specific activity of 10 μ Ci/mL glucose at 37 °C for 3 h. The oxidative PPP flux was stopped by injecting 0.3 mL of 50% TCA through one of the holes on the top, and at the same time ¹⁴CO₂ released was trapped by injecting

0.3 mL of Hyamine Hydroxide into a small cup placed on the 10-cm dish through the second hole. Krebs cycle measurements, obtained in parallel samples incubated with [6-¹⁴C]-glucose, were used to correct the oxidative PPP flux measurements obtained from samples incubated with [1-¹⁴C]-glucose. Each dish was completely re-sealed with parafilm and incubated overnight at room temperature. Hyamine Hydroxide in the small cup was dissolved into 60% methanol and directly subjected to scintillation counting.

Cell viability assays. 5×10^6 cells were seeded in 6-well plates and incubated with indicated drug concentrations at 37°C for 36-48 hours. Relative cell viability was determined by trypan blue exclusion using a TC10 Automated Cell Counter (BioRad). Combination index (CI) values were calculated using ComboSyn program.

Apoptosis assay. 1×10^5 cells were treated with indicated drug concentrations for 24 hours, then collected and stained using FITC-conjugated annexin V labeling reagent (BD Pharmingen) and PI (Sigma) followed by FACS analysis for apoptotic cell population.

Intracellular reactive oxygen species (ROS) production. The amount of intracellular ROS was measured by detecting dichlorodihydrofluorescein, which is the cleavage product of carboxy-H₂DCFDA (Invitrogen) by ROS. 1×10^5 cells were seeded in 6-well plate and treated with drug at indicated concentrations. Two hours after treatment, cells were washed with PBS and loaded with 5 μ M carboxy-

H₂DCFDA for 30 min. The cells were harvested, resuspended in PBS and analyzed using a FACS (BD Biosciences; excitation and emission at 490 and 530 nm, respectively).

Xenograft studies. For drug evaluation using xenograft mice, the drug was administered by daily intraperitoneal injection (S3: 5 mg/kg/day; DHA: 2.5 mg/kg/day; S3 + DHA: 5 + 2.5 mg/kg/day) from 3 days after subcutaneous injection of 5×10^6 K562 cells on the *right* flank of each mouse. Tumor growth was recorded by measurement of two perpendicular diameters using the formula $4\pi/3 \times (\text{width}/2)^2 \times (\text{length}/2)$. The tumors were harvested and weighed at the experimental endpoint, and the masses of tumors (g) treated with vehicle control (DMSO) and drug treated groups were compared by a two-tailed unpaired Student's *t* test.

Complete blood counts. For complete blood counts, blood was collected retro-orbitally and immediately applied to a HemaVet 950FS (Drew Scientific) for generation of complete hematology profile.

Primary tissue samples from patients with leukemia and healthy donors.

Approval of use of human specimens was given by the Institutional Review Board of Emory University School of Medicine. All clinical samples were obtained with informed consent with approval by the Emory University Institutional Review Board. Clinical information for the patients was obtained from the pathologic files at

Emory University Hospital under the guidelines and with approval from the Institutional Review Board of Emory University School of Medicine and according to the Health Insurance Portability and Accountability Act. Only samples from patients that were not previously treated with chemotherapy or radiation therapy were used. Mononuclear cells and RBCs were isolated from PB and bone marrow samples from patients with leukemia or from healthy donors using lymphocyte separation medium (Cellgro). Cells were cultured in RPMI 1640 medium supplemented with 10% fetal bovine serum and penicillin/streptomycin and incubated with indicated drug concentrations for 48 hours

3.3.3. Results

Targeting the oxidative pentose phosphate pathway by stable KD of G6PD or 6PGD sensitizes K562 human leukemia cells to anti-malarial agent DHA.

We began by testing our hypothesis in K562 human leukemia cells, an erythroleukemia cell line whose hematopoietic properties resemble RBCs (140). To determine whether attenuation of oxidative PPP flux sensitizes leukemia cells to DHA as it does in dehydrogenase deficient patients, we first generated K562 cells with stable KD of G6PD (Figure 1.3.3A) or 6PGD (Figure 1.3.3B), both of which display significantly decreased oxidative PPP flux compared to vector control cells (A and B, *middle panels*). We then exposed KD cells to increasing concentrations of DHA for 36 hours, and found that indeed, both G6PD and 6PGD KD cells were significantly more sensitive to DHA treatment in a dose dependent manner compared to vector control cells.

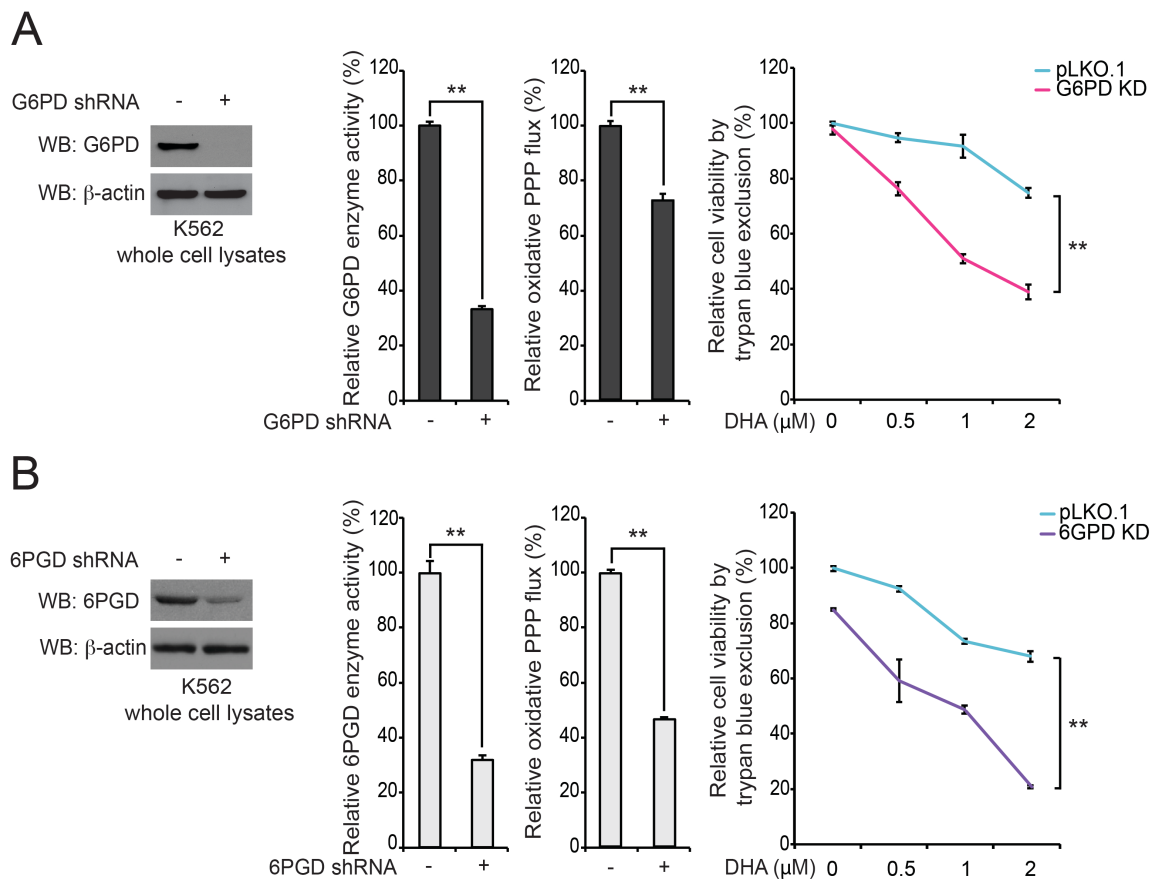


Figure 1.3.3. Targeting the oxidative pentose phosphate pathway by stable KD of G6PD or 6PGD sensitizes K562 human leukemia cells to anti-malarial agent DHA. Attenuation of oxidative PPP flux in K562 leukemia cells by stable KD of G6PD (A) or 6PGD (B) renders cells significantly more sensitive to anti-malarial agent DHA compared to vector control cells. Stable KD of G6PD and 6PGD was confirmed by Western blot. Cell viability was determined 36 hours post DHA-treatment. The error bars represent mean values \pm SD from three replicates of each sample. *p* values were determined by two-tailed Student's *t* test (*0.01 < *p* < 0.05; **0.001 < *p* < 0.01).

6PGD inhibitor Physcion, but not G6PD inhibitor DHEA, in combination with DHA leads to synergistic inhibition of K562 cell viability and induction of apoptosis.

We thus proceeded to develop a treatment strategy using G6PD and 6PGD inhibitors combined with DHA. In order to allow for synergistic activity, which we define as the combined effect being greater than the sum of effects of both drugs, we first aimed to determine sub-lethal dosing windows for each compound to be used in the combination. We performed a dose curve for DHA in K562 cells, where we defined a sub-lethal dose to be $\leq 40\%$ inhibition of cell viability (Figure 2.3.3A). To determine appropriate doses for G6PD and 6PGD inhibitors, we performed dose curves followed by enzyme activity assays to determine the dose at which each drug could significantly inhibit enzyme activity without significantly inhibiting cell viability. DHEA, an abundantly produced adrenal steroid, is a known non-competitive inhibitor of G6PD. Dose escalation of DHEA (Figure 2.3.3B) followed by G6PD enzyme activity assay (Figure 2.3.3C) in K562 cells revealed 50 μM DHEA to be an appropriate sub-lethal dose that could still significantly inhibit G6PD enzyme activity. However, we found that combined treatment with 50 μM DHEA + sub-lethal doses of DHA in K562 cells did not lead to dose dependent synergistic inhibition of cell viability (Figure 2.3.3D), nor apoptosis induction (Figure 2.3.3E). While we did observe that targeted downregulation of G6PD by shRNA significantly sensitized cells to DHA (Figure 1.3.3A), DHEA may not be an ideal compound for combination therapy given its high IC_{50} and myriad of other intracellular targets (141-143). We thus focused on the combination of our selective 6PGD inhibitor Physcion with DHA.

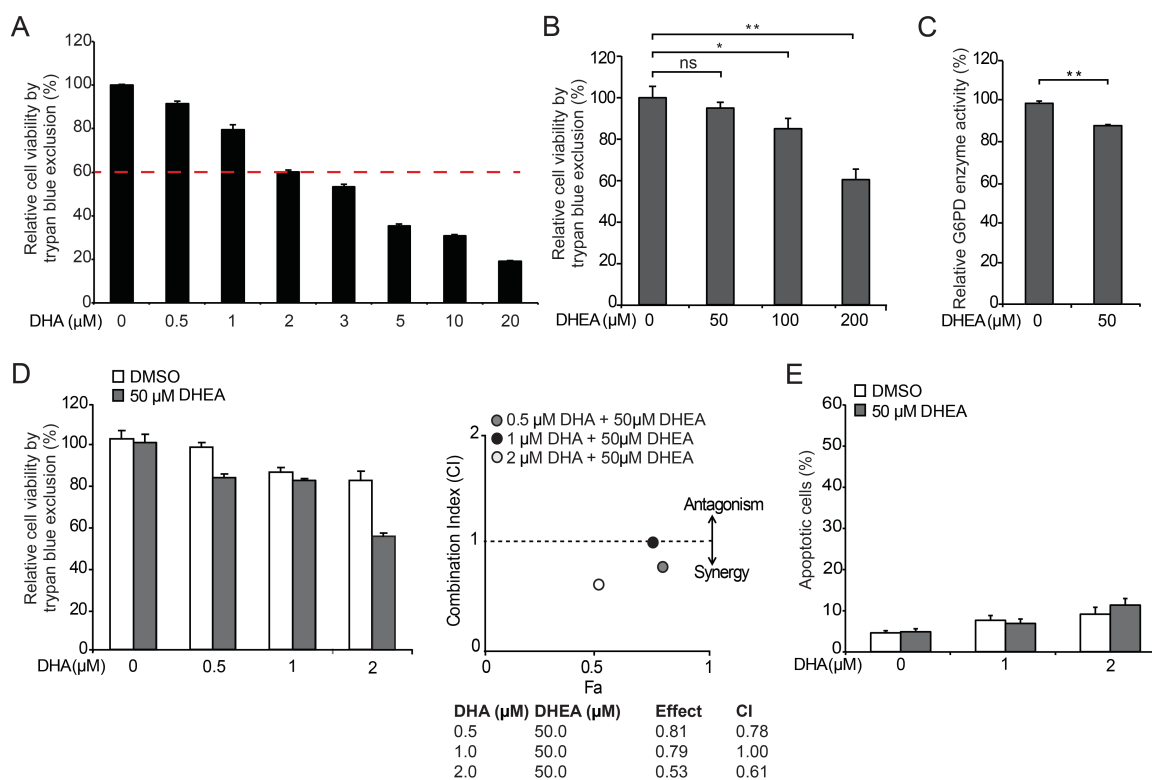


Figure 2.3.3. G6PD inhibitor DHEA in combination with DHA does not synergistically inhibit K562 cell viability. (A) Dose escalation in K562 cells with DHA to determine sub-lethal window ($\leq 40\%$ inhibition of cell viability) for combined treatment. (B) DHEA dose curve in K562 cells to determine concentration that would not cause significant cell death but could still significantly decrease G6PD activity (C). Combined treatment with DHEA + DHA does not lead to synergistic inhibition of cell viability in a dose dependent manner nor (E) significant induction of apoptosis. The combination index plot (D, right panel) shows the combination index (CI) for each drug combination. $CI < 1$ denotes synergy. The error bars represent mean values \pm SD from three replicates of each sample. p values were determined by two-tailed Student's *t* test (* $0.01 < p < 0.05$; ** $0.001 < p < 0.01$; ns, not significant).

Following our approach for DHEA dosing, we likewise performed dose escalation of inhibitor Phycion (Figure 3.3.3A) followed by 6PGD enzyme activity assay (Figure 3.3.3B) in K562 cells, and found 5 μ M Phycion to be an appropriate sub-lethal dose for 6PGD inhibition. Combined treatment of K562 cells with 5 μ M Phycion + sub-lethal doses of DHA did indeed induce synergistic inhibition of cell viability (Figure 3.3.3C), as well as significant induction of apoptosis compared to control untreated cells or cells treated with Phycion or DHA alone (Figure 3.3.3D).

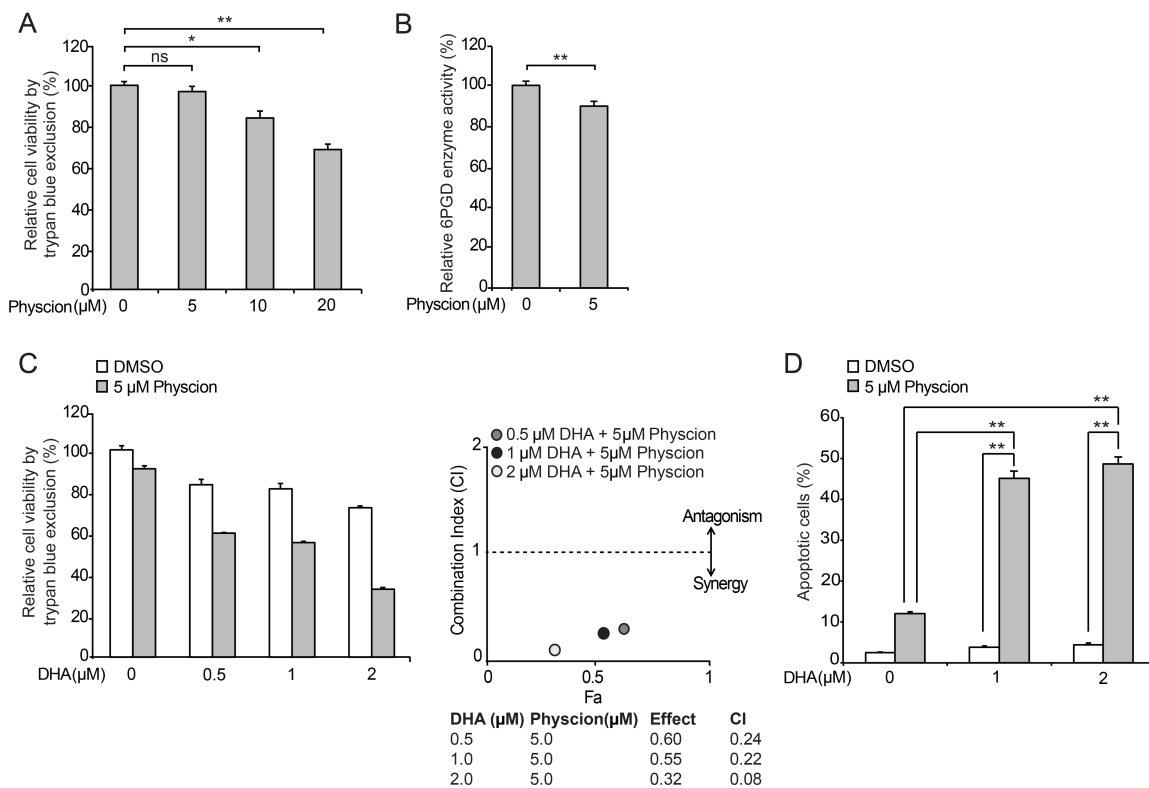


Figure 3.3.3. 6PGD inhibitor Physcion in combination with DHA leads to synergistic inhibition of K562 cell viability and induction of apoptosis. (A) Physcion dose curve in K562 cells to determine concentration that does not cause significant cell death but still significantly decreases 6PGD activity (B). (C) Combined treatment with Physcion + DHA leads to synergistic inhibition of cell viability in a dose dependent manner and (D) significant induction of apoptosis compared to control untreated cells and cells treated with Physcion or DHA alone. The combination index plot (C, right panel) shows the CI for each drug combination. $\text{CI} < 1$ denotes synergy. The error bars represent mean values +SD from three replicates of each sample. p values were determined by two-tailed Student's *t* test (* $0.01 < p < 0.05$; ** $0.001 < p < 0.01$; ns, not significant).

Combination treatment with Physcion + DHA leads to synergistic inhibition of cell viability in diverse human leukemia cell lines.

Heretofore, we established our combination treatment strategy in K562 erythroleukemia cells representative of BCR-ABL positive CML. In order to determine whether the combined treatment of Physcion + DHA shows general anti-leukemia activity, we tested this combination in diverse human leukemia cell lines. Among those tested were HEL erythroleukemia cells representative of Jak2 V617F positive MPN (Figure 4.3.3A), KG1a BM-derived myeloblast cells representative of FOP-FGFR1 positive AML (Figure 4.3.3B), and Molm14 PB-derived myeloblast cells representative of the FLT3-ITD positive acute monocytic leukemia subtype of AML (Figure 4.3.3C). In each cell line, we found that Physcion + DHA treatment induced synergistic anti-leukemia activity in a dose-dependent manner. This suggests that Physcion + DHA may represent a common anti-leukemia treatment strategy.

Furthermore, this suggests that while patients with 6PGD or G6PD deficiency are thought to experience hemolytic anemia as a result of oxidative damage due to the uncompensated role of the PPP in RBCs, another mechanism is likely at work in leukemia cells. Like all cancer cells, leukemia cells are well equipped to handle oxidative stress, and have several mechanisms in place for the maintenance of redox status in addition to the PPP. Furthermore, while we initially chose K562 cells to test our concept due to their erythroid nature, Molm14 and KG1a cells are myeloblast cells that have already diverged from the erythroid lineage, and thus no longer retain erythroid properties. This suggests that the mechanisms underlying the

synergistic action of Physcion + DHA combination treatment may differ from the mechanisms underlying non-immune hemolytic anemia, and may not depend primarily upon oxidative damage.

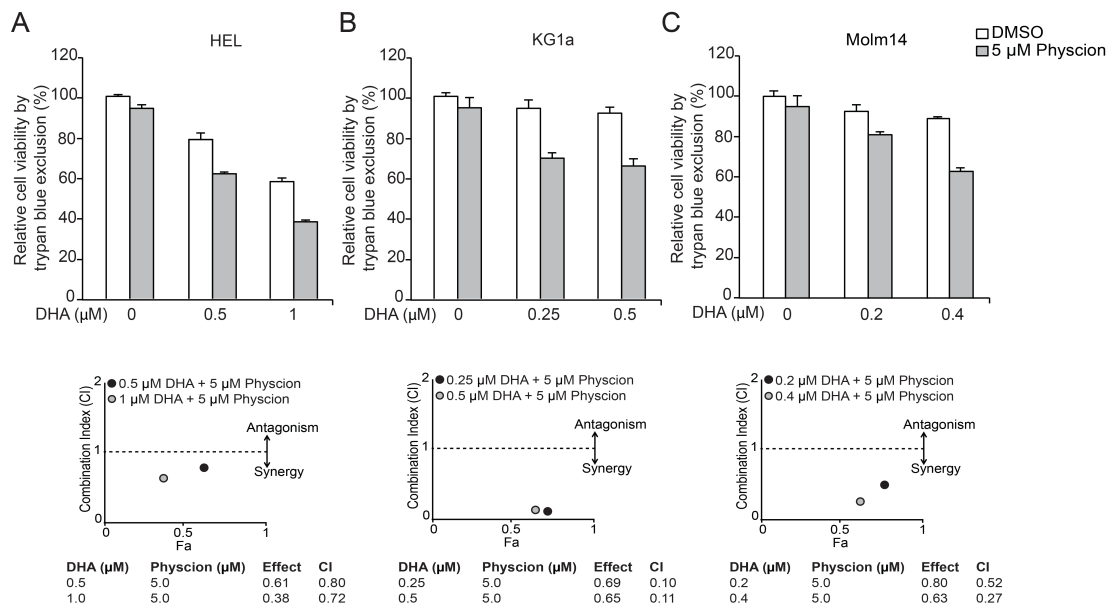


Figure 4.3.3. Combination treatment with Physcion + DHA leads to synergistic inhibition of cell viability in diverse human leukemia cell lines. Physcion + DHA combination treatment demonstrates synergistic inhibitory efficacy in diverse leukemia cell lines, including HEL erythroleukemia cells representative of Jak2 V617F positive MPN (A), KG1a bone marrow-derived myeloblast cells representative of FOP-FGFR1 positive AML (B), and Molm14 PB-derived myeloblast cells representative of the FLT3-ITD acute monocytic leukemia subtype of AML (C). The combination index plots (*lower panels*) show the CIs for each drug combination. $\text{CI} < 1$ denotes synergy.

Synergistic inhibition of cell viability in K562 leukemia cells treated with Physcion + DHA is mediated in part by activation of AMPK.

Indeed, while we did find increased ROS levels in K562 cells treated with Physcion + DHA compared to cells treated with Physcion or DHA alone, neither cell viability nor apoptosis could be rescued with antioxidant NAC treatment suggesting that oxidative damage is not principally responsible for the decreased cell viability observed in Physcion + DHA treated cells (Figure 5.3.3).

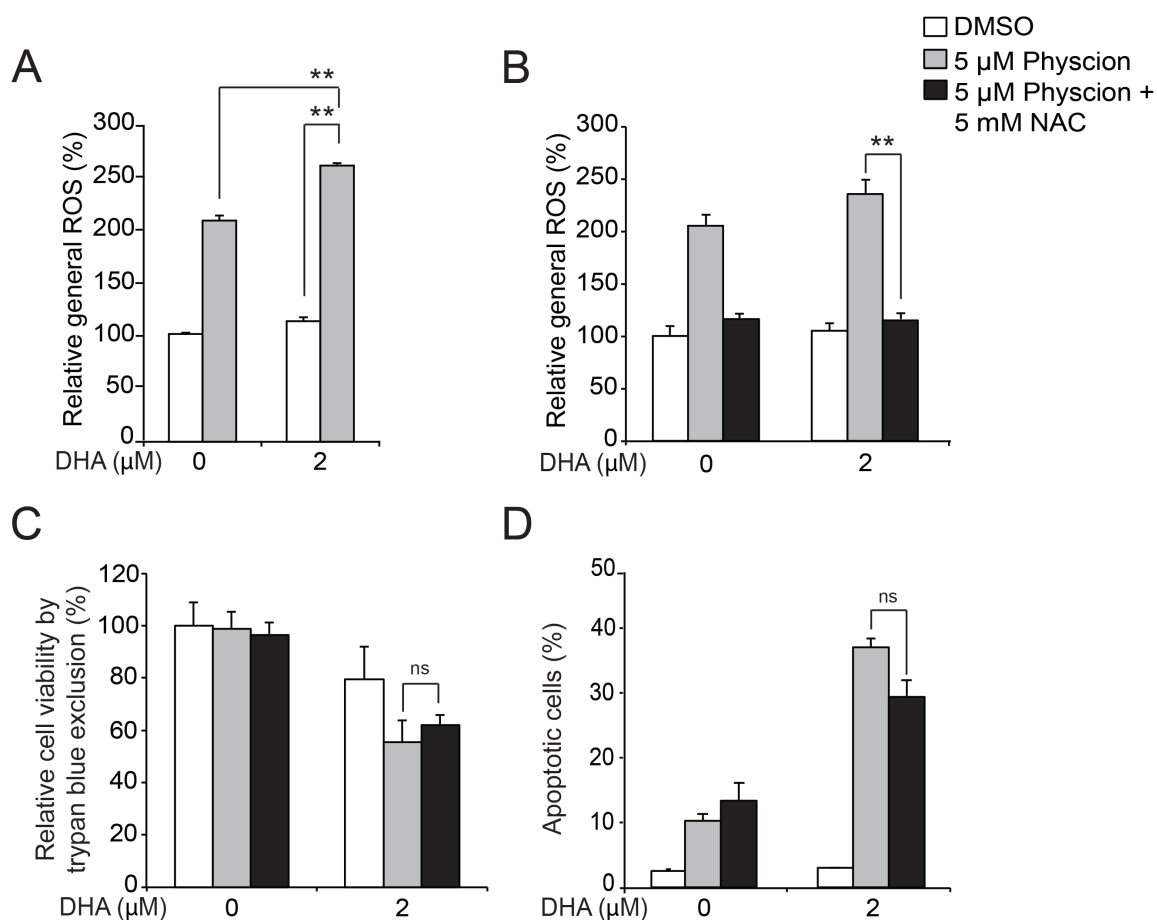


Figure 5.3.3. Synergistic inhibition of cell viability in K562 leukemia cells treated with Physcion + DHA is mediated in part by activation of AMPK. (A) General ROS levels are significantly increased in K562 cells treated with Physcion + DHA compared to K562 cells treated with Physcion or DHA alone. (B) Treatment with 5 mM NAC significantly reduces general ROS levels back to baseline in K562 cells treated with Physcion + DHA. (C) Treatment with 5 mM NAC does not rescue the decreased viability in K562 cells treated with Physcion + DHA. (D) Treatment with 5 mM NAC does not rescue Physcion + DHA-treated K562 cells from apoptotic cell death. The error bars represent mean values +SD from three replicates of each sample. *p* values were determined by two-tailed Student's *t* test (*0.01 < *p* < 0.05; **0.001 < *p* < 0.01; ns, not significant).

Interestingly, several of the medications known to induce hemolysis in dehydrogenase deficient patients have been shown to function through shared mechanisms, including inhibition of cyclooxygenase (COX) gene expression and/or activation of AMPK (144-147). To investigate the mechanism underlying Physcion + DHA induced synergy, we first examined gene expression of COX2 in Physcion + DHA treated K562 cells. We found that COX2 mRNA and protein levels were unaltered in Physcion + DHA treated cells compared to control untreated cells or cells treated with Physcion or DHA alone (data not shown).

Our previous studies on 6PGD demonstrated that targeted downregulation of 6PGD by shRNA or Physcion treatment leads to AMPK activation by alleviating Ru-5-P-mediated inhibition of AMPK upstream kinase LKB1. Although the intracellular targets of DHA remain poorly understood, we postulated that Physcion and DHA may activate AMPK via distinct mechanisms, leading to synergistically increased AMPK activation levels and consequently synergistic inhibition of cell viability. We thus assessed AMPK activation as measured by T172 phosphorylation levels in K562 cells treated with Physcion + DHA (Figure 6.3.3A). We found that while sub-lethal concentrations of Physcion and DHA alone were unable to induce detectable levels of active AMPK, combined treatment led to substantially increased AMPK phosphorylation levels. This indicates that AMPK activation may play a role in mediating the synergistic effects observed in Physcion + DHA treated cells.

To further dissect the role of AMPK in Physcion + DHA induced inhibition of cell viability, we generated K562 cells with stable KD of AMPK. We found that KD of AMPK could significantly rescue cell viability in Physcion + DHA treated K562 cells (Figure 6.3.3B). Moreover, treatment of K562 cells with a sub-lethal concentration of AMPK inhibitor Compound C similarly renders cells significantly resistant to Physcion + DHA treatment (Figure 6.3.3C). Together, these data suggest that the inhibitory effects on cell viability induced by Physcion + DHA are mediated at least in part by AMPK.

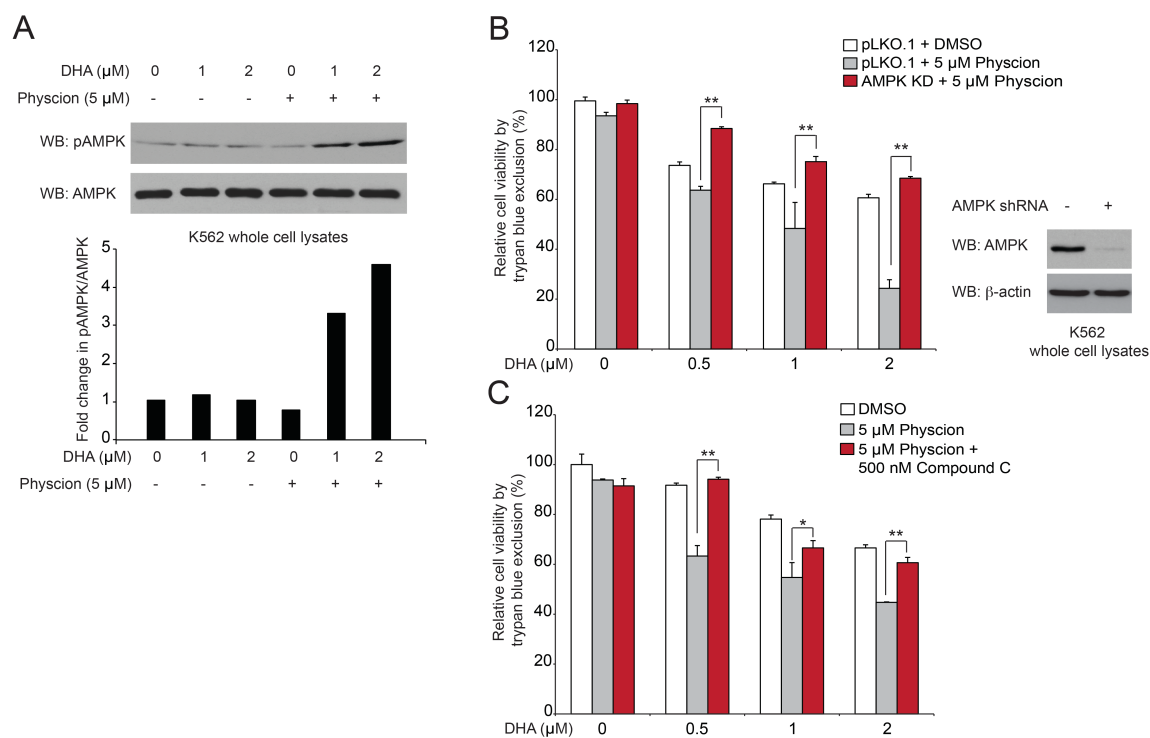


Figure 6.3.3. Synergistic inhibition of cell viability in K562 leukemia cells treated with Physcion + DHA is mediated in part by activation of AMPK. (A) AMPK activation, as assessed by phosphorylation of AMPK at T172, is increased in K562 cells treated with Physcion + DHA compared to Physcion or DHA treatment alone. (B) Stable KD of AMPK renders cells significantly less sensitive to Physcion + DHA treatment compared to vector control cells. Stable KD of AMPK was confirmed by Western blot. (C) Treatment with AMPK inhibitor Compound C significantly rescues the synergistic inhibition of cell viability in Physcion + DHA treated K562 cells. The error bars represent mean values +SD from three replicates of each sample. *p* values were determined by two-tailed Student's *t* test (*0.01 < *p* < 0.05; **0.001 < *p* < 0.01).

Combination treatment with Physcion + AMPK activator A769662 leads to synergistic inhibition of cell viability in diverse human leukemia cell lines.

We next sought to expound upon our observation that the synergistic inhibition of cell viability observed in Physcion + DHA treated cells is mediated through AMPK activation. To further develop this concept, we established a second combinatorial treatment utilizing AMPK activator A769662. A769662 directly activates AMPK by mimicking AMP, thus leading to allosteric activation and inhibition of dephosphorylation at T172 (148). The effects of A769662 are independent of the upstream kinase utilized, thus representing a mechanism of AMPK activation that is distinct from 6PGD inhibition. We therefore reasoned that combined treatment with Physcion + A769662 may induce synergistic inhibition of cell viability in a manner similar to Physcion + DHA. Indeed, we found that treatment with Physcion + A769662 led to markedly increased AMPK activation compared to Physcion or A769662 alone (Figure 7.3.3A), as well as a synergistic decrease in cell viability (Figure 7.3.3B) and significant apoptosis induction (Figure 7.3.3C). Moreover, we found this combination treatment to be similarly effective in diverse leukemia cell lines including HEL (Figure 7.3.3D), KG1a (Figure 7.3.3E), and Molm14 (Figure 7.3.3F).

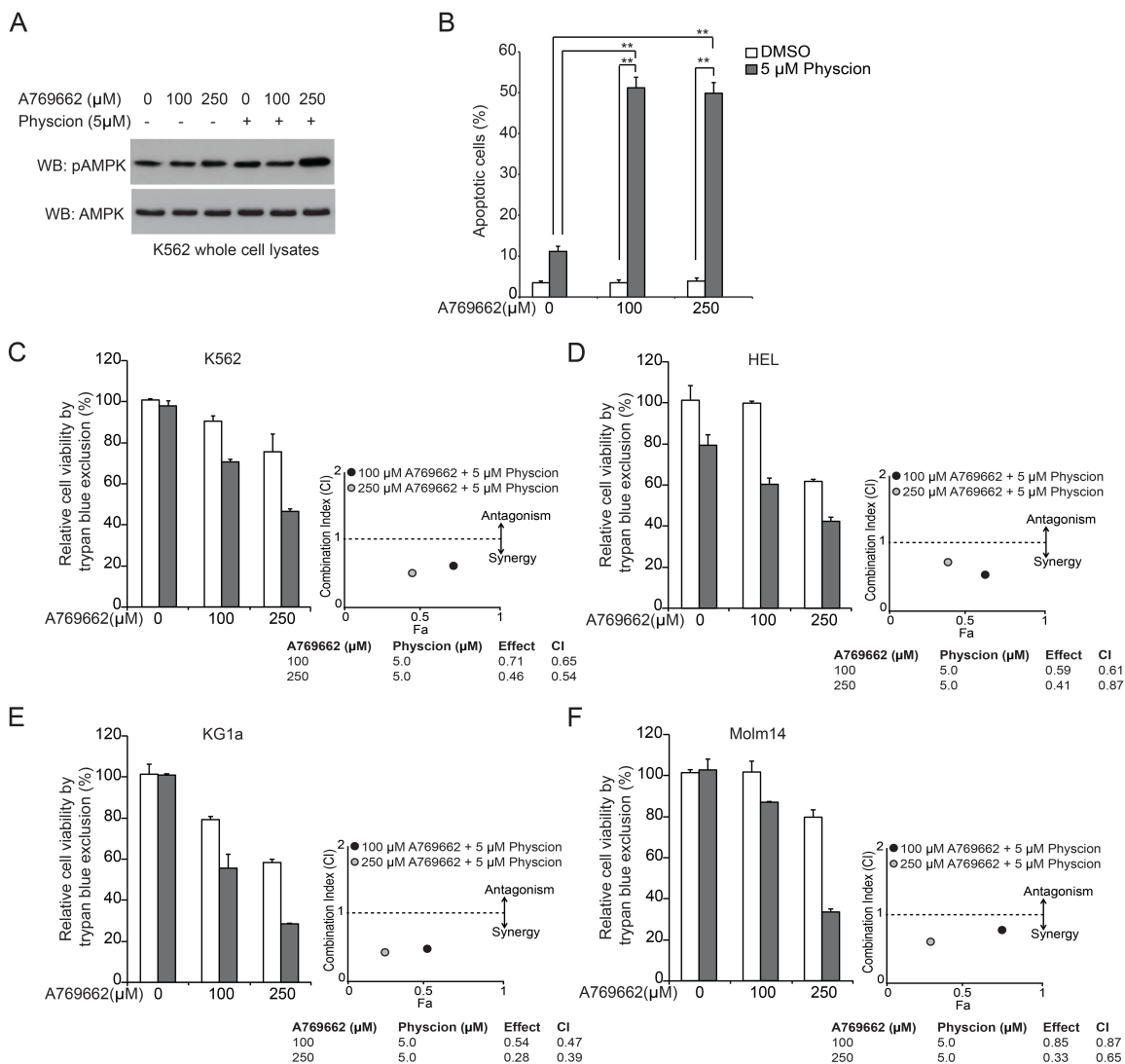


Figure 7.3.3. Combination treatment with Physcion + AMPK activator A769662 leads to synergistic inhibition of cell viability in diverse human leukemia cell lines. (A) AMPK activation, as assessed by phosphorylation of AMPK at T172, is increased in K562 cells treated with Physcion + A769662 compared to Physcion or A769662 treatment alone. (B) K562 cells treated with Physcion + A769662 exhibit significantly increased apoptosis induction (C) synergistically decreased cell viability. (D-F) Physcion + A769662 combination treatment demonstrated synergistic inhibitory efficacy in diverse leukemia cell lines, including Jak2 V617F positive HEL erythroleukemia cells representing MDS (D), FOP-FGFR1 positive KG1a cells representing AML, (E), and FLT3-ITD positive Molm14 blast cells representing the acute monocytic leukemia subtype of AML (F). The combination index plots (C-F, right panels) show the combination index (CI) for each drug combination. The error bars represent mean values \pm SD from three replicates of each sample. p values were determined by two-tailed Student's *t* test (* $0.001 < p < 0.01$). CI <1 denotes synergy.

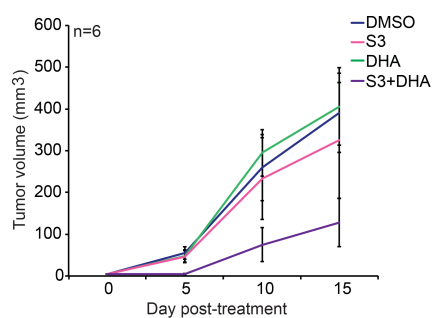
Physcion derivative S3 in combination with DHA induces anti-leukemia activity *in vivo* in a K562 leukemia cell xenograft model.

We next performed an *in vivo* drug treatment experiment using Physcion derivative S3 + DHA. Initial toxicity studies by chronic injection of S3 + DHA to nude mice for 30 days revealed that 5 mg/kg/day S3 + 2.5 mg/kg/day DHA administered intraperitoneally is a well-tolerated dose. We found that continuous treatment with 5 mg/kg/day S3 + 2.5 mg/kg/day DHA did not significantly alter body weight or the hematopoietic properties of nude mice. Importantly, we observed that both hemoglobin (Hb) and RBC levels fell within the normal range in mice treated with S3 + DHA, suggesting no evidence of RBC damage (Figure 8.3.3A). These results demonstrate that S3 + DHA combination treatment has minimal toxicity *in vivo*. We next performed *in vivo* drug treatment using a xenograft model in which nude mice were subcutaneously injected with K562 cells on the right flank. Three days post-injection, mice were randomly divided into four groups and treated with DMSO, S3 (5 mg/kg/day), DHA (2.5 mg/kg/day), or S3 + DHA (5 mg/kg/day + 2.5 mg/kg/day) for 15 days. S3 + DHA treatment resulted in significantly decreased K562 leukemia cell-derived tumor growth (Figure 8.3.3B) and masses (Figure 8.3.3C) compared to tumors derived from mice treated with DMSO, S3, or DHA alone. Moreover, tumor cell lysates from S3 + DHA treated mice demonstrated increased levels of pAMPK compared to DMSO, S3 or DHA treated mice (Figure 8.3.3D), suggesting that S3 + DHA-mediated attenuation of tumor growth is mediated at least in part by AMPK activation *in vivo*.

A

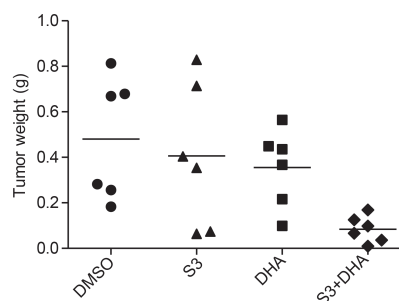
Test name	Normal range	DMSO (mean)	5 mg/kg/day S3 (mean)	2.5 mg/kg/day DHA (mean)	S3 + DHA (mean)
WBC (K/ μ L)	1.8-10.7	6.5 \pm 0.53	6.6 \pm 0.69	7.2 \pm 1.37	9.4 \pm 1.12
LYM (K/ μ L)	0.9-9.3	3.2 \pm 0.86	3.6 \pm 0.04	4.3 \pm 1.27	4.8 \pm 1.14
MONO (K/ μ L)	0.0-0.4	0.24 \pm 0.16	0.3 \pm 0.13	0.2 \pm 0.03	0.3 \pm 0.15
GRAN (K/ μ L)	0.1-2.4	2.8 \pm 0.81	2.6 \pm 0.84	2.6 \pm 0.54	4.1 \pm 0.23
HCT (%)	35.1-45.4	49.7 \pm 4.17	42.6 \pm 8.08	52.9 \pm 4.2	46.6 \pm 5.72
MCV (fL)	45.4-60.3	59.0 \pm 1.57	59.3 \pm 1.1	59.7 \pm 2.13	60.4 \pm 2.23
RDW _a (%)	12.4-27.0	15.6 \pm 0.26	15.5 \pm 0.21	15.7 \pm 0.49	17.3 \pm 0.26
Hb (g/dL)	11.0-15.1	12.9 \pm 1.25	11.1 \pm 2.48	13.5 \pm 0.85	11.8 \pm 1.70
MCHC (g/dL)	30.2-34.2	26.1 \pm 0.62	25.8 \pm 1.04	25.5 \pm 0.52	25.3 \pm 1.50
RBC (M/mL)	6.36-9.42	8.4 \pm 0.50	7.2 \pm 1.27	8.9 \pm 0.92	7.7 \pm 0.67
MCH (pg)	14.1-19.3	15.4 \pm 0.52	15.3 \pm 0.89	15.2 \pm 0.67	15.3 \pm 1.00
PLT (K/ μ L)	592-2972	905.3 \pm 198	991.7 \pm 117	985 \pm 38.6	1120 \pm 488.09
MPV (fL)	5.0-20.0	5.5 \pm 0.26	5.7 \pm 0.26	5.2 \pm 0.06	6.2 \pm 0.72

B



Treatment	p value	Significance
DMSO versus combination	0.01	*
S3 versus combination	0.04	*
DHA versus combination	0.04	*
DMSO versus S3	0.31	ns
DMSO versus DHA	0.46	ns

C



Treatment	p value	Significance
DMSO versus combination	0.002	**
S3 versus combination	0.017	*
DHA versus combination	0.002	**
DMSO versus S3	0.337	ns
DMSO versus DHA	0.179	ns

D

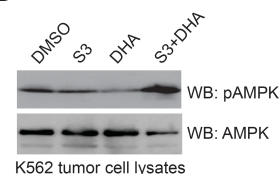


Figure 8.3.3. S3 + DHA combination treatment results in significantly attenuated leukemia K562 cell tumor growth *in vivo*. (A) Athymic nude mouse hematology. Nude mice were treated with vehicle control, S3 alone (5 mg/kg/day), DHA alone (2.5 mg/kg/day), or S3+DHA for 30 days. CBC analysis shows no significant difference in the hematopoietic properties between the two groups of mice. Notably, hemoglobin (Hb) and RBC levels were within the normal range, suggesting that the combination treatment does not induce hemolytic anemia at the whole organism level. (B-C) Tumor growth (B) and tumor size (C) in xenograft nude mice injected with K562 cells were compared between groups of mice treated with vehicle control, 5 mg/kg/day S3, 2.5 mg/kg/day DHA, or S3 + DHA. (D) Western blot analysis of resected tumors from representative vehicle control and drug treated mice shows increased AMPK activation, as assessed by T172 phosphorylation, in tumor lysates derived from combination treated mice compared to vehicle control or single-drug treated mice. . p values were determined by two-tailed Student's *t* test (*0.01 < p < 0.05; **0.001 < p < 0.01; ns, not significant).

Physcion + DHA shows anti-leukemia activity in primary leukemia cells from human patients.

Finally, we found that Physcion + DHA treatment significantly inhibited viability of primary leukemia cells from patients with diverse types and subtypes of leukemia (Figure 9.3.3A), including the acute promyelocytic leukemia (APL) subtype of AML, AML, and CML. In contrast, neither drug alone nor the combination affected cell viability of mononucleocytes (WBC) or RBCs isolated from the PB of healthy human donors (Figure 9.3.3B), suggesting promising anti-leukemia potential with minimal toxicity to human blood cells. The results of these translational studies suggest that the novel combination of selective 6PGD inhibitors Physcion and S3 with DHA represents a promising therapeutic strategy for treatment of human leukemia.

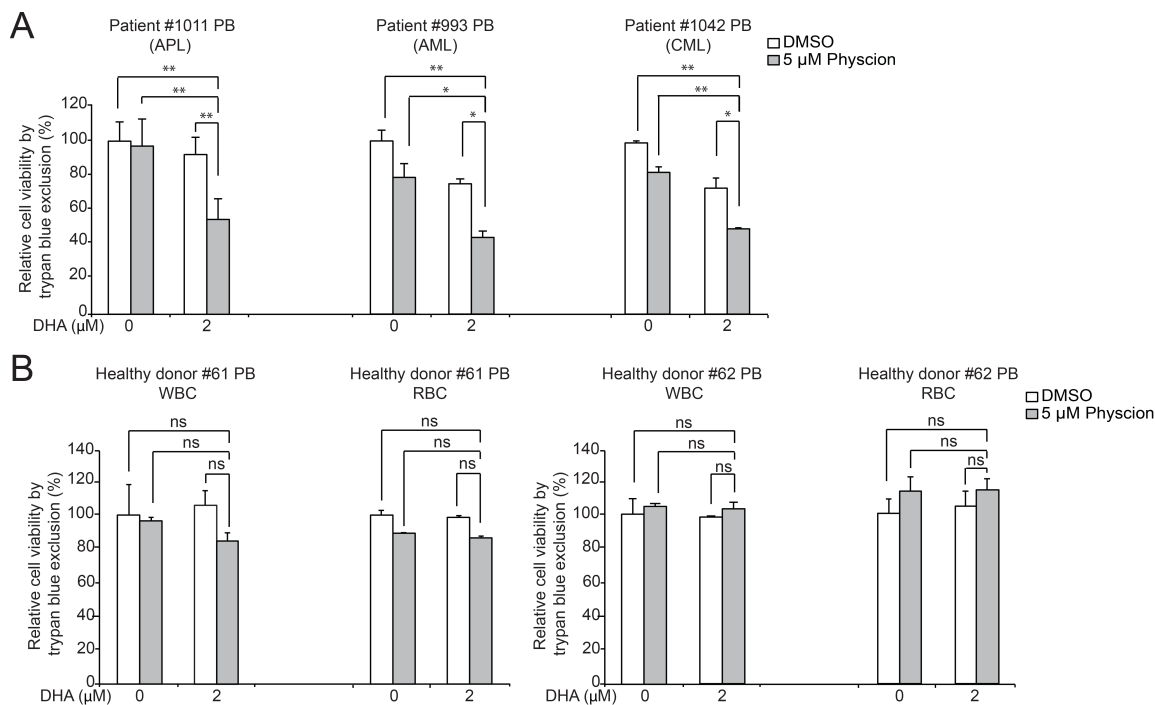


Figure 9.3.3. Physcion + DHA leads to significant inhibition of cell viability in primary leukemia cells from human patients with a spectrum of disease types. (A) Effects of combined Physcion + DHA treatment on cell viability of human primary leukemia cells isolated from representative APL, AML, and CML patients. (B) Combined Physcion + DHA treatment does not affect viability of mononucleocytes or RBCs isolated from the PB of representative healthy human donors. The error bars represent mean values +SD from three replicates of each sample. p values were determined by two-tailed Student's *t* test (*0.01 < p < 0.05; **0.001 < p < 0.01; ns, not significant).

3.3.4. Discussion

Taken together, our findings suggest that inhibition of the oxidative PPP by targeting G6PD or 6PGD sensitizes leukemia cells to anti-malarial agent DHA. Moreover, we developed a novel treatment strategy using our own selective 6PGD inhibitors Physcion or S3 combined with DHA, which demonstrates synergistic anti-leukemia activity in diverse human leukemia cell lines and primary leukemia cells from patients, as well as in leukemia xenograft mice *in vivo*.

Our combination strategy was devised to “hijack” the concept behind drug-induced hemolysis in 6PGD and G6PD deficient patients and utilize it against leukemia cells. Importantly, we were able to establish an optimal dosing window for our drug combination that selectively and synergistically killed leukemia cells but left RBCs unscathed. The increased sensitivity of leukemia cells to this drug combination may be partially due to the fact the leukemia cells are highly proliferative and rely heavily on anabolic biosynthesis with elevated oxidative PPP flux compared to normal hematopoietic cells, including RBCs. Developing erythroprotective treatment strategies is of paramount importance for leukemia patients in particular, as they are already at risk of developing anemia due to the “crowding out” of RBCs upon the accumulation of leukemic cells in the blood and bone marrow.

While 6PGD and G6PD deficient red cells are likely destroyed upon exposure to anti-malarial drugs due to unopposed oxidative damage, our findings suggest that

another mechanism underlies Physcion + DHA-mediated leukemia cell death. We demonstrated that K562 leukemia cells treated with Physcion + DHA exhibit markedly increased levels of AMPK activation compared to cells treated with Physcion or DHA alone. Downregulation of AMPK activity by shRNA or Compound C treatment renders cells significantly less sensitive to Physcion + DHA treatment, suggesting that AMPK is the predominant effector to mediate Physcion + DHA-induced cell death. While the intracellular targets of DHA remain unclear, our own 6PGD studies demonstrated that inhibition of 6PGD leads to activation of AMPK by alleviating 6PGD product Ru5P-dependent inhibition of AMPK upstream kinase LKB1. Several possibilities exist to explain the mechanism by which Physcion + DHA converge to increase AMPK activation: Physcion and DHA may synergistically activate LKB1, or DHA may activate an alternative upstream kinase to AMPK. Alternatively, DHA may inhibit an AMPK phosphatase, preventing dephosphorylation at T172. The mechanism by which DHA activates AMPK certainly warrants further exploration.

Our translational studies suggest that Physcion + DHA may represent a promising pan-leukemia therapy with minimal off-target toxicity, as this combination was observed to be efficacious in various leukemia disease types without affecting viability of blood cells from healthy donors. In G6PD and 6PGD deficient patients, hemolysis of RBCs occurs episodically, and consequently does not present as a sustained complication in most cases. We thus acknowledge that patients undergoing this combination treatment would need to have RBC counts carefully

monitored to ensure the absence of hemolytic episodes. However, it is important to note that complete blood counts of mice treated with S3 + DHA were monitored weekly over the course of 30 days with no evidence of RBC destruction. These translational studies provide “proof of principle” to suggest the novel combination of 6PGD inhibition + DHA as a promising therapy in clinical treatment of human leukemias.

While the development of this combinatorial anti-leukemia treatment strategy began as a lesson learned from non-immune hemolytic anemia, our findings in turn shed light on the molecular mechanisms that may trigger hemolytic anemia in 6PGD and G6PD deficient patients. Our studies suggest that, in addition to a diminished capacity for oxidative damage, activation of AMPK may also contribute to hemolysis. In mice, AMPK has been shown to play an important role in preserving RBC integrity and lifespan, with targeted deletion of the catalytic alpha-1 subunit leading to defective red cell maturation, structural abnormalities, and increased red cell destruction (149-150). However, little is known about the effect of AMPK activation on RBCs. It is worth exploring whether 6PGD and G6PD deficient RBCs exhibit increased AMPK activation, and whether this increase is potentiated in response to anti-malarial drugs or aspirin. This would be particularly important for 6PGD and G6PD deficient patients undergoing treatment with known AMPK activators, including anti-diabetic drug metformin. Conversely, this indicates that treatment with sub-lethal doses of anti-malarials may represent a powerful anti-cancer strategy in leukemia patients with G6PD or 6PGD deficiency.

Chapter 4: Discussion

4.1. Summary

The past several decades have seen tremendous progress in the treatment of leukemia, particularly due to the introduction of BCR-ABL inhibitors for the treatment of CML, which has improved survival rates for CML patients nearly three-fold (151). Nonetheless, the “magic bullet” to cure leukemia remains elusive. Resistance to BCR-ABL inhibitors remains a significant clinical problem, even with the advent of second and third generation derivatives. Moreover, while CML is a largely homogenous disease with 95% of patients exhibiting BCR-ABL mutations, AML, ALL, and CLL are quite heterogeneous, with more complicated molecular and cytogenetic features, and thus have yet to benefit from such pathway-directed therapy. Despite the Herculean efforts involved in advancing leukemia therapies during the 60 years, from the advent of bone marrow transplantation in the 1950s, to the discovery and development of Gleevec® in 2001, to sequencing the AML genome in 2008, we have yet to come upon therapies that can treat leukemia as one disease. This requires the identification of targets common to the leukemic cell, whether myeloid or lymphoid, acute or chronic.

In this work, we sought to develop pan-leukemia therapies by targeting leukemogenic signal transduction and leukemia cell metabolism. Our approach for targeting leukemogenic signal transduction involved identifying common

downstream effectors of discrete LTKs associated with distinct leukemia disease types. Guided by our phospho-proteomics studies that identified p90RSK2 as a downstream effector of FGFR3-related hematopoietic malignancies, we examined whether RSK2 may be a common substrate among diverse LTK signaling pathways. Indeed, we found RSK2 to be activated by multiple LTKs, including CML-associated BCR-ABL and AML-associated FLT3-ITD. However, murine BMT assays revealed that while RSK2 is indeed required for FLT3-ITD-induced myeloid transformation, it is dispensable for BCR-ABL-induced myeloproliferative neoplasm in mice. Likewise, targeting RSK2 with selective RSK inhibitor fmk in FLT3-ITD positive cell lines and AML patient samples caused significant cell death, but didn't affect viability of BCR-ABL positive cell lines or patient samples, further suggesting that RSK2 is a promising therapeutic target for FLT3-ITD positive AML, but not BCR-ABL positive CML. Together, these data demonstrate that while LTK signaling may converge upon common downstream substrates, the requirement of those substrates for malignant transformation, cell proliferation, and survival can differ quite substantially.

While our phospho-proteomics studies showed a number of additional kinases as being phosphorylated by OTKs, numerous enzymes involved in cellular metabolism were also identified. Pursuant to the recent revival of Otto Warburg's tumor cell metabolism hypothesis, we sought to evaluate leukemia cell metabolism as an anti-leukemia targeting strategy. This permitted us to focus on a phenomenon potentially more common to leukemia cells as whole, rather than particular genetic features associated with distinct leukemia disease types. Of the metabolic enzymes

we found to be tyrosine phosphorylated by LTKs, we were particularly interested in glycolytic enzyme PGAM1 due to unique position as at the branching point between glycolysis and anabolic biosynthetic pathways, and its marked upregulation in leukemia and other cancers. We screened and characterized a novel PGAM1 inhibitor, PGMI-004A, which was effective in inhibiting proliferation of diverse leukemia cell lines and primary cells from patients with both myeloid and lymphoid leukemias. We also characterized the *in vivo* efficacy of PGMI-004A, and found it to significantly attenuate tumor growth in xenograft mice with minimal toxicity to the hematopoietic system and vital organ homeostasis.

Our PGAM1 studies established a novel link between glycolysis and the oxidative pentose phosphate pathway in which PGAM1 substrate 3-PG competitively inhibits 6PGD in the oxidative PPP. This subsequently drew our attention to 6PGD as an additional target for anti-leukemia therapy. We found that while 6PGD expression is not upregulated in leukemia, its activity is significantly increased due to acetylation at two distinct lysine sites. We screened and characterized 6PGD inhibitor Physcion and its derivative S3, both of which effectively decreased leukemia cell viability in cell lines and primary cells from patients with distinct disease types. Moreover, we found that *in vivo* treatment with S3 attenuated leukemia cell-derived tumor growth in xenograft mice with minimal toxicity off-target toxicity.

In investigating the potential side effects that may be involved in anti-6PGD therapy, we learned that genetic deficiency of both 6PGD and G6PD have been identified in

humans, with the latter representing the most common human enzyme defect in the world. Patients with these genetic deficiencies are typically asymptomatic, but can experience episodes of hemolytic anemia upon exposure to certain triggers, including aspirin and anti-malarial drugs. We attempted to translate this concept into a novel combinatorial anti-leukemia therapy using our selective 6PGD inhibitors and anti-malarial drug DHA. We found that indeed, targeting 6PGD in combination with DHA exposure leads to synergistic inhibition of cell viability in diverse leukemia cell lines. We also found that combination treatment of primary cells from leukemia patient samples with different disease types led to a significant decrease in cell viability, but didn't affect isolated WBCs or RBCs from healthy human donors. In a leukemia cell xenograft model, we found that our combination treatment strategy led to significantly attenuated tumor growth with minimal toxicity to hematopoietic cells and vital organs, and induced no evidence of RBC destruction. This suggests that combining 6PGD inhibitors with anti-malarials may represent a common anti-leukemia treatment strategy without inducing hemolytic anemia.

Collectively, this work represents an effort to identify novel strategies to target leukemia as one disease rather than by disease type. Importantly, our initial studies on leukemogenic signal transduction identified critical differences in the signaling properties of LTKs despite transmission through a mutual downstream substrate, reminding us that apparent commonalities do not promise a functionally overlapping target. In general however, our pre-clinical, translational studies using

a vast array of leukemia patient samples demonstrate the potential effectiveness of our targeting strategies in human patients irrespective of disease type. Though we can't yet rule out the potential adverse effects of these compounds on overall human health and homeostasis, our use of *in vivo* drug treatment models and healthy human PB and bone marrow cells serves to demonstrate that our compounds exhibit minimal off-target toxicity.

4.2. Future Directions

While our studies have established a broad spectrum of novel therapeutic approaches for leukemia treatment, numerous avenues remain to be explored.

Certainly, efforts to target leukemogenic signal transduction have been underway for quite some time, and have successfully introduced targeted therapies to the clinic. However, moving forward, identifying common effectors of diverse leukemogenic signaling pathways will not only promote a shift from disease-type specific therapy towards the development of pan-leukemia therapies, but will help overcome common obstacles associated with small molecule TKI treatment, including drug resistance and adverse side effects. Our phospho-proteomics studies alone reveal multiple additional hits that could potentially represent targetable convergence points among diverse leukemogenic signaling pathways.

Within our studies on RSK2, several questions remain. First, a number of additional leukemia cell lines expressing different leukemogenic tyrosine kinases and representing different disease types demonstrated RSK2 activation but were unexplored in this work. Among those were EOL-1 that expresses FIP1L1-PDGFR α fusion tyrosine kinase and is associated with idiopathic HES, and HEL that expresses the constitutively active JAK2 V617F mutant and is associated with MPN. This suggests that RSK2 may still represent a common therapeutic target among leukemias transformed by different leukemogenic tyrosine kinases, despite the fact that BCR-ABL positive CML is not among them. It is worth investigating the role of RSK2 in FIP1L1-PDGFR α positive HES and Jak2 V617F positive MPN to determine whether RSK2 may represent a therapeutic target for treatment of these diseases in addition to FLT3-ITD positive AML.

Moreover, understanding the molecular mechanisms underlying RSK2-mediated transformation and myeloid lineage determination in FLT3-ITD positive leukemias would help further the development of anti-RSK2 as a therapeutic approach for FLT3-ITD positive AML. Examining the frequency of hematopoietic progenitor populations as well as myeloid colony forming ability in FLT3-ITD transformed WT versus RSK2 KO bone marrow cells would provide initial insight into the role of RSK2 as a myeloid lineage determinant. Additionally, RSK2 has been shown to phosphorylate and inactivate GSK3, which in turn prevents degradation of β -catenin. Under conditions of GSK3 inhibition, β -catenin translocates from the cytosol to the nucleus where it regulates transcription of growth promoting genes as well as

self-renewal of leukemia stem cells (LSCs). Loss of β -catenin has been shown to impair the self-renewal of normal and CML stem cells, which leads to a profound reduction in the ability of mice to develop BCR-ABL-induced CML, while allowing progression of B-ALL (152). A similar mechanism may be at work in FLT3-ITD-induced AML, and it is thus worth exploring whether RSK2 regulates β -catenin in LSCs and/or myeloid progenitors, but not lymphoid progenitors, to mediate FLT3-ITD-induced myeloid leukemia. This would provide a more comprehensive understanding of the FLT3-ITD/RSK2-regulated myeloid transforming network in FLT3-ITD positive AML, and may potentially reveal additional strategies for therapeutic intervention.

In contrast to leukemogenic signal transduction, the therapeutic potential of targeting leukemia cell metabolism has yet to be fully ascertained. The major concern associated with targeting cancer cell metabolism lies in the fact that all cells utilize the same life-sustaining metabolic networks, and disruption of any of these metabolic processes has the potential to adversely affect cancer cells and normal cells alike. Most metabolic enzymes implicated in the pathogenesis of cancer are not mutated, and are expressed both in transformed cells and normal cells throughout the body. This presents a considerable set of challenges with regard to achieving specificity in targeting cancer cells versus normal cells. However, the altered metabolism in cancer cells does provide a window for therapeutic intervention. Though most metabolic enzymes are not mutated in cancer, there is increasing evidence to suggest that many are aberrantly regulated by oncogenes, which can in

turn create addictions to specific metabolic pathways (53). Dissecting how oncogenes regulate metabolic enzymes and pathways will certainly provide insight into potential therapeutic strategies that exploit the altered metabolism in leukemia cells. For instance, our PGAM1 studies demonstrate that leukemogenic tyrosine kinases serve to enhance PGAM1 activation, which contributes to enhanced cancer cell proliferation and tumor growth through effects on the glycolytic pathway, the oxidative PPP, and the serine biosynthesis pathway. Our 6PGD studies have yet to identify the upstream oncogenic signals that regulate the acetyltransferases and deacetylase that in turn modulate 6PGD activity, but preliminary studies show that both DLAT and ACAT2 display increased protein expression in leukemia cell lines expressing diverse leukemogenic tyrosine kinases compared to normal proliferating cells. Indeed, this merits future studies to identify the leukemogenic pathways that regulate DLAT, ACAT2, and HDAC4 activity.

Despite the growing host of potential therapeutic targets in leukemia cell metabolism, drug discovery and development efforts are still in their infancy. Currently, the IDH inhibitors developed by Agios Pharmaceuticals (51, 153) represent the only targeted therapy against leukemia metabolism poised to enter clinical trials. While this is a tremendous advance for leukemia patients harboring IDH mutations, it again represents a mutation-type specific therapy that is not broadly applicable to the altered metabolism of all leukemias, regardless of mutation status or disease type. Though both our PGAM1 and 6PGD inhibitors were broadly effective across leukemia types and subtypes, a number of additional

directions remain. PGMI-004A, Physcion, and S3 would all benefit from structure-activity relationship (SAR) studies to improve both solubility and potency. Physcion in particular, though effective in providing proof-of-concept that 6PGD represents a promising anti-leukemia target alone and in combination therapy, is quite insoluble due to its hydrophobic nature, and displays relatively weak affinity for 6PGD. Both limitations could be improved by SAR studies. Furthermore, our 2,000 compound library possesses inherent shortcomings due to its small size, and certainly much more comprehensive libraries (up to ~300,000 compounds) are available. Screening larger libraries will facilitate the identification of additional small molecule PGAM1 and 6PGD inhibitors, which will allow for further development of anti-PGAM1 and anti-6PGD as therapeutic strategies in leukemia treatment.

In addition to monotherapies targeting single metabolic enzymes or pathways, there are a number of novel combinatorial strategies that have yet to be explored. In accordance with mimicking the concept of drug-induced hemolytic anemia in G6PD and 6PGD deficient patients, several possibilities remain. In addition to DHA, G6PD and 6PGD deficient patients are intolerant to various other compounds that have been shown to have anti-cancer effects in their own right, including the anti-malarial agent chloroquine and the analgesic compound aspirin. Further studies are warranted to expand the concept of anti-6PGD in combination with compounds known to induce hemolytic anemia in G6PD and 6PGD deficient patients for leukemia therapy.

Beyond the combinatorial approach presented in this work, combination therapies targeting complementary metabolic pathways is an important anti-leukemia therapeutic strategy to be investigated as well. For example, leukemia cells rely primarily on glycolysis for ATP production, but inhibiting glycolysis would in theory drive cells towards oxidative phosphorylation as an ATP source. Targeting both glycolysis and oxidative phosphorylation would likely lead to severe depletion of intracellular ATP levels and consequently cell death. This concept has been explored in a prostate cancer model using glycolytic inhibitor 2-deoxyglucose (2-DG) and oxidative phosphorylation inhibitor metformin. It was shown that prostate cancer cells displayed significant sensitivity to this combination, while normal prostate cells were only moderately affected (154). Interestingly, our PGAM1 inhibitor attenuates the upper glycolytic process in leukemia cells, but has no effect on ATP levels, suggesting a compensatory mechanism may be at work to sustain intracellular ATP. Combining PGMI-004A with metformin or other inhibitors of oxidative phosphorylation may lead to enhanced or synergistic inhibition of leukemia cell viability through ATP depletion similar to the combination of 2-DG and metformin in prostate cancer cells.

An alternative strategy involves the combined inhibition of distinct biosynthetic pathways. In cancer cells, glucose and glutamine serve as primary carbon sources for ATP production and biosynthesis (155). Glutamine has recently been shown to be crucial for *de novo* lipogenesis in cells under hypoxia. Normally, precursors for fatty-acid synthesis are generated from glucose-derived pyruvate through the

oxygen-dependent TCA cycle. However, proliferating cells undergoing aerobic glycolysis and those grown under hypoxic conditions use reductive carboxylation of glutamine-derived α -ketoglutarate to synthesize lipid precursors, with the latter relying almost exclusively on this pathway for *de novo* lipogenesis (156). This may indeed be the case in leukemic cells residing under hypoxia in the bone marrow, and inhibition of this pathway would disrupt *de novo* lipid biosynthesis in these cells. In addition to its effects on the upper glycolytic pathway, PGMI-004A also leads to inhibition both nucleotide biosynthesis and serine biosynthesis through its indirect effects on 6PGD and PHGDH, respectively. Therefore, combined inhibition of the reductive glutamine pathway together with PGMI-004A would block three different biosynthetic pathways from two different carbon sources, which may in turn lead to enhanced or synergistic inhibition of leukemia cell viability particularly under hypoxia.

Is it worth noting that an outstanding concern regarding PGMI-004A was potential toxicity in normal post-mitotic, metabolically active cells. The aforementioned combinations using PGMI-004A would permit reduced doses of the drug, which in turn could limit the effect it may have on normal, glycolytic cells.

Lastly, as we move forward in the search for features common to leukemia cells for the development of pan-leukemia therapies, it is imperative to consider the leukemic stem cell, which is thought to be a common denominator in many human leukemias regardless of the lineage along which the disease manifests. Because LSCs

are typically quiescent, they elude cytotoxic therapies and serve to reconstitute the disease, leading to relapse. Though not broached in this work, leukemia stem cell signaling and metabolism represent important avenues to be explored in the search for pan-leukemia vulnerabilities.

References

1. Leukemia Facts & Statistics. The Leukemia & Lymphoma Society. Accessed 2013-05-06.
2. SEER Stat Fact Sheets: Leukemia. National Cancer Institute. Accessed 2013-05-06.
3. Gratwohl A, Baldomero H, Aljurf M, Pasquini MC, Bouzas LF, Yoshimi A, Szer J, Lipton J, Schwendener A, Gratwohl M, Frauendorfer K, Niederwieser D, Horowitz M, Kodaera Y. Hematopoietic stem cell transplantation: A Global Perspective. *JAMA*. 2010 April 28; 303(16): 1617–1624.
4. Goker H, Haznedaroglu IC, Chao NJ. Acute graft-vs-host disease: pathobiology and management. *Exp Hematol*. 2001 Mar;29(3):259-77.
5. Gilliland DG, Griffin JD. The roles of FLT3 in hematopoiesis and leukemia. *Blood*. 2002 Sep 1;100(5):1532-42.
6. Takahashi S. Current findings for recurring mutations in acute myeloid leukemia. *J Hematol Oncol*. 2011 Sep 14;4:36. Review.
7. Frohling S, Scholl C, Gilliland DG, Levine RL. Genetics of myeloid malignancies: pathogenetic and clinical implications. *J Clin Oncol* 2005, 23:6285-6295.
8. Kelly LM, Gilliland DG: Genetics of myeloid leukemias. *Annu Rev Genomics Hum Genet* 2002, 3:179-198.
9. Ren R. Mechanisms of BCR-ABL in the pathogenesis of chronic myelogenous leukaemia. *Nat Rev Cancer*. 2005 Mar;5(3):172-83.
10. Hantschel O, Superti-Furga G. Regulation of the c-Abl and Bcr-Abl tyrosine kinases. *Nat Rev Mol Cell Biol*. 2004 Jan;5(1):33-44.
11. Zheng X, Oancea C, Henschler R, Moore MA, Ruthardt M. Reciprocal t(9;22) ABL/BCR fusion proteins: leukemogenic potential and effects on B cell commitment. *PLoS One*. 2009 Oct 30;4(10):e7661.
12. Cilloni D, Saglio G. Molecular pathways: BCR-ABL. *Clin Cancer Res*. 2012 Feb 15;18(4):930-7.
13. Gilliland DG, Jordan CT, Felix CA. The molecular basis of leukemia. *Hematology Am Soc Hematol Educ Program*. 2004:80-97.
14. Grundler R, Miething C, Thiede C, Peschel C, Duyster J. FLT3-ITD and tyrosine kinase domain mutants induce 2 distinct phenotypes in a murine bone marrow transplantation model. *Blood*. 2005 Jun 15;105(12):4792-9.
15. Lee BH, Williams IR, Anastasiadou E, Boulton CL, Joseph SW, Amaral SM, Curley DP, Duclos N, Huntly BJ, Fabbro D, Griffin JD, Gilliland DG. FLT3 internal tandem duplication mutations induce myeloproliferative or lymphoid disease in a transgenic mouse model. *Oncogene*. 2005 Nov 24;24(53):7882-92.
16. Lee BH, Tothova Z, Levine RL, Anderson K, Buza-Vidas N, Cullen DE, McDowell EP, Adelsperger J, Fröhling S, Huntly BJ, Beran M, Jacobsen SE, Gilliland DG. FLT3 mutations confer enhanced proliferation and survival properties to multipotent progenitors in a murine model of chronic myelomonocytic leukemia. *Cancer Cell*. 2007 Oct;12(4):367-80.

17. Rocnik JL, Okabe R, Yu JC, Lee BH, Giese N, Schenkein DP, Gilliland DG. Roles of tyrosine 589 and 591 in STAT5 activation and transformation mediated by FLT3-ITD. *Blood*. 2006 Aug 15;108(4):1339-45.
18. Hatlen MA, Wang L, Nimer SD. AML1-ETO driven acute leukemia: insights into pathogenesis and potential therapeutic approaches. *Front Med*. 2012 Sep;6(3):248-62. Review.
19. Look AT. Oncogenic transcription factors in the human acute leukemias. *Science*. 1997 Nov 7;278(5340):1059-64. Review.
20. Rosenbauer F, Tenen DG. Transcription factors in myeloid development: balancing differentiation with transformation. *Nat Rev Immunol*. 2007 Feb;7(2):105-17.
21. Wichmann C, Grez M, Lausen J. Molecular targeting of aberrant transcription factors in leukemia: strategies for RUNX1/ETO. *Curr Drug Targets*. 2010 Sep;11(9):1181-91.
22. Gao C, Dimitrov T, Yong KJ, Tatetsu H, Jeong HW, Luo HR, Bradner JE, Tenen DG, Chai L. Targeting transcription factor SALL4 in acute myeloid leukemia by interrupting its interaction with an epigenetic complex. *Blood*. 2013 Feb 21;121(8):1413-21.
23. Druker BJ, Tamura S, Buchdunger E, Ohno S, Segal GM, Fanning S, Zimmermann J, Lydon NB. Effects of a selective inhibitor of the Abl tyrosine kinase on the growth of Bcr-Abl positive cells. *Nat Med* 1996;2:561-566.
24. Druker BJ, Talpaz M, Resta D et al. Clinical efficacy and safety of an ABL specific tyrosine kinase inhibitor as targeted therapy for chronic myelogenous leukemia. *Blood* 1999;94:697a.
25. Druker BJ, Lydon NB. Lessons learned from the development of an abl tyrosine kinase inhibitor for chronic myelogenous leukemia. *J Clin Invest* 2000;105:3-7.
26. Talpaz M, Sawyers CL, Kantarjian H et al. Activity of an Abl specific tyrosine kinase inhibitor in patients with Bcr-Abl positive acute leukemias, including chronic myelogenous leukemia in blast crisis. *Proc Am Soc Clin Oncol* 2000;19:4a.
27. Druker BJ, Talpaz M, Resta DJ, Peng B, Buchdunger E, Ford JM, Lydon NB, Kantarjian H, Capdeville R, Ohno-Jones S, Sawyers CL. Efficacy and safety of a specific inhibitor of the BCR-ABL tyrosine kinase in chronic myeloid leukemia. *N Engl J Med* 2001;344:1038-1042.
28. Druker BJ, Sawyers CL, Kantarjian H, Resta DJ, Reese SF, Ford JM, Capdeville R, Talpaz M. Activity of a specific inhibitor of the BCR-ABL tyrosine kinase in the blast crisis of chronic myeloid leukemia and acute lymphoblastic leukemia with the Philadelphia chromosome. *N Engl J Med* 2001;344:1038-1042.
29. Lemonick MD, Park A. New hope for cancer. *TIME*. 2001 May 28;157(21):62-9.
30. Agrawal M, Garg RJ, Kantarjian H, Cortes J. Chronic myeloid leukemia in the tyrosine kinase inhibitor era: what is the "best" therapy? *Curr Oncol Rep*. 2010 Sep;12(5):302-13.

31. Sawyers CL. Even better kinase inhibitors for chronic myeloid leukemia. *N Engl J Med*. 2010 Jun 17;362(24):2314-5.
32. Gorre ME, Mohammed M, Ellwood K, Hsu N, Paquette R, Rao PN, Sawyers CL. Clinical resistance to STI-571 cancer therapy caused by BCR-ABL gene mutation or amplification. *Science*. 2001 Aug 3;293(5531):876-80.
33. Gorre ME, Sawyers CL. Molecular mechanisms of resistance to STI571 in chronic myeloid leukemia. *Curr Opin Hematol*. 2002 Jul;9(4):303-7.
34. le Coutre P, Tassi E, Varella-Garcia M, Barni R, Mologni L, Cabrita G, Marchesi E, Supino R, Gambacorti-Passerini C. Induction of resistance to the Abelson inhibitor STI571 in human leukemia cells through gene amplification. *Blood* 2000;95:1758-1766.
35. Weisberg E, Griffin JD. Mechanism of resistance to the ABL tyrosine kinase inhibitor STI571 in BCR/ABL-transformed hematopoietic cell lines. *Blood* 2000;95:3498-3505.
36. Mahon FX, Deininger MW, Schultheis B, Chabrol J, Reiffers J, Goldman JM, Melo JV. Selection and characterization of BCR-ABL positive cell lines with differential sensitivity to the tyrosine kinase inhibitor STI571: diverse mechanisms of resistance. *Blood* 2000;96:1070-1079.
37. Bixby D, Talpaz M. Mechanisms of resistance to tyrosine kinase inhibitors in chronic myeloid leukemia and recent therapeutic strategies to overcome resistance. *Hematology Am Soc Hematol Educ Program*. 2009:461-76.
38. Das J, Chen P, Norris D, Padmanabha R, Lin J, Moquin RV, Shen Z, Cook LS, Dowejko AM, Pitt S, Pang S, Shen DR, Fang Q, de Fex HF, McIntyre KW, Shuster DJ, Gillooly KM, Behnia K, Schieven GL, Wityak J, Barrish JC. 2-aminothiazole as a novel kinase inhibitor template. Structure-activity relationship studies toward the discovery of N-(2-chloro-6-methylphenyl)-2-[[6-[4-(2-hydroxyethyl)-1-piperazinyl]]-2-methyl-4-pyrimidinyl]amino]-1,3-thiazole-5-carboxamide (dasatinib, BMS-354825) as a potent pan-Src kinase inhibitor. *J Med Chem*. 2006 Nov 16;49(23):6819-32.
39. Talpaz M, Shah NP, Kantarjian H, Donato N, Nicoll J, Paquette R, Cortes J, O'Brien S, Nicaise C, Bleickardt E, Blackwood-Chirchir MA, Iyer V, Chen TT, Huang F, Decillis AP, Sawyers CL. Dasatinib in imatinib-resistant Philadelphia chromosome-positive leukemias. *N Engl J Med*. 2006 Jun 15;354(24):2531-41.
40. Kantarjian H, Giles F, Wunderle L, Bhalla K, O'Brien S, Wassmann B, Tanaka C, Manley P, Rae P, Mietlowski W, Bochinski K, Hochhaus A, Griffin JD, Hoelzer D, Albitar M, Dugan M, Cortes J, Alland L, Ottmann OG. Nilotinib in imatinib-resistant CML and Philadelphia chromosome-positive ALL. *N Engl J Med*. 2006 Jun 15;354(24):2542-51.
41. Dufies M, Cassuto O, Jacquelin A, Robert G, Auberger P. Ponatinib circumvents all types of imatinib resistance in chronic myelogenous leukemia cell lines. *Cell Cycle*. 2013 May 10;12(11).
42. Pokras SM, Divino V, Ferrufino CP, R J G A, Huang H. The economic burden of dasatinib and nilotinib treatment failure in chronic myeloid leukemia (cml) patients: a real-world analysis. *Value Health*. 2013 May;16(3):A137.

43. Broekman F, Giovannetti E, Peters GJ. Tyrosine kinase inhibitors: Multi-targeted or single-targeted? *World J Clin Oncol*. 2011 Feb 10;2(2):80-93.
44. Bixby D, Talpaz M. Seeking the causes and solutions to imatinib-resistance in chronic myeloid leukemia. *Leukemia*. 2011 Jan;25(1):7-22.
45. Cairns RA, Harris IS, Mak TW. Regulation of cancer cell metabolism. *Nat Rev Cancer*. 2011 Feb;11(2):85-95.
46. Kroemer G, Pouyssegur J. Tumor cell metabolism: cancer's Achilles' heel. *Cancer Cell*. 2008 Jun;13(6):472-82.
47. Ward PS, Thompson CB. Metabolic Reprogramming: A Cancer Hallmark Even Warburg Did Not Anticipate. *Cancer Cell*. 2012 March 20; 21(3): 297–308.
48. Vander Heiden MG, Cantley LC, Thompson CB. Understanding the Warburg Effect: The Metabolic Requirements of Cell Proliferation. *Science*. 2009 May 22; 324(5930): 1029–1033.
49. Mardis ER, Ding L, Dooling DJ, Larson DE, McLellan MD, Chen K, Koboldt DC, Fulton RS, Delehaunty KD, McGrath SD, Fulton LA, Locke DP, Magrini VJ, Abbott RM, Vickery TL, Reed JS, Robinson JS, Wylie T, Smith SM, Carmichael L, Eldred JM, Harris CC, Walker J, Peck JB, Du F, Dukes AF, Sanderson GE, Brummett AM, Clark E, McMichael JF, Meyer RJ, Schindler JK, Pohl CS, Wallis JW, Shi X, Lin L, Schmidt H, Tang Y, Haipek C, Wiechert ME, Ivy JV, Kalicki J, Elliott G, Ries RE, Payton JE, Westervelt P, Tomasson MH, Watson MA, Baty J, Heath S, Shannon WD, Nagarajan R, Link DC, Walter MJ, Graubert TA, DiPersio JF, Wilson RK, Ley TJ. Recurring mutations found by sequencing an acute myeloid leukemia genome. *N Engl J Med*. 2009 Sep 10;361(11):1058-66.
50. Cazzola M. IDH1 and IDH2 mutations in myeloid neoplasms--novel paradigms and clinical implications. *Haematologica*. 2010 Oct;95(10):1623-7.
51. Wang F, Travins J, DeLaBarre B, Penard-Lacronique V, Schalm S, Hansen E, Straley K, Kernytsky A, Liu W, Gliser C, Yang H, Gross S, Artin E, Saada V, Mylonas E, Quivoron C, Popovici-Muller J, Saunders JO, Salituro FG, Yan S, Murray S, Wei W, Gao Y, Dang L, Dorsch M, Agresta S, Schenkein DP, Biller SA, Su SM, de Botton S, Yen KE. Targeted inhibition of mutant IDH2 in leukemia cells induces cellular differentiation. *Science*. 2013 May 3;340(6132):622-6.
52. Broome JD. L-Asparaginase: discovery and development as a tumor-inhibitory agent. *Cancer Treat Rep*. 1981;65 Suppl 4:111-4.
53. Vander Heiden MG. Targeting cancer metabolism: a therapeutic window opens. *Nat Rev Drug Discov*. 2011 Aug 31;10(9):671-84.
54. Cairo MS. Adverse reactions of L-asparaginase. *Am J Pediatr Hematol Oncol*. 1982 Fall;4(3):335-9.
55. Kang S, Dong S, Gu TL, Guo A, Cohen MS, Lonial S, Khoury HJ, Fabbro D, Gilliland DG, Bergsagel PL, Taunton J, Polakiewicz RD, Chen J. FGFR3 activates RSK2 to mediate hematopoietic transformation through tyrosine phosphorylation of RSK2 and activation of the MEK/ERK pathway. *Cancer Cell*. 2007 Sep;12(3):201-14.

56. Elf S, Blevins D, Jin L, Chung TW, Williams IR, Lee BH, Lin JX, Leonard WJ, Taunton J, Khoury HJ, Kang S. p90RSK2 is essential for FLT3-ITD- but dispensable for BCR-ABL-induced myeloid leukemia. *Blood*. 2011 Jun 23;117(25):6885-94.
57. Hitosugi T, Kang S, Vander Heiden MG, Chung TW, Elf S, Lythgoe K, Dong S, Lonial S, Wang X, Chen GZ, Xie J, Gu TL, Polakiewicz RD, Roesel JL, Boggon TJ, Khuri FR, Gilliland DG, Cantley LC, Kaufman J, Chen J. Tyrosine phosphorylation inhibits PKM2 to promote the Warburg effect and tumor growth. *Sci Signal*. 2009 Nov 17;2(97):ra73.
58. Fan J, Hitosugi T, Chung TW, Xie J, Ge Q, Gu TL, Polakiewicz RD, Chen GZ, Boggon TJ, Lonial S, Khuri FR, Kang S, Chen J. Tyrosine phosphorylation of lactate dehydrogenase A is important for NADH/NAD(+) redox homeostasis in cancer cells. *Mol Cell Biol*. 2011 Dec;31(24):4938-50.
59. Hitosugi T, Fan J, Chung TW, Lythgoe K, Wang X, Xie J, Ge Q, Gu TL, Polakiewicz RD, Roesel JL, Chen GZ, Boggon TJ, Lonial S, Fu H, Khuri FR, Kang S, Chen J. Tyrosine phosphorylation of mitochondrial pyruvate dehydrogenase kinase 1 is important for cancer metabolism. *Mol Cell*. 2011 Dec 23;44(6):864-77.
60. Hitosugi T, Zhou L, Fan J, Elf S, Zhang L, Xie J, Wang Y, Gu TL, Alečković M, Leroy G, Kang Y, Kang HB, Seo JH, Shan C, Jin P, Gong W, Lonial S, Arellano ML, Khoury HJ, Chen GZ, Shin DM, Khuri FR, Boggon TJ, Kang S, He C, Chen J. Tyr26 phosphorylation of PGAM1 provides a metabolic advantage to tumours by stabilizing the active conformation. *Nat Commun*. 2013;4:1790.
61. Hitosugi T, Zhou L, Elf S, Fan J, Kang HB, Seo JH, Shan C, Dai Q, Zhang L, Xie J, Gu TL, Jin P, Alečković M, LeRoy G, Kang Y, Sudderth JA, DeBerardinis RJ, Luan CH, Chen GZ, Muller S, Shin DM, Owonikoko TK, Lonial S, Arellano ML, Khoury HJ, Khuri FR, Lee BH, Ye K, Boggon TJ, Kang S, He C, Chen J. Phosphoglycerate mutase 1 coordinates glycolysis and biosynthesis to promote tumor growth. *Cancer Cell*. 2012 Nov 13;22(5):585-600.
62. Caprari P, Caforio MP, Cianciulli P, Maffi D, Pasquino MT, Tarzia A, Amadori S, Salvati AM. 6-Phosphogluconate dehydrogenase deficiency in an Italian family. *Ann Hematol*. 2001 Jan;80(1):41-4.
63. Frank JE. Diagnosis and management of G6PD deficiency. *Am Fam Physician*. 2005 Oct 1;72(7):1277-82.
64. Beutler E. G6PD deficiency. *Blood*. 1994 Dec 1;84(11):3613-36.
65. Jones SW, Erikson E, Blenis J, Maller JL, Erikson RL. A *Xenopus* ribosomal protein S6 kinase has two apparent kinase domains that are each similar to distinct protein kinases. *Proc Natl Acad Sci U S A*. 1988;85:3377-3381.
66. Fisher TL, Blenis J. Evidence for two catalytically active kinase domains in pp90rsk. *Mol Cell Biol*. 1996;16:1212-1219.
67. Sturgill TW, Ray LB, Erikson E, Maller JL. Insulin-stimulated MAP-2 kinase phosphorylates and activates ribosomal protein S6 kinase II. *Nature*. 1988;334:715-718.
68. Blenis J. Signal transduction via the MAP kinases: proceed at your own RSK. *Proc Natl Acad Sci U S A*. 1993;90:5889-5892.

69. Frodin M, Gammeltoft S. Role and regulation of 90 kDa ribosomal S6 kinase (RSK) in signal transduction. *Mol Cell Endocrinol.* 1999;151:65-77.
70. Anjum R, Blenis J. The RSK family of kinases: emerging roles in cellular signalling. *Nat Rev Mol Cell Biol.* 2008;9:747-758.
71. Trivier E, De Cesare D, Jacquot S, et al. Mutations in the kinase Rsk-2 associated with Coffin-Lowry syndrome. *Nature.* 1996;384:567-570.
72. Kang S, Dong S, Guo A, et al. Epidermal growth factor stimulates RSK2 activation through activation of the MEK/ERK pathway and src-dependent tyrosine phosphorylation of RSK2 at Tyr-529. *J Biol Chem.* 2008;283:4652-4657.
73. Kang S, Elf S, Dong S, et al. Fibroblast growth factor receptor 3 associates with and tyrosine phosphorylates p90 RSK2, leading to RSK2 activation that mediates hematopoietic transformation. *Mol Cell Biol.* 2009;29:2105-2117.
74. Leighton IA, Dalby KN, Caudwell FB, Cohen PT, Cohen P. Comparison of the specificities of p70 S6 kinase and MAPKAP kinase-1 identifies a relatively specific substrate for p70 S6 kinase: the N-terminal kinase domain of MAPKAP kinase-1 is essential for peptide phosphorylation. *FEBS Lett.* 1995;375:289-293.
75. Buck M, Poli V, Hunter T, Chojkier M. C/EBPbeta phosphorylation by RSK creates a functional XEXD caspase inhibitory box critical for cell survival. *Mol Cell.* 2001;8:807-816.
76. Gavin AC, Ni Ainle A, Chierici E, Jones M, Nebreda AR. A p90(rsk) mutant constitutively interacting with MAP kinase uncouples MAP kinase from p34(cdc2)/cyclin B activation in *Xenopus* oocytes. *Mol Biol Cell.* 1999;10:2971-2986.
77. Dalby KN, Morrice N, Caudwell FB, Avruch J, Cohen P. Identification of regulatory phosphorylation sites in mitogen-activated protein kinase (MAPK)-activated protein kinase-1a/p90rsk that are inducible by MAPK. *J Biol Chem.* 1998;273:1496-1505.
78. Yang TT, Xiong Q, Graef IA, Crabtree GR, Chow CW. Recruitment of the extracellular signal-regulated kinase/ribosomal S6 kinase signaling pathway to the NFATc4 transcription activation complex. *Mol Cell Biol.* 2005;25:907-920.
79. Cho YY, Yao K, Bode AM, et al. RSK2 mediates muscle cell differentiation through regulation of NFAT3. *J Biol Chem.* 2007;282:8380-8392.
80. Yang X, Matsuda K, Bialek P, et al. ATF4 is a substrate of RSK2 and an essential regulator of osteoblast biology; implication for Coffin-Lowry Syndrome. *Cell.* 2004;117:387-398.
81. Wingate AD, Campbell DG, Peggie M, Arthur JS. Nur77 is phosphorylated in cells by RSK in response to mitogenic stimulation. *Biochem J.* 2006;393:715-724.
82. He Z, Ma WY, Liu G, Zhang Y, Bode AM, Dong Z. Arsenite-induced phosphorylation of histone H3 at serine 10 is mediated by Akt1, extracellular signal-regulated kinase 2, and p90 ribosomal S6 kinase 2 but not mitogen- and stress-activated protein kinase 1. *J Biol Chem.* 2003;278:10588-10593.

83. Shimamura A, Ballif BA, Richards SA, Blenis J. Rsk1 mediates a MEK-MAP kinase cell survival signal. *Curr Biol.* 2000;10:127-135.
84. Dehan E, Bassermann F, Guardavaccaro D, et al. betaTrCP- and Rsk1/2-mediated degradation of BimEL inhibits apoptosis. *Mol Cell.* 2009;33:109-116.
85. Anjum R, Roux PP, Ballif BA, Gygi SP, Blenis J. The tumor suppressor DAP kinase is a target of RSK-mediated survival signaling. *Curr Biol.* 2005;15:1762-1767.
86. Sutherland C, Leighton IA, Cohen P. Inactivation of glycogen synthase kinase-3 beta by phosphorylation: new kinase connections in insulin and growth-factor signalling. *Biochem J.* 1993;296 (Pt 1):15-19.
87. Takahashi E, Abe J, Gallis B, et al. p90(RSK) is a serum-stimulated Na⁺/H⁺ exchanger isoform-1 kinase. Regulatory phosphorylation of serine 703 of Na⁺/H⁺ exchanger isoform-1. *J Biol Chem.* 1999;274:20206-20214.
88. Fujita N, Sato S, Tsuruo T. Phosphorylation of p27Kip1 at threonine 198 by p90 ribosomal protein S6 kinases promotes its binding to 14-3-3 and cytoplasmic localization. *J Biol Chem.* 2003;278:49254-49260.
89. Marques Pereira P, Schneider A, Pannetier S, Heron D, Hanauer A. Coffin-Lowry syndrome. *Eur J Hum Genet.* 2009.
90. Kang S, Elf S, Lythgoe K, et al. p90 ribosomal S6 kinase 2 promotes invasion and metastasis of human head and neck squamous cell carcinoma cells. *J Clin Invest;*120:1165-1177.
91. Xian W, Pappas L, Pandya D, et al. Fibroblast growth factor receptor 1-transformed mammary epithelial cells are dependent on RSK activity for growth and survival. *Cancer Res.* 2009;69:2244-2251.
92. Clark DE, Errington TM, Smith JA, Frierson HF, Jr., Weber MJ, Lannigan DA. The serine/threonine protein kinase, p90 ribosomal S6 kinase, is an important regulator of prostate cancer cell proliferation. *Cancer Res.* 2005;65:3108-3116.
93. David JP, Mehic D, Bakiri L, et al. Essential role of RSK2 in c-Fos-dependent osteosarcoma development. *J Clin Invest.* 2005;115:664-672.
94. Chen J, Williams IR, Lee BH, et al. Constitutively activated FGFR3 mutants signal through PLCgamma-dependent and -independent pathways for hematopoietic transformation. *Blood.* 2005;106:328-337.
95. Lin JX, Spolski R, Leonard WJ. Critical role for Rsk2 in T-lymphocyte activation. *Blood.* 2008;111:525-533.
96. Schwaller J, Parganas E, Wang D, et al. Stat5 is essential for the myelo- and lymphoproliferative disease induced by TEL/JAK2. *Mol Cell.* 2000;6:693-704.
97. Dash AB, Williams IR, Kutok JL, et al. A murine model of CML blast crisis induced by cooperation between BCR/ABL and NUP98/HOXA9. *Proc Natl Acad Sci U S A.* 2002;99:7622-7627.
98. Kelly LM, Liu Q, Kutok JL, Williams IR, Boulton CL, Gilliland DG. FLT3 internal tandem duplication mutations associated with human acute myeloid leukemias induce myeloproliferative disease in a murine bone marrow transplant model. *Blood.* 2002;99:310-318.

99. Schwaller J, Frantsve J, Aster J, et al. Transformation of hematopoietic cell lines to growth-factor independence and induction of a fatal myelo- and lymphoproliferative disease in mice by retrovirally transduced TEL/JAK2 fusion genes. *PG* - 5321-33. *Embo J*. 1998;17.
100. David E, Sun SY, Waller EK, Chen J, Khuri FR, Lonial S. The combination of the farnesyl transferase inhibitor lonafarnib and the proteasome inhibitor bortezomib induces synergistic apoptosis in human myeloma cells that is associated with down-regulation of p-AKT. *Blood*. 2005;106:4322-4329.
101. Lopes de Menezes DE, Peng J, Garrett EN, et al. CHIR-258: a potent inhibitor of FLT3 kinase in experimental tumor xenograft models of human acute myelogenous leukemia. *Clin Cancer Res*. 2005;11:5281-5291.
102. Lee SH, Lopes de Menezes D, Vora J, et al. In vivo target modulation and biological activity of CHIR-258, a multitargeted growth factor receptor kinase inhibitor, in colon cancer models. *Clin Cancer Res*. 2005;11:3633-3641.
103. Cohen MS, Zhang C, Shokat KM, Taunton J. Structural bioinformatics-based design of selective, irreversible kinase inhibitors. *Science*. 2005;308:1318-1321.
104. Yagasaki F, Wakao D, Yokoyama Y, et al. Fusion of ETV6 to fibroblast growth factor receptor 3 in peripheral T-cell lymphoma with a t(4;12)(p16;p13) chromosomal translocation. *Cancer Res*. 2001;61:8371-8374.
105. Dufresne SD, Bjorbaek C, El-Haschimi K, et al. Altered extracellular signal-regulated kinase signaling and glycogen metabolism in skeletal muscle from p90 ribosomal S6 kinase 2 knockout mice. *Mol Cell Biol*. 2001;21:81-87.
106. Choudhary C, Schwable J, Brandts C, et al. AML-associated Flt3 kinase domain mutations show signal transduction differences compared with Flt3 ITD mutations. *Blood*. 2005;106:265-273.
107. Choudhary C, Brandts C, Schwable J, et al. Activation mechanisms of STAT5 by oncogenic Flt3-ITD. *Blood*. 2007;110:370-374.
108. Cuadrado A, Nebreda AR. New insights into RSK activation and hematopoietic cancer. *Cancer Cell*. 2007;12:187-189.
109. Elstrom RL, Bauer DE, Buzzai M, Karnauskas R, Harris MH, Plas DR, Zhuang H, Cinalli RM, Alavi A, Rudin CM, Thompson CB. Akt stimulates aerobic glycolysis in cancer cells. *Cancer Res*. 2004 Jun 1;64(11):3892-9.
110. Gottschalk S, Anderson N, Hainz C, Eckhardt SG, Serkova NJ. Imatinib (STI571)-mediated changes in glucose metabolism in human leukemia BCR-ABL-positive cells. *Clin Cancer Res*. 2004 Oct 1;10(19):6661-8.
111. Ren F, Wu H, Lei Y, Zhang H, Liu R, Zhao Y, Chen X, Zeng D, Tong A, Chen L, Wei Y, Huang C. Quantitative proteomics identification of phosphoglycerate mutase 1 as a novel therapeutic target in hepatocellular carcinoma. *Mol Cancer*. 2010 Apr 19;9:81.
112. Liu L, Wang S, Zhang Q, Ding Y. Identification of potential genes/proteins regulated by Tiam1 in colorectal cancer by microarray analysis and proteome analysis. *Cell Biol Int*. 2008 Oct;32(10):1215-22.
113. Corcoran CA, Huang Y, Sheikh MS. The regulation of energy generating metabolic pathways by p53. *Cancer Biol Ther*. 2006 Dec;5(12):1610-3.

114. Tennant DA, Durán RV, Boulahbel H, Gottlieb E. Metabolic transformation in cancer. *Carcinogenesis*. 2009 Aug;30(8):1269-80.
115. Tennant DA, Durán RV, Gottlieb E. Targeting metabolic transformation for cancer therapy. *Nat Rev Cancer*. 2010 Apr;10(4):267-77.
116. Evans MJ, Saghatelian A, Sorensen EJ, Cravatt BF. Target discovery in small-molecule cell-based screens by in situ proteome reactivity profiling. *Nat Biotechnol*. 2005 Oct;23(10):1303-7.
117. Evans MJ, Morris GM, Wu J, Olson AJ, Sorensen EJ, Cravatt BF. Mechanistic and structural requirements for active site labeling of phosphoglycerate mutase by spiroepoxides. *Mol Biosyst*. 2007 Jul;3(7):495-506.
118. Jiang P, Du W, Wang X, Mancuso A, Gao X, Wu M, Yang X. p53 regulates biosynthesis through direct inactivation of glucose-6-phosphate dehydrogenase. *Nat Cell Biol*. 2011 Mar;13(3):310-6.
119. Shackelford DB, Shaw RJ. The LKB1-AMPK pathway: metabolism and growth control in tumour suppression. *Nat Rev Cancer*. 2009 Aug;9(8):563-75.
120. Nicklin P, Bergman P, Zhang B, Triantafellow E, Wang H, Nyfeler B, Yang H, Hild M, Kung C, Wilson C, Myer VE, MacKeigan JP, Porter JA, Wang YK, Cantley LC, Finan PM, Murphy LO. Bidirectional transport of amino acids regulates mTOR and autophagy. *Cell*. 2009 Feb 6;136(3):521-34.
121. Engel M, Mazurek S, Eigenbrodt E, Welter C. Phosphoglycerate mutase-derived polypeptide inhibits glycolytic flux and induces cell growth arrest in tumor cell lines. *J Biol Chem*. 2004 Aug 20;279(34):35803-12.
122. Bailey-Serres J, Tom J, Freeling M. Expression and distribution of cytosolic 6-phosphogluconate dehydrogenase isozymes in maize. *Biochem Genet*. 1992 Jun;30(5-6):233-46.
123. Bravard A, Luccioni C, Muleris M, Lefrancois D, Dutrillaux B. Relationships between UMPK and PGD activities and deletions of chromosome 1p in colorectal cancers. *Cancer Genet Cytogenet*. 1991 Oct 1;56(1):45-56.
124. Basu J, Duttagupta C, Vermund SH, Ahn C, Palan PR, Romney SL. Alterations in erythrocyte glutathione metabolism associated with cervical dysplasias and carcinoma in situ. *Cancer Invest*. 1993;11(6):652-9.
125. Jonas SK, Benedetto C, Flatman A, Hammond RH, Micheletti L, Riley C, Riley PA, Spargo DJ, Zonca M, Slater TF. Increased activity of 6-phosphogluconate dehydrogenase and glucose-6-phosphate dehydrogenase in purified cell suspensions and single cells from the uterine cervix in cervical intraepithelial neoplasia. *Br J Cancer*. 1992 Jul;66(1):185-91.
126. Giusti L, Iacconi P, Ciregia F, Giannaccini G, Donatini GL, Basolo F, Miccoli P, Pinchera A, Lucacchini A. Fine-needle aspiration of thyroid nodules: proteomic analysis to identify cancer biomarkers. *J Proteome Res*. 2008 Sep;7(9):4079-88.
127. Brocklehurst D, Champion AE, Cheek TR, Dewhurst DG. The value of 6-phosphogluconate dehydrogenase (6-PGDH) activity as a marker of tumour cellularity and prognostic indicator in primary breast cancer. *Tumour Biol*. 1986;7(2-3):99-104.
128. Schauerte JA, Gafni A. Long-lived tryptophan fluorescence in phosphoglycerate mutase. *Biochemistry*. 1989 May 2;28(9):3948-54.

129. Sommercorn J, Freedland RA. Regulation of hepatic phosphofructokinase by 6-phosphogluconate. *J Biol Chem.* 1982 Aug 25;257(16):9424-8.
130. Tian WN, Braunstein LD, Pang J, Stuhlmeier KM, Xi QC, Tian X, Stanton RC. Importance of glucose-6-phosphate dehydrogenase activity for cell growth. *J Biol Chem.* 1998 Apr 24;273(17):10609-17.
131. Farquharson C, Milne J, Loveridge N. Mitogenic action of insulin-like growth factor-I on human osteosarcoma MG-63 cells and rat osteoblasts maintained in situ: the role of glucose-6-phosphate dehydrogenase. *Bone Miner.* 1993 Aug;22(2):105-15.
132. Tian WN, Braunstein LD, Apse K, Pang J, Rose M, Tian X, Stanton RC. Importance of glucose-6-phosphate dehydrogenase activity in cell death. *Am J Physiol.* 1999 May;276(5 Pt 1):C1121-31.
133. Li D, Zhu Y, Tang Q, Lu H, Li H, Yang Y, Li Z, Tong S. A new G6PD knockdown tumor-cell line with reduced proliferation and increased susceptibility to oxidative stress. *Cancer Biother Radiopharm.* 2009 Feb;24(1):81-90.
134. Schafer ZT, Grassian AR, Song L, Jiang Z, Gerhart-Hines Z, Irie HY, Gao S, Puigserver P, Brugge JS. Antioxidant and oncogene rescue of metabolic defects caused by loss of matrix attachment. *Nature.* 2009 Sep 3;461(7260):109-13.
135. Ke S, Wei Y, Shi L, Yang Q, Yang Z. Synthesis of Novel Steroid Derivatives Derived from Dehydroepiandrosterone as Potential Anticancer Agents. *Anticancer Agents Med Chem.* 2013 Apr 1.
136. Budihardjo II, Walker DL, Svingen PA, Buckwalter CA, Desnoyers S, Eckdahl S, Shah GM, Poirier GG, Reid JM, Ames MM, Kaufmann SH. 6-Aminonicotinamide sensitizes human tumor cell lines to cisplatin. *Clin Cancer Res.* 1998 Jan;4(1):117-30.
137. Galal AM, Gul W, Slade D, Ross SA, Feng S, Hollingshead MG, Alley MC, Kaur G, ElSohly MA. Synthesis and evaluation of dihydroartemisinin and dihydroartemisinin acetal dimers showing anticancer and antiprotozoal activity. *Bioorg Med Chem.* 2009 Jan 15;17(2):741-51.
138. Ba Q, Zhou N, Duan J, Chen T, Hao M, Yang X, Li J, Yin J, Chu R, Wang H. Dihydroartemisinin exerts its anticancer activity through depleting cellular iron via transferrin receptor-1. *PLoS One.* 2012;7(8):e42703.
139. Wang Z, Hu W, Zhang JL, Wu XH, Zhou HJ. Dihydroartemisinin induces autophagy and inhibits the growth of iron-loaded human myeloid leukemia K562 cells via ROS toxicity. *FEBS Open Bio.* 2012 May 23;2:103-12.
140. Villeval JL, Pelicci PG, Tabilio A, Titeux M, Henri A, Hoesche F, Thomopoulos P, Vainchenker W, Garbaz M, Rochant H, Breton-Gorius J, Edwards PA, Testa U. Erythroid properties of K562 cells. Effect of hemin, butyrate and TPA induction. *Exp Cell Res.* 1983 Jul;146(2):428-35.
141. Kalimi M, Shafagoj Y, Loria R, Padgett D, Regelson W. Anti-glucocorticoid effects of dehydroepiandrosterone (DHEA). *Mol Cell Biochem.* 1994 Feb 23;131(2):99-104.

142. Chen F, Knecht K, Birzin E, Fisher J, Wilkinson H, Mojena M, Moreno CT, Schmidt A, Harada S, Freedman LP, Reszka AA. Direct agonist/antagonist functions of dehydroepiandrosterone. *Endocrinology*. 2005 Nov;146(11):4568-76.
143. Lindschau C, Kirsch T, Klinge U, Kolkhof P, Peters I, Fiebeler A. Dehydroepiandrosterone-induced phosphorylation and translocation of FoxO1 depend on the mineralocorticoid receptor. *Hypertension*. 2011 Sep;58(3):471-8.
144. Wang SJ, Sun B, Cheng ZX, Zhou HX, Gao Y, Kong R, Chen H, Jiang HC, Pan SH, Xue DB, Bai XW. Dihydroartemisinin inhibits angiogenesis in pancreatic cancer by targeting the NF- κ B pathway. *Cancer Chemother Pharmacol*. 2011 Dec;68(6):1421-30.
145. Di JM, Pang J, Sun QP, Zhang Y, Fang YQ, Liu XP, Zhou JH, Ruan XX, Gao X. Toll-like receptor 9 agonists up-regulates the expression of cyclooxygenase-2 via activation of NF-kappaB in prostate cancer cells. *Mol Biol Rep*. 2010 Apr;37(4):1849-55.
146. Din FV, Valanciute A, Houde VP, Zibrova D, Green KA, Sakamoto K, Alessi DR, Dunlop MG. Aspirin inhibits mTOR signaling, activates AMP-activated protein kinase, and induces autophagy in colorectal cancer cells. *Gastroenterology*. 2012 Jun;142(7):1504-15.e3.
147. Hawley SA, Fullerton MD, Ross FA, Schertzer JD, Chevtzoff C, Walker KJ, Peggie MW, Zibrova D, Green KA, Mustard KJ, Kemp BE, Sakamoto K, Steinberg GR, Hardie DG. The ancient drug salicylate directly activates AMP-activated protein kinase. *Science*. 2012 May 18;336(6083):918-22.
148. Göransson O, McBride A, Hawley SA, Ross FA, Shpiro N, Foretz M, Viollet B, Hardie DG, Sakamoto K. Mechanism of action of A-769662, a valuable tool for activation of AMP-activated protein kinase. *J Biol Chem*. 2007 Nov 9;282(45):32549-60.
149. Foretz M, Guihard S, Leclerc J, Fauveau V, Couty JP, Andris F, Gaudry M, Andreelli F, Vaulont S, Viollet B. Maintenance of red blood cell integrity by AMP-activated protein kinase alpha1 catalytic subunit. *FEBS Lett*. 2010 Aug 20;584(16):3667-71.
150. Wang S, Dale GL, Song P, Viollet B, Zou MH. AMPKalpha1 deletion shortens erythrocyte life span in mice: role of oxidative stress. *J Biol Chem*. 2010 Jun 25;285(26):19976-85.
151. Pray L. Gleevec: the breakthrough in cancer treatment. *Nature Education* 2008; 1(1).
152. Zhao C, Blum J, Chen A, Kwon HY, Jung SH, Cook JM, Lagoo A, Reya T. Loss of beta-catenin impairs the renewal of normal and CML stem cells in vivo. *Cancer Cell*. 2007 Dec;12(6):528-41.
153. Rohle D, Popovici-Muller J, Palaskas N, Turcan S, Grommes C, Campos C, Tsoi J, Clark O, Oldrini B, Komisopoulou E, Kunii K, Pedraza A, Schalm S, Silverman L, Miller A, Wang F, Yang H, Chen Y, Kernytsky A, Rosenblum MK, Liu W, Biller SA, Su SM, Brennan CW, Chan TA, Graeber TG, Yen KE, Mellinghoff IK. An inhibitor of mutant IDH1 delays growth and promotes differentiation of glioma cells. *Science*. 2013 May 3;340(6132):626-30.

154. Ben Sahra I, Laurent K, Giuliano S, Larbret F, Ponzio G, Gounon P, Le Marchand-Brustel Y, Giorgetti-Peraldi S, Cormont M, Bertolotto C, Deckert M, Auberger P, Tanti JF, Bost F. Targeting cancer cell metabolism: the combination of metformin and 2-deoxyglucose induces p53-dependent apoptosis in prostate cancer cells. *Cancer Res.* 2010 Mar 15;70(6):2465-75.
155. Wellen KE, Lu C, Mancuso A, Lemons JM, Ryczko M, Dennis JW, Rabinowitz JD, Collier HA, Thompson CB. The hexosamine biosynthetic pathway couples growth factor-induced glutamine uptake to glucose metabolism. *Genes Dev.* 2010 Dec 15;24(24):2784-99.
156. Metallo CM, Gameiro PA, Bell EL, Mattaini KR, Yang J, Hiller K, Jewell CM, Johnson ZR, Irvine DJ, Guarente L, Kelleher JK, Vander Heiden MG, Iliopoulos O, Stephanopoulos G. Reductive glutamine metabolism by IDH1 mediates lipogenesis under hypoxia. *Nature.* 2011 Nov 20;481(7381):380-4.